COLUMBIA RADIATION LABORATORY

RESEARCH INVESTIGATION DIRECTED TOWARD EXTENDING THE USEFUL RANGE OF THE ELECTROMAGNETIC SPECTRUM

JOINT SERVICES ELECTRONICS PROGRAM

Annual Progress Report No. 39

October 1, 1988 - September 30, 1989

Contract DAAL03-88-C-0009

Object of the Research:

Basic research in the fields of quantum electronics; electromagnetic propagation, detection and sensing; materials processing and solid state electronics.

The research reported in this document was made possible through support extended to the Columbia Radiation Laboratory, Columbia University, by the Joint Services Electronics Program (U.S. Army Research Office, Office of Naval Research, and the Air Force Office of Scientific Research) under Contract DAAL03-88-C-0009.

Submitted by: George W. Flynn and Richard M. Osgood, Jr.
Co-Directors, Columbia Radiation Laboratory

Coordinated by: Columbia Radiation Laboratory Staff
Karen Wingate, Departmental Administrator
Barbara Blegen, Secretary

COLUMBIA UNIVERSITY in the City of New York
Columbia Radiation Laboratory
500 West 120th St.
253 Engineering Terrace
New York, New York 10027

December 31, 1989

RESEARCH SUPPORT

The research reported in this document was made possible through support extended to the Columbia Radiation Laboratory, Columbia University, by the Joint Services Electronics Program (U.S. Army Research Office, Office of Naval Research, and the Air Force Office of Scientific Research) under Contract DAAL03-88-C-0009.

Portions of this work were also supported by:

AIR FORCE OFFICE OF SCIENTIFIC RESEARCH

Contract F49620-86-C-0067

ARMY RESEARCH OFFICE

Contract DAAL03-89-K-0028

NATIONAL SCIENCE FOUNDATION

Grant CHE 88-16581
Grant PHY-88-20540

DEPARTMENT OF ENERGY

Contract DE-FG02-88-ER-13937

OFFICE OF NAVAL RESEARCH

Contract N00014-86-K-0694
Contract N00014-88-K-0299

SEMICONDUCTOR RESEARCH CORPORATION

SRC-88-SJ-055

IBM CORPORATION

The support of these agencies and corporations is acknowledged in the text.

SECURITY CLASSIFICATION OF THIS PAGE

REPORT DOCUMENTATION PAGE

Form Approved OMB No. 0704-0188

1a. REPORT SECURITY CLASSIFICATION Unclassified	1b. RESTRICTIVE MARKINGS
2a. SECURITY CLASSIFICATION AUTHORITY	3. DISTRIBUTION/AVAILABILITY OF REPORT Approved for public release; distribution unlimited.
2b. DECLASSIFICATION/DOWNGRADING SCHEDULE	
4. PERFORMING ORGANIZATION REPORT NUMBER(S) ANNUAL PROGRESS REPORT NO. 39	5. MONITORING ORGANIZATION REPORT NUMBER(S)
6a. NAME OF PERFORMING ORGANIZATION COLUMBIA UNIVERSITY COLUMBIA RADIATION LABORATORY 6b. OFFICE SYMBOL (If applicable)	7a. NAME OF MONITORING ORGANIZATION Department of the Army
6c. ADDRESS (City, State, and ZIP Code) Columbia Radiation Laboratory Columbia University, 253 Engineering Ter. 500 W. 120th St., New York, NY 10027	7b. ADDRESS (City, State, and ZIP Code) U.S. Army Research Office, P.O. Box 12211 Research Triangle Park, NC 27709-2211
8a. NAME OF FUNDING/SPONSORING ORGANIZATION Department of the Army 8b. OFFICE SYMBOL (If applicable)	9. PROCUREMENT INSTRUMENT IDENTIFICATION NUMBER DAAL03-88-C-0009
8c. ADDRESS (City, State, and ZIP Code) P.O. Box 12211 Research Triangle Park, NC 27709-2211	10. SOURCE OF FUNDING NUMBERS PROGRAM ELEMENT NO. / PROJECT NO. / TASK NO. / WORK UNIT ACCESSION NO.

11. TITLE (Include Security Classification)
RESEARCH INVESTIGATION DIRECTED TOWARD EXTENDING THE USEFUL RANGE OF THE ELECTROMAGNETIC SPECTRUM

12. PERSONAL AUTHOR(S) Richard M. Osgood, Jr. and George W. Flynn, Co-Directors
Columbia Radiation Laboratory, Columbia University

13a. TYPE OF REPORT	13b. TIME COVERED	14. DATE OF REPORT (Year, Month, Day)	15. PAGE COUNT
Annual Progress Report	FROM 10/01/88 TO 09/30/89	December 31, 1989	97 pages

16. SUPPLEMENTARY NOTATION The views, opinions and/or findings contained in this report are those of the author(s) and should not be construed as an official Department of the Army position, policy, or decision, unless so designated by other documentation.

17. COSATI CODES			18. SUBJECT TERMS (Continue on reverse if necessary and identify by block number)
FIELD	GROUP	SUB-GROUP	See attached "KEYWORDS"

19. ABSTRACT (Continue on reverse if necessary and identify by block number)

See attached "ABSTRACT"

20. DISTRIBUTION/AVAILABILITY OF ABSTRACT ☒ UNCLASSIFIED/UNLIMITED ☐ SAME AS RPT. ☐ DTIC USERS	21. ABSTRACT SECURITY CLASSIFICATION Unclassified
22a. NAME OF RESPONSIBLE INDIVIDUAL George W. Flynn and/or Richard M. Osgood	22b. TELEPHONE (Include Area Code) (212) 854-3265 22c. OFFICE SYMBOL

DD Form 1473, JUN 86 Previous editions are obsolete. SECURITY CLASSIFICATION OF THIS PAGE

ABSTRACT

JSEP research has yielded two new laser microprobes for use in electronics fabrication. The development of such probes is increasingly important because of the need for precision in situ monitoring in advanced electronics fabrication. In the first, photoelectric emission induced by a focused UV laser beam (λ=257 nm) has been used for the first time to make a scanning photoemission microscope for probing semiconductor surfaces. With this instrument it was possible to map regions of different doping levels on a silicon surface. The spatial resolution was found to be limited only by the laser beam spot size. In addition, Raman microprobe spectroscopy has been used to profile locally doped regions in GaAs with micrometer-level resolution. This is an important in-situ diagnostic technique for compound semiconductors.

Two new experimental systems have been established at Columbia for fundamental studies of layer and bulk compound semiconductor surfaces and bulk crystals. In the first, a unique high-resolution laser two-photon photo-electron system has been built and tested. This system will be used to study Fermi-level band-structure of interfaces, insulator band structure, and electron dynamics. In the second, the photoluminescence from ZnSe epilayers on GaAs, bulk crystalline ZnSe, and ZnSe/$ZnMn_xSe_{1-x}$ superlattices had been studied when these materials were subjected to hydrostatic pressure in a diamond anvil cell. These measurements have provided an improved value for the hydrostatic deformatic potential for ZnSe. This study will aid the development of optical and electronic devices based on wide-band-gap II-VI semiconductors.

We have investigated ways of making improved sources of silent light (also known as photon-number-squeezed light or sub-Poisson light), and determined how such light behaves when it impinges on simple optical elements such as dielectric beamsplitters. In addition, we have used the novel ultrafast optical technique of time-delayed-four-wave-mixing (TDFWM) to measure optical dephasing phenomena in semiconductor doped glasses. Dephasing times as short as 18 fsec were observed at room temperature with no evidence of modulated structure.

In device physics, a simple theoretical model has been developed which explains the bimetal Schottky-barrier behavior observed in our UHV experiments over the last two years. Within this model, the functional dependence of the barrier height on the inner metal thickness is interpreted in terms of the metal effective screening and the interface trap states. The results indicate that the potential drop inside the metal electrode of a Schottky contact is not negligible, in contrast to the common assumption.

Keywords: light ; photons, Poisson density functions, Quantum theory, Semiconductors, Electromagnetic

A simple method for producing hot electrons and studying their collisions with molecules in the gas phase has been developed. A key and novel feature of the experiments is the resolution, 0.0003cm^{-1} or approximately 4 x 10^{-8} eV! This compares with standard electron scattering experiments which have a typical energy resolution of about 80 cm^{-1} or 10 meV. The high resolution is obtained by observing the molecular collision partner rather than the scattered electron as is normal in most electron scattering experiments. Such studies are providing fundamental insight into the mechanisms and processes which are important in plasma etching reactors. Considerable interest in this technique has been exhibited by scientists working on plasma etching diagnostics in the electronics industry.

KEYWORDS

silent light
sub-Poisson light
photon-number statistics
atmospheric transmission
random media
1/f noise
shot noise
attosecond
time-delayed four-wave mixing
optical pumping
spectroscopy
exponential decay
time delayed four wave mixing
nile blue
inhomogeneous broadening
bimetal Schottky diode
metal screening
chlorine atoms
chemical reactions
cold rotations
diode lasers
electrons
electron scattering
recoil velocity
vibrational energy
plasma etching
ZnMnSe
superlattice
diamond anvil cell
Raman scattering
squeezed light
beamsplitter
lightwave communications
K distribution
irradiance fluctuation
photodetector noise
atomic vapor
quantum beat
superfluorescence
cesium
photon echoes
optical dephasing
organic dyes
homogeneous broadening
auto correlation
Schottky barrier
interface morphology
Cl, D_2S, DCl, C_6D_{12}, S_2Cl_2
transition state
hot vibrations
excimer lasers
collision dynamics
surfaces
angular momentum
electron collisions
ZnSe
epilayer
high pressure
photoluminescence

JSEP ANNUAL PROGRESS REPORT No. 39
October 1, 1988 - September 30, 1989

TABLE OF CONTENTS

PUBLICATIONS i
PRESENTATIONS iv
COLUMBIA SEMINARS x

I. QUANTUM GENERATION AND DETECTION OF RADIATION

A. SILENT LIGHT, Malvin C. Teich, Principal Investigator
Research Area I, Work Unit 1 1

B. OPTICAL COHERENT TRANSIENT SPECTROSCOPY
Sven R. Hartmann, Principal Investigator
Research Area I, Work Unit 2
1. Attosecond Beats in Atomic Vapors 7
2. Broad-Band Time-Delayed Four-Wave Mixing 8
3. Two-photon Cooperative Cascade Superfluorescence 16
4. Local Field Contribution to the Nonlinear Response 18

II. SOLID-STATE ELECTRONICS (MATERIALS AND PROCESSING)

A. ELECTRONIC STATES AT METAL/SEMICONDUCTOR INTERFACES
Edward S. Yang, Principal Investigator
Research Area II, Work Unit 1
1. Fermi-level Movement in GaAs Bimetal Schottky Diodes 20

B. NEW OPTICAL MATERIALS AND SOURCES
Irving P. Herman, Principal Investigator
Research Area II, Work Unit 2.
1. Optical Studies of II-VI Semiconductor Structures 28
2. Optical Studies of Compound Semiconductors After Processing 33

C. ULTRAVIOLET LASER INDUCED ELECTRON AND ION EMISSION FROM SEMICONDUCTORS
Richard M. Osgood, Jr., Principal Investigator
Research Area II, Work Unit 3
1. Photoemissive Scanning Microscopy of Doped Regions on Semiconductor Surfaces 37
2. UV Laser Photoemission Studies of Compound Semiconductor Surfaces 43

D. GENERATION AND DYNAMIC PROPERTIES OF METASTABLE SPECIES FOR QUANTUM ELECTRONICS AND LASER MICROPROCESSING
George W. Flynn, Principal Investigator
Research Area II, Work Unit 4
1 Diode Laser Probing of CO_2 Vibrational Excitation Produced by Collisions with High Energy Electrons from 193 nm Excimer Laser Photolysis of Iodine 49
2 Chemical Dynamics of the Reaction Between Chlorine Atoms and Deuterated Cyclohexane 61
3. Diode Laser Probe of Vibrational, Rotational, and Translational Excitation of CO_2 following Collisions with $O(^1D)$: 1. Inelastic Scattering 66

SIGNIFICANT ACCOMPLISHMENTS 75
TECHNOLOGY TRANSITIONS 77
PERSONNEL 78

PUBLICATIONS

J. Z. Chou, S. A. Hewitt, J. F. Hershberger, B. B. Brady, G. B. Spector, L Chia, and G. W. Flynn, "Diode Laser Probing of the High Frequency Vibrational Modes of Baths of CO_2, N_2O and CO Excited by Relaxation of Highly Excited NO_2," J. Chem. Phys. 91, 5392 (1989).

J. F. Hershberger, S. A. Hewitt, S. K. Sarkar, and G. W. Flynn, "Quantum State-Resolved Study of Pure Rotational Excitation of CO_2 by Hot Atoms," J. Chem. Phys. 91, 4636 (1989).

J. M. Hossenlopp, J. F. Hershberger, and G. W. Flynn, "Kinetics and Product Vibrational Energy Disposal Dynamics in the Reaction of Chlorine Atoms with D_2S," accepted for publication, J. Phys. Chem.

T. G. Kreutz, F. A. Khan, and G. W. Flynn, "Inversion of Experimental Data to Generate State-to-State Cross Sections for Ro-Vibrationally Inelastic Scattering of CO_2 by Hot Hydrogen Atoms," accepted for publication, J. Chem. Phys.

J. F. Hershberger, J. M. Hossenlopp, Y. Lee, and G. W. Flynn, "Chemical Dynamics of the Reaction between Chlorine Atoms and Deuterated Cyclohexane," submitted for publication, J. Chem. Phys.

G. W. Flynn, "Chemical Cartography: Finding the Keys to the Kinetic Labyrinth," Science, accepted for publication.

F. A. Khan, T. G. Kreutz, G. W. Flynn, and R. E. Weston, Jr., "State Resolved Vibrational, Rotational, and Translational Energy Deposition in $CO_2(00^01)$ Excited by Collisions with Hot Hydrogen Atoms, submitted for publication, J. Chem. Phys.

L. Zhu, T. G. Kreutz, and G. W. Flynn, "Diode Laser Probing of Vibrational, Rotational, and Translational Excitation of CO_2 Following Collisions with $O(^1D)$: Inelastic Scattering," submitted for publication, J. Chem. Phys.

T. G. Kreutz and G. W. Flynn, "Analysis of Translational, Rotational, and Vibrational Energy Transfer in Collisions between CO_2 and Hot Hydrogen Atoms: The Three Dimensional 'Breathing Ellipse' Model," submitted for publication, J. Chem. Phys.

F. A. Khan, T. G. Kreutz, J. A. O'Neill, C. X. Wang, and G. W. Flynn, "State Resolved Vibrational, Rotational, and Translational Energy Deposition in $CO_2(01^11)$ Excited by Collisions with Hot Hydrogen Atoms," submitted for publication, J. Chem. Phys.

R. Friedberg, S. R. Hartmann, and J. T. Manassah, "Frequency Shift in 3-Photon Resonance," Phys. Rev. A39, 93 (1989)

R. Friedberg, S. R. Hartmann, and J. T. Manassah, "3-Photon Frequency Shift On Noncolinear Excitation," J. of Phys. B: At. Mol. Opt. Phys. 22, 2211 (1989)

R. Friedberg, S. R. Hartmann, and J. T. Manassah, "The Mirrorless Optical Bistability Condition," Phys Rev. A39, 3444 (1989)

R. Friedberg, S. R. Hartmann, and Jamal T. Manassah, "Effect of Local Field Correction on a Strongly Pumped Resonance, Phys. Rev. A40, 2446 (1989).

F. Moshary, R. Kichinski, R. J. Beach, and S. R. Hartmann, "Spectroscopy and Multiwave Mixing in Pr^{3+}:LaF_3," Phys. Rev. A40, 4426 (1989).

R. Friedberg, S. R. Hartmann, and J. T. Manassah, "Time Delayed Four-Wave Mixing with Incoherent Light: The Inhomogeneous Limit for a System with Multilevel Structure," submitted to J. of Phys. B: At. Mol. Opt. Phys.

R. Friedberg, S. R. Hartmann, and J. T. Manassah, "Frequency Shift in the Reflection Coefficient from a Gas of Two-Level Atoms," submitted to Opt. Comm.

D. DeBeer, E. Usadi, and S. R. Hartmann, "Attosecond Modulation in Sodium Vapor," to be published in the Proceedings of the International Conference on Lasers 1988.

D. DeBeer, E. Usadi and S. R. Hartmann, "Attosecond Beats in Sodium Vapor," to be published in the Proceedings of the Fourth International Laser Science Conference1988.

B. Quiniou, R. Scarmozzino, Z. Wu and R. M. Osgood, Jr., "Photoemissive Scanning Microscopy of Doped Regions on Semiconductor Surfaces," Appl. Phys. Lett. 55, 481 (1989).

B. Quiniou, R. Scarmozzino, Z. Wu and R. M. Osgood, Jr., "Microscopic Photoemissive Probing of Doped Regions on Semiconductor Surfaces," to be published in the Proceedings for the Spring '89 CLEO Meeting.

T. J. Licata, D. V. Podlesnik, H. Tang, I. P. Herman and R. M. Osgood, Jr., "CW Laser-Doping of Micrometer-Sized Features in GaAs Using a DMZn Ambient," submitted to J. Vac. Sci. Technol. (October 1989).

J. A. Tuchman, Z. Sui, I. P. Herman, R. L. Gunshor, L. A. Kolodziejski, D. A. Cammack, and M. Shone, "Photoluminescence of ZnSe Epilayers on GaAs under Hydrostatic Pressure," submitted to Mat. Res. Soc. Symp. Proc. 161, (1990).

P. Shaw, J. A. O'Neill, E. Sanchez, Z. Wu and R. M. Osgood, Jr., "The Spectroscopy and Surface Chemistry of Metal-Alkyl Molecules," Mat. Res. Soc. Proc., Dec.1988 Meeting (1989).

R. A. Campos, B. E. A. Saleh, and M. C. Teich, "Quantum-mechanical Lossless Beamsplitter: SU(2) Symmetry and Photon Statistics," Phys. Rev. A 40, 1371 (1989).

M. C. Teich and P. Diament, "Multiply Stochastic Representations for K Distributions and their Poisson Transforms," J. Opt. Soc. Am. A6, 80 (1989).

S. B. Lowen and M. C. Teich, "Generalized 1/f Shot Noise," Electronics Lett. 25, 1072 (1989).

M. C. Teich, "Fractal Character of the Auditory Neural Spike Train," IEEE Trans. Biomed. Eng. 36, 150 (1989) [Special issue on neurosystems and neuroengineering].

S. M. Khanna and M. C. Teich, "Spectral Characteristics of the Responses of Primary Auditory-Nerve Fibers to Amplitude-Modulated Signals," Hearing Res. 39, 143 (1989).

S. M. Khanna and M. C. Teich, "Spectral Characteristics of the Responses of Primary Auditory-Nerve Fibers to Frequency-Modulated Signals," Hearing Res. 39, 159 (1989).

L. F. Luo, H. L. Evans, and E. S. Yang, "A Heterojunction Bipolar Transistor with Separate Carrier Injection and Confinement," IEEE Trans. Elec. Dev. 36, 1845 (1988).

X. Wu and E. S. Yang, "Interface Capacitance in Metal-Semiconductor Junctions," J. Appl. Phys. 65, 3560 (1988).

Q. Y. Ma, T. J. Licata, X. Wu, E. S. Yang and C.-A. Chang, "High Tc Superconducting Thin-Films by Rapid Thermal Annealing of Cu/BaO/Y_2O_3 Layered Structures," Appl. Phys. Lett. 53, 2229, (1988).

X. Wu, M. T. Schmidt and E. S. Yang, "Control of the Schottky Barrier Using an Ultra-thin Interface Metal Layer," Appl. Phys. Lett. 54, 268 (1989).

Q. Y. Ma, M. T. Schmidt, T. J. Licata, D. V. Rossi, E. S. Yang, C.-A. Chang and C. E. Farrell, "Processing and Substrate Effects on YBaCuO Thin Films Formed by Rapid Thermal Annealing of Cu/BaO/Y_2O_3 Layered Structures," Proc. of 3rd Ann. Conf. on Superconductivity and Applications, Buffalo, NY (Sept. 1989).

X. Wu, E. S. Yang, and H. L. Evans, "Negative Capacitance at Metal-Semiconductor Interfaces," sub. for publications.

X. Wu, E. S. Yang, and N. D. Theodore, "Structural Characterization of Ti and Pt Thin Films on GaAs(100) Substrate," submitted for publication.

PRESENTATIONS

G. Flynn, "Diode Laser Probes of Collisonal Relaxation," University of Pennsylvania, Philadelphia, PA (October 1988).

G. Flynn, "Diode Laser Probes of Collisonal Relaxation," University of California, Los Angeles, CA (November 1988).

G. Flynn, "Diode Laser Probes of Collisonal Relaxation," University of California, Irvine, CA (November 1988).

G. Flynn, "Diode Laser Probes of Collisonal Relaxation," IBM Almaden Research Labs, San Jose, CA (November 1988).

G. Flynn, "Super High Resolution Studies of Chemical and Collision Dynamics," Yale University, New Haven, CT (January 1989).

G. Flynn, "Super High Resolution Studies of Chemical and Collision Dynamics," Polytechnic University, Brooklyn, NY (February 1989).

G. Flynn, "Super High Resolution Studies of Chemical and Collision Dynamics," Southern Illinois University, Carbondale, IL (March 1989).

G. Flynn, "Super High Resolution Studies of Chemical and Collision Dynamics," University of Kansas, Lawrence, KA (March 1989).

G. Flynn, "Super High Resolution Studies of Chemical and Collision Dynamics," Joint Institute for Laboratory Astrophysics, University of Colorado (April 1989).

G. Flynn, "Super High Resolution Studies of Chemical and Collision Dynamics," Swiss Federal Institute of Technology(ETH), Zurich, Switzerland (September 1989).

G. Flynn, "High Resolution Lasers in The Study of Chemical Dynamics," Conference on Lasers and Electroptics, Baltimore, MD (April 1989).

G. Flynn, "Energy Science from Confuscius to Buck Rogers," Consolidated Edison Lecture, Columbia University, New York, NY (May 1989).

G. Flynn, "Lasers from Rabi to Javan: Super High Resolution Studies of Molecular Collisions and How They Came to Be," Gordon Conference on Molecular Energy Transfer, Wolfboro, NH (July 1989).

G. Flynn, "Super High Resolution Studies of High Energy Molecular Relaxation Phenomena," Workshop on Dynamics of Laser-induced Molecular Processes, Gottingen, West Germany (September 1989).

J. Chou, "Diode Laser Probing of the Vibrational/Translational Energy in Baths of CO_2, N_2O and CO Excited by Relaxation of Highly Excited NO_2," Columbia Radiation Lab Symposium, Arden House Symposium, Columbia University, NY, NY, June 2, 1989.

F. A. Khan, "Collisional Excitation of CO_2 by Hot Hydrogen Atoms: Experimental Results for Several Important Inelastic Scattering Channels," Physical Chemistry Seminar, Chemistry Department, Columbia University, NY, NY, October 12, 1989.

F. A. Khan, "Initial State Dependence of the Translational and Ro-vibrational Excitation of CO_2 by Hot Hydrogen Atoms," Arden House Symposium, Columbia University, NY, NY, June 2, 1989.

F. A. Khan, "Diode Laser Probe of the Translational and Ro-Vibrational Excitation of CO_2 by Hot Hydrogen Atoms," Conference on the Dynamics of Molecular Collisions, Asilomar, California, July 20, 1989.

T. G. Kreutz, "State-to-State Dynamics; A Simple Picture of Collisional Energy Transfer between Hot Hydrogen Atoms and CO_2," Columbia University Physical Chemistry Seminar, Columbia University Department of Chemistry, NY, NY, 1989.

T. G. Kreutz, "Theoretical Investigations of State-to-State Collisional Energy Transfer between Hot Hydrogen Atoms and CO_2," Brookhaven National Laboratory Research Colloquium, Brookhaven National Laboratory, Brookhaven, NY, 1989.

T. G. Kreutz, "Inversion of Experimental Data to Generate State-to-State Cross Sections for Ro-Vibrationally Inelastic Scattering of CO_2 by Hot Hydrogen Atoms," Gordon Conference on Molecular Energy Transfer, Brewster Academy, Brewster, NY, 1989.

T. G. Kreutz, "Tunable Diode Laser Absorption Probes of State-Resolved Molecular Dynamics," University of Virginia Physical Chemistry Seminar, University of Virginia Department of Chemistry, 1988.

L. Zhu, "Energy Deposition in the Quenching of O(1D) by CO_2," Arden House Symposium, Columbia University, NY, NY, June, 1989.

L. Zhu, "Rovibrational Excitation of OCS by Hot Hydrogen Atoms," Conference on the Dynamics of Molecular Collisions, Asilomer, California, July 20, 1989.

S. Hartmann with F. Moshary and M. Arend, "Femtosecond Relaxation in Organic Dyes and Color Filters," Invited Paper, 5th Interdisciplinary Laser Science Conference (ILS-V), Stanford University, CA (August 1989).

D. DeBeer, E. Usadi and S. R. Hartmann, "Attosecond Beats in Sodium Vapor," Fourth International Laser Science Conference, Atlanta, Georgia (October 1988).

D. DeBeer, E. Usadi and S. R. Hartmann, "Attosecond Modulation in Sodium Vapor," International Conference on Lasers '88, Lake Tahoe, Nevada (December 1988).

R. Osgood, "Local Area Processing for IC's," SRC TECHCON, Dallas, TX, (October 1988).

R. Osgood, "Laser Surface Chemistry of Metal Alkyls," Materials Research Society Meeting, Boston, MA, (November 1988).

R. Scarmozzino, "Laser Induced Atomic Chlorine Etching of Silicon," Materials Research Society Meeting, Boston, MA, (November 1988).

M. Ruberto, "Photogenerated Carrier Confinement During the Laser-Controlled Etching of AlGaAs/GaAs Heterostructures," Materials Research Society Meeting, Boston, MA (November 1988).

R. Osgood, "Laser Applications in Surface Science," American Vacuum Society Meeting, (November 1988).

D. Podlesnik, "Photogenerated-Carrier Induced Surface Reactions: Oxygen on GaAs," American Vacuum Society Meeting, (November 1988).

M. Schmidt, "Ultraviolet-Laser-Induced Photochemistry on GaAs Surfaces," American Vacuum Society Meeting, (November 1988).

R. Osgood, "Laser Processing Physics and Devices," Yale Seminar, Yale University, CT, (December 1988).

R. Osgood, "Laser Chemical Processing," Short Courses, Materials Research Society (December 1988).

A. Willner, "Laser Direct Writing of Integrated Optical Components in the GaAs/AlGaAs System," Electrochemical Society Meeting (October 1988).

R. Osgood, "Optical Surface Chemistry of Semiconductors," NIST Seminar, (January 1989).

R. Osgood, "Techniques and Basic Surface Physics," NIST Seminar, Washington, DC (January 1989).

D. Podlesnik, "Laser-Assisted Processing for Integrated Optics," Topical Meeting on Integrated and Guided Wave Optics, Houston, TX (January 1989).

D. Podlesnik, "Chemically Modified GaAs Schottky Barrier Variation," Conference on Physics and Chemistry of Semiconductor Interfaces, Bozeman, MT (February 1989).

R. Osgood, "Laser Surface Interactions and Applications," Max Planck Institut Fur Physical and Biologische Chemie, Gottingen, West Germany (March 1989).

P. Shaw, "The Surface Spectroscopic Study of Organometallic Molecules," IBM, Yorktown Heights, NY (March 1989).

D. Podlesnik, "Laser-Controlled Processing for Microelectronics," Lectures on Interdisciplinary Areas of Laser Science, Rutgers University, Rutgers, New Jersey (March 1989).

R. Osgood, "Laser Surface Interactions and Comments on their Applications," Max Planck Institut fur Quantenoptik, Garching, West Germany (March 1989).

R. Osgood, "Laser Assisted Fabrication for Microelectronics," SIEMENS, Munchen, West Germany, (April 1989).

R. Osgood, "Laser Aqueous Etching," Max Planck Institut fur Quantenoptik, Garching, West Germany (April 1989).

R. Osgood, "Advanced Photon Processing for VLSI," MIT, Cambridge, MA (May 1989).

R. Osgood, "Laser Chemical Processing of Materials," DuPont, Wilmington, Delaware (May 1989).

D. Podlesnik, "Laser-Controlled Fabrication of Optoelectronic Devices," AT&T Bell Laboratories, Murray Hill, NJ (May 1989).

D. Podlesnik, "Laser Processing of Materials for Optoelectronic Devices," Eastman Kodak, Corporate Research Lab., Rochester, NY (June 1989).

R. Osgood, "Laser-Surface Chemical Interactions and Applications," Fritz-Haber-Institut Der Max-Planck-Gesellschaft, Berlin, Germany (June 1989).

D. Podlesnik, "Laser-Controlled Modification of Semiconductor Surfaces," Third International Symposium on Surface Modification Technologies, Neuchatel, Switzerland (June 1989).

D. Podlesnik, "An Overview of Laser-Assisted Processing of Semiconductors for Integrated-Optic Device Applications," IBM, Zurich Research Laboratory, Rueschlikon Switzerland (June 1989).

D. Podlesnik, "Photochemistry of Adsorbed Oxygen on GaAs," IBM, East Fishkill Facilities, Hopewell Jct., New York (June 1989).

D. Podlesnik, "Laser-Controlled Processing of Electronic Materials," IBM, T. J. Watson Research Labs., Yorktown Heights, New York (July 1989).

D. Podlesnik, "Laser Processing of Materials for Optoelectronic Devices," Eastman Kodak, Corporate Research Lab., Rochester, NY (June 1989).

M. Ruberto, "The Maskless Photochemical Etching of Optical Components on GaAs/AlGaAs Heterostructures," LEOS Conference, Orlando, FL (October 1989).

T. Licata, "CW Laser-Doping of Micrometer-Sized Features in GaAs Using a DMZn Ambient," American Vacuum Society Meeting (October 1989).

R. Osgood, "American Business and Technology: How Competitive Are We?," Columbia University Alumni Club, Fairfield, CT (October 1989).

R. Osgood, "Laser Photochemical Techniques for In Situ Processing," SRC Review, MIT, Boston, MA (June 1989).

R. Osgood, "Laser Induced Chemical Surface Modification," Max-Planck-Institut fur Biophysikalische Chemie, Schloss Ringberg, Germany (June 1989).

R. Osgood, "Microphotoelectrochemistry for the Fabrication of Integrated Optical Devices," Non-Linear Optics and Ultra-fast Phenomena Symposium, Electrochem;ical Society Meeting, Hollywood, FL (October 1989).

R. Osgood, "Advanced Photon Processing for VLSI," Laser Processing Seminar, Digital, Shrewsbury, MA (October 1989).

M. Ruberto, "The Maskless Photochemical Etching of Optical Components on Ga/As/AlGaAs Heterostructures," LEOS Conference, Orlando, FL (October 1989).

J. Shor, "Characterization of n-Type 3C Silicon Carbide Strain Gauges," Electrochemical Society Meeting (October 1989).

R. Osgood, "Novel Optoelectronic Devices Made with Laser-Assisted Processing," DARPA Site Visit, University of Southern California, Los Angeles, CA (July 1989).

R. Osgood, "Photochemistry of Surface-Bound Metal Alkyls," Sykmposium on Surface Photochemistry, American Chemical Society Meeting, Miami, FL (September 1989).

R. Osgood, "Laser Chemical Processing - A Tutorial Overview," Short Course, IBM, T. J. Watson Research Laboratories, Yorktown Heights, NY (September 1989).

M. Teich, "Nonclassical Photon Statistics," Invited Lecture, Annual Meeting of the Optical Society of America, Santa Clara, California (October 1988).

M. Teich, "Characteristics of the Auditory Neural Spike Train," Speech and Hearing Science Seminar, Department of Physiology, University of California, San Francisco, California (November 1988).

M. Teich with S. M. Khanna, "Spectral Characteristics of the Responses of Primary Auditory-Nerve Fibers to Frequency-Modulated Signals," Annual Meeting of the Acoustical Society of America, Honolulu, Hawaii (November 1988).

M. Teich, "Fractal Character of the Auditory Neural Spike Train," Annual Meeting of the Acoustical Society of America, Honolulu, Hawaii (November 1988).

M. Teich with S. M. Khanna, "Loss of Synchrony in Auditory Nerve Fibers," Annual Meeting of the Association for Research in Otolaryngology, St. Petersburg Beach, Florida (February 1989).

M. Teich with D. H. Johnson and A. R. Kumar, "Spontaneous Rate Fluctuations and Fractional Power-Law Noise Recorded from Cat Auditory Nerve Fibers," Annual Meeting of the Association for Research in Otolaryngology, St. Petersburg Beach, Florida (February 1989).

M. Teich, "Fractal Character of Action Potentials in the Auditory Nerve," Speech and Hearing Research Seminar, Northwestern University, Evanston, Illinois (April 1989).

M. Teich, "Squeezed Light," Electrical Engineering Seminar, Northwestern University, Evanston, Illinois (April 1989).

M. Teich, "Fiber-Optic Communications," Invited Tutorial Presentation, Electro '89, New York, New York (April 1989).

M. Teich, "Semiconductor Photodetectors, Guided-Wave and Fiber Optics, Coherent Communications and Fundamental Limits," Lecture Series, Center for Telecommunications Research, Columbia University, New York, New York (May 1989).

M. Teich with B. E. A. Saleh, "Noise Properties of Superlattice Avalanche Photodiodes in Quantum-Limited Detection," Invited Lecture, Topical Meeting on Quantum Limited Imaging and Information Processing II, North Falmouth, Massachusetts (June 1989).

M. Teich with R. A. Campos and B. E. A. Saleh, "Photon-Number Distributions for Homodyne Photomixing at a Lossless Beamsplitter," Sixth Rochester Conference on Coherence and Quantum Optics, Rochester, New York (June 1989).

M. Teich, "Squeezed Light," Invited Lecture, USSR/USA Popov-Society/IEEE Joint Workshop on Electro-Optics, Moscow, USSR (September 1989).

M. Teich, "Quantum Squeezed-State Light Fields," Invited Colloquium, Faculty of Physics, Moscow State University, Moscow, USSR (September 1989).

X. Wu and E. Yang, "Thomas-Fermi Screening and Fermi-level Position at Metal-GaAs Interfaces," Materials Research Society Meeting, San Diego, CA (April 1989).

Q. Ma, C. Yu, X. Wu, M. Schmidt, E. Yang and C. Chang, "Interdiffusion between Substrates and SYBaCuO Films Formed by Rapid Thermal Annealing of Cu/BaO/Y_2O_3 Layered Structures," Materials Research Society Meeting, San Diego, CA (April 1989).

Q. Ma, M. Schmidt, T. Licata, D. Rossi, E. Yang, C. Chang and C. Farrell, "Processing and Substrate Effects on YBaCuO Thin Films Formed by Rapid Thermal Annealing of Cu/BaO/Y_2O_3 Layered Structures," 3rd Annual Conference on Superconductivity and Applications, Buffalo, New York (September 1989).

COLUMBIA RESONANCE SEMINARS

"Generation of Subpicosecond Electrical Pulses and their Spectroscopic Applications," Dan Grischkowsky, IBM, October 7, 1988

"Squeezed States for Ultra-Sensitive Optical & Microwave Spectroscopy," Ed Whittaker, Stevens Institute of Technology, October 21, 1988.

"Toward a Classical Atom: Rydberg Electron Wave Packet," Carlos Stroud, University of Rochester, November 11, 1988.

"Laser Cooling Below the Limit (The Coldest Gas in the Universe)," Bill Phillips, National Institute of Standards and Technology, November 18, 1988.

"Atomic Polarizability at Very High Laser Field Strength," Joe Eberly, University of Rochester, March 10, 1989.

"Diode Array Pumped Solid State Lasers," Dr. Toomas Allik, Science Applications International, Inc., May 23, 1989.

"Optical Coherence and Raman Heterodyne Spectroscopy of Ruby," Alex Szabo, National Research Council, March 31, 1989.

"Optoelectronics: Present Status," Paul Liao, Bell Communications Research, April 14, 1989.

COLUMBIA RADIATION LABORATORY SEMINAR SERIES ON PURE AND APPLIED SCIENCE

"New Quantum and Memory Devices: Physics and Circuit Applications," Federico Capasso, AT&T Bell Laboratories, October 11, 1988.

"Two-Dimensional Magnetism and High T_c Superconductivity," Marc Kastner, MIT, October 25, 1988.

"Recent Advances in Lasers for Optical Communication," Aram Mooradian, MIT Lincoln Laboratory, November 15, 1988.

"Electronic Excitations in Response to Gas-Surface Interactions," Mark Cardillo, AT&T Bell Laboratories, February 14, 1989.

"From Photon Echoes to Optical Holeburning: A New Approach to the Study of Complex Solids," Michael Fayer, Stanford University, April 18, 1989.

"Atomic-Scale Physics of Metal-Semiconductor Interfaces," Leonard Brillson, Xerox Webster Research Center, May 9, 1989.

I. QUANTUM GENERATION AND DETECTION OF RADIATION

A. SILENT LIGHT

Malvin C. Teich, Principal Investigator (212) 854-3117
Research Area I, Work Unit 1

We have been investigating ways of making improved sources of silent light (also known as photon-number-squeezed light or sub-Poisson light),[1] and determining how such light behaves when it impinges on simple optical elements. We have determined the photon statistics at the output of a lossless beamsplitter when photon number states are incident at the inputs.[2] As described in (a) below, the results reflect unexpected interferences of photon pairs with themselves. For optical signals transmitted through random media such as the atmosphere, rather than through an optical fiber, the K distribution and its Poisson transform turn out to be of interest.[3] These families of distributions can be represented in multiply stochastic (compound) form, as discussed in (b). Detectors of nonclassical and classical light can exhibit 1/f-type noise under a variety of experimental conditions.[4] As we show in (c), a generalized form of 1/f shot noise can be used to describe these fluctuations.

(a) Quantum-mechanical beamsplitter[2]

A number of authors have considered the behavior of the quantum-mechanical beamsplitter in the past few years. We have provided a comprehensive approach that treats the photon statistics arising from the homodyne photomixing of (not necessarily independent) light beams of arbitrary statistical composition. It turns out that important mathematical tools can be borrowed directly from a different, but fully equivalent, physical model: the quantization of angular momentum. By employing a two-dimensional boson-operator algebra, Schwinger reformulated the theory of angular momentum.[5] The technique, viewed in reverse, is ideally suited to the beamsplitter. Schwinger's formalism has been considered by Yurke et al.,[6] who showed that interferometry with beamsplitters may be viewed geometrically as abstract rotations of angular momenta on a sphere. We have extended this approach, carrying over to quantum optics many of the well established mathematical methods and results from the theory of angular momentum.

For optical homodying, the matrix representation of a lossless beamsplitter belongs to the SU(2) group of unimodular second-order unitary matrices. The connection between this group and the rotation group in three dimensions permits the field density operators at the input and output ports of the beamsplitter to be related by means of well-known

angular-momentum transformations. This, in turn, provides the joint output photon-number distribution, which may be written as a Fourier series in the relative phase shift imparted by the beamsplitter, for a general joint state at its inputs. The series collapses to a single term if one of the input fields is diagonal in the number-state representation. If the inputs to both ports are further restricted to be pure number states, the joint, as well as the marginal photon-number distributions, turn out to be directly proportional to the square of Jacobi polynomials in the beamsplitter transmittance. These photon-number probabilities are invariant to a set of physical and time-reversal symmetries. When one of the input photon-number states is the vacuum, the beamsplitter simply deletes photons from the other port in Bernoulli fashion, as if they were classical particles. The output photon number is then described by the binomial distribution. If the inputs at the two ports are different number states, neither of which is the vacuum, the photon-number distribution is expressible in terms of summed and weighted products of the results for photomixing with the vacuum. If the inputs at the two ports are identical number states, and a beamsplitter of transmittance $\tau=1/2$ is used, the photon-number distribution assumes a simple but interesting form. It vanishes for odd photon numbers, indicating that the photons assemble in pairs at each output port. Finally, it is shown that homodyning quantum fluctuations can be reduced by using a balanced photomixer for arbitrary input states.

In Figure 1 we provide a comparison of the beamsplitter-output photon-number probability distributions when there are a total of 10 photons at the input ports, and the beamsplitter transmittance $\tau=1/2$. The unimodal binomial distribution for a vacuum-state input at one port ($|10,0\rangle$) evolves into a distribution in which odd photon numbers are absent when there are equal numbers of photons at each input port ($|5,5\rangle$), illustrating the results described above.

(b) Compound representation for K distributions[3]

In optics the K distribution provides a useful statistical description for problems involving fluctuations of the irradiance (and electric field) of light that has been scattered or transmitted through random media (e.g., the turbulent atmosphere). The Poisson transform of the K distribution describes the photon-counting statistics of light whose irradiance is K-distributed.

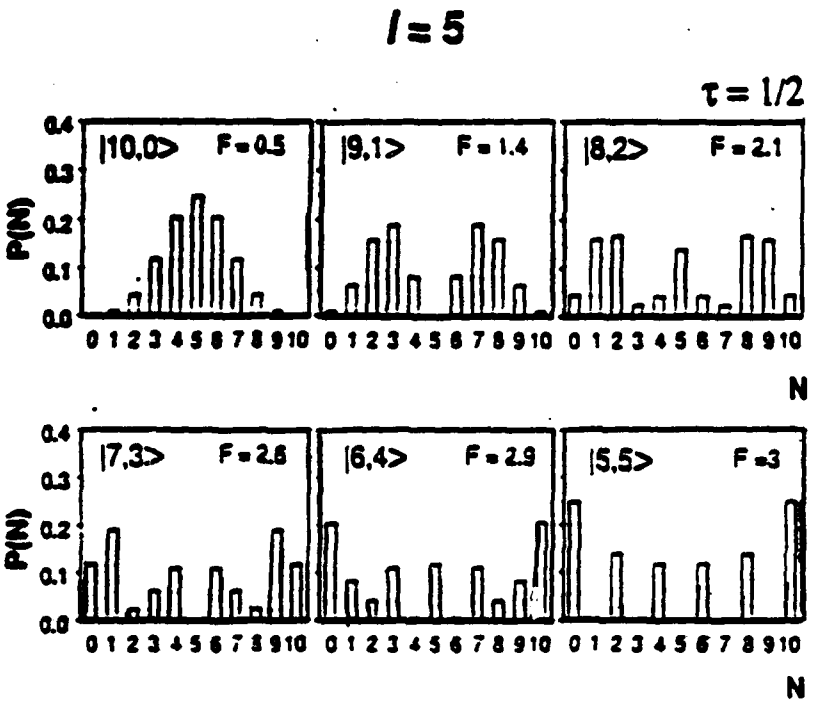

Figure 1. Beamsplitter-output photon-number probability distributions when there are a total of 10 photons at the input ports, and the beamsplitter transmittance τ=1/2. The binomial distribution obtains when all of the photons impinge on one of the ports (|10,0>) whereas a distribution in which odd photon numbers are absent obtains when equal numbers of photons are incident at each input port (|5,5>).

The K_0 distribution was first used in the biological sciences in the 1950's;[7] however, its first application in optics appears to be in connection with the problem of doubly-scattered laser light.[8] A general approach for problems involving the field and irradiance in scattering, speckle, and the propagation of light through turbulent media has been developed.[9] This model has also been used to describe non-Rayleigh microwave sea echo.[10] A number of generalizations of the K distribution, including the I-K[11] and the generalized-K[12] distributions, have been set forth. The K distribution has also been obtained in the context of a quantum-mechanical formulation.[13]

Two physically distinct doubly stochastic representations are available for the K distribution and for some of its generalizations. In the first, the second moment of a Rayleigh distribution is smeared by a gamma distribution. In the second, the mean of a gamma distribution is smeared by another gamma distribution. It has been shown that the generalized K distribution can be represented as a Rician distribution with both its mean-

square noise component and its coherent amplitude varying in correlated fashion, according to a gamma distribution.[12] The Poisson transform of the K distribution, describing the photon-counting detection of light whose field (or irradiance) is K-distributed, has been written in terms of Whittaker functions.[8]

We have been able to demonstrate that the K-distribution family can be represented in multiply stochastic (compound) form, whereby the mean of a gamma distribution is itself stochastic and described by a member of the gamma-family of distributions. Similarly, the family of Poisson transforms of the K distributions can be alternatively represented as a family of negative-binomial transforms of the gamma distributions, or as Whittaker distributions. These multiply stochastic representations provide an alternate route to the random-walk models in understanding the genesis of these distributions and their Poisson transforms. Using these representations we have developed a new transform pair as a useful addition to the K-distribution family. All of these distributions decay slowly and are difficult to calculate accurately by conventional formulas. A recursion relation, together with a generalized method of steepest descent, has been developed to evaluate numerically the photon-counting distributions, and their factorial moments, to excellent accuracy.

A schematic representation for the effects of a scattering (or atmospheric) medium of fluctuating transmission (with characteristic fluctuation time τ_a), imposing a random modulation on the mean irradiance W of a light source passing through it, is provided in Figure 2(a). For purposes of illustration, we have taken the fluctuations of the mean irradiance imposed by the medium to be gamma-distributed. These fluctuations result in an overall mean aW for the light that emerges from the medium, where a is a scaling factor introduced by the medium. Light sources also exhibit intrinsic irradiance fluctuations (characterized by the coherence time τ_c). The integrated irradiance of chaotic (or thermal) light, for example, is gamma-distributed. A gamma-fluctuating light source, whose mean is smeared by a random medium in accordance with another gamma distribution, results in a doubly stochastic distribution for the integrated intensity that is given by the K' distribution. A unity quantum efficiency detector of the integrated irradiance provides a direct measure of this distribution. In Figure 2(b), the fluctuating medium and the light source have the same properties as those considered above. The integrated intensity is therefore again describable by the K' distribution, but in this case a photon-counting detector is used. It measures the Poisson transform of the integrated intensity, rather than the integrated intensity itself. The resultant discrete photon-counting distribution, which we refer to as A(n), is therefore the Poisson transform of the K' distribution. For a unity quantum efficiency counter, it registers the same overall mean count aW as does the integrated-irradiance detector.

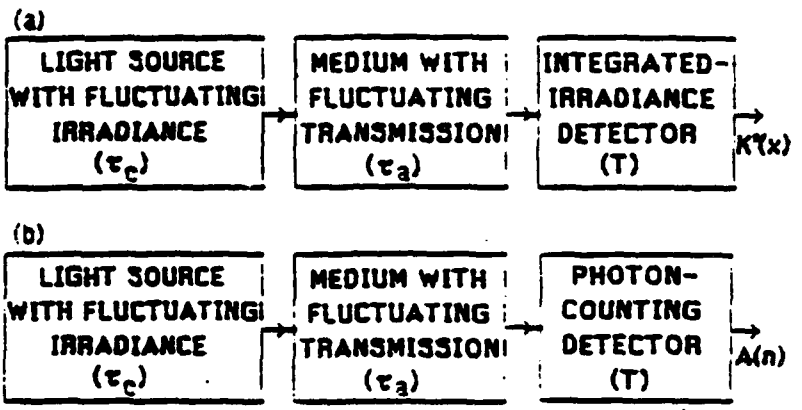

Figure 2. Models representing the effects of a medium with fluctuating transmission (or a scattering medium) on the statistical properties of a light source observed at the output of a detector. (a) The medium (with characteristic fluctuation time τ_a) stochastically modulates the mean irradiance of the source, the source exhibits intrinsic irradiance fluctuations (with coherence time τ_c), and the detector records the overall (continuous) integrated irradiance (in the time T). (b) Same as (a), but now the detector records the overall (discrete) photon count (in the time T).

(c) Generalized 1/f shot noise in semiconductor detectors[4]

The semiconductor detectors used to detect light exhibit 1/f-type noise under a variety of experimental conditions. One widely used theoretical approach to this problem makes use of a superposition of relaxation processes of different time constants. We have used an alternative approach based on a generalized form of 1/f shot noise that we have developed. The impulse response functions assume a time-decaying power-law form with power $-\beta$. For $0 < \beta < 1$, the 1/f shot-noise process can serve as a source of $1/f^{\alpha}$ noise, for any $\alpha = 2(1-\beta)$ in the range $0 < \alpha < 2$. The first-order moment generating function has been developed for $0 < \beta < 1$, from which first-order statistics may be numerically computed. For $\beta > 1$, the amplitude has a Levy-stable probability density function.

The research in this report was supported by the Joint Services Electronics Program.

References

1. M. C. Teich and B. E. A. Saleh, "Photon bunching and antibunching," in Progress in Optics, edited by E. Wolf (North-Holland, Amsterdam, 1988), Vol. 26, pp. 1-104.

2. R. A. Campos, B. E. A. Saleh, and M. C. Teich, "Quantum-mechanical lossless beamsplitter: SU(2) symmetry and photon statistics," Phys. Rev. A 40, 1371 (1989).

3. M. C. Teich and P. Diament, "Multiply stochastic representations for K distributions and their Poisson transforms," J. Opt. Soc. Am. A 6, 80 (1989).

4. S. B. Lowen and M. C. Teich, "Generalized 1/f shot noise," Electronics Lett. 25, 1072 (1989).

5. J. Schwinger, U.S. Atomic Energy Commission Report No NYO-3071 (US GPO, Washington, DC, 1952); reprinted in Quantum Theory of Angular Momentum, edited by L. C. Biedenharn and H. van Dam (Academic, New York, 1965).

6. B. Yurke, S. L. McCall, and J. R. Klauder, Phys. Rev. A 33, 4033 (1986).

7. S. R. Broadbent and D. G. Kendall, "The random walk of trichostrongylus retortaeformis," Biometrics 9, 460 (1953).

8. M. Bertolotti, B. Crosignani, and P. DiPorto, "On the statistics of Gaussian light scattered by a Gaussian medium," J. Phys. A 3, L37-L38 (1970).

9. E. Jakeman, "On the statistics of K-distributed noise," J. Phys. A 13, 31 (1980).

10. E. Jakeman and P. N. Pusey, "A model for non-Rayleigh sea echo," IEEE Trans. Ant. Prop. AP-24, 806 (1976).

11. L. C. Andrews and R. L. Phillips, "Mathematical genesis of the I-K distribution for random optical fields," J. Opt. Soc. Am. A 3, 1912 (1986).

12. E. Jakeman and R. J. A. Tough, "Generalized K distribution: a statistical model for weak scattering," J. Opt. Soc. Am. A 4, 1764 (1987).

13. E. B. Rockower, "Quantum derivation of K-distributed noise for finite <N>," J. Opt. Soc. Am. A 5, 730 (1988).

B. OPTICAL COHERENT TRANSIENT SPECTROSCOPY

Sven R. Hartmann, Principal Investigator (212) 854-3272
Research Area I, Work Unit 2

1. Attosecond Beats in Atomic Vapors

(D. DeBeer, E. Usadi, S. Hartmann)

We are continuing our study of beating effects in time-delayed four-wave mixing experiments. In an experiment in sodium vapor, we have observed sub-femtosecond modulation of the signal intensity as a function of delay time.[1] The excitation fields contained frequency components corresponding to the two fine-structure split levels of the first excited state. The frequency of the modulation was the sum of the frequencies of these two levels. The same excitation scheme is now being employed in an experiment in potassium vapor. The excitation fields are the second harmonics of the fields from two coherent (laser) sources tuned respectively to the fine-structure split levels of the 4S-6P transition. The sum of these frequencies, and therefore the expected modulation frequency, is 1.7 ¥ 10^{15} Hz. This implies a beat period of 575 attoseconds (1 asec = 10^{-18} sec) which we believe will be the fastest such quantum beat observed.

These beats have not yet been observed in our potassium experiment. However the experimental apparatus is completely assembled, and the search for the expected modulation is nearing its climax. A schematic representation of the apparatus is presented in the figure below. The relative delay between the fields in the $\mathbf{k}_1$ and $\mathbf{k}_2$ directions is controlled by moving one mirror in a Michelson-type interferometer with a piezoelectric crystal. Since one complete modulation of the signal occurs for every 575 asec of increasing (or decreasing) delay, all mirrors in the interferometer must be stable to much better than 1/4 of one wavelength (λ = 3447Å). We have been successful in stabilizing the delay jitter to well within the limit required for this experiment. To achieve a reasonable signal intensity, pulses of area π are desirable. This implies a needed laser intensity of 448 watts / sq. cm. (compared to 0.24 watts / sq. cm. in the sodium experiment). This consideration and the fact that we achieve an 8% second harmonic conversion efficiency in generating the ultraviolet excitation fields necessitate the use of two amplifiers for each dye laser.

At present fluctuations in the four-wave mixing signal have prevented observation of the beats. Initially it was thought that amplitude jitter in the pump beams was the main

---

1 D. DeBeer, E. Usadi, and S. R. Hartmann, Phys. Rev. Lett. 60, 1262 (1988)

culprit. Small jitter in our Nd:YAG laser amplitude is magnified by three nonlinear processes: dye laser pumping, 2nd harmonic generation, and four wave mixing. An attempt was made to eliminate this source of noise by software-selecting data based on pump laser amplitude. Large four wave mixing amplitude jitter persisted even with the use of this data acquisition software. We now believe that the fluctuations are due largely to frequency jitter in the dye lasers. The doppler-broadened width of the potassium resonance lines is 1 GHz. Each laser operates in several longitudinal modes (with a mode spacing of less than 1 GHz and a total bandwidth of about 6 GHz) and hops freely between them. We are now setting up dye lasers which operate in a single longitudinal mode and have a time-averaged bandwidth of less than 150 MHz.[2] It is hoped that this will result in a more stable four-wave mixing signal and enable us to observe attosecond beats in potassium vapor.
Schematic diagram of the apparatus used to generate sum-frequency beats in the TDFWM signal as a function of time delay: Each dye laser consists of one oscillator and two amplification stages with a spatial filter after each stage. The KDP crystal doubles the frequency of each of the laser beams. All subsequent optical components are coated to reflect only these second harmonic UV beams, so no residual visible light reaches the potassium cell. M1 is mounted on a piezoelectric-driven translation stage. M2, made of two perpendicular mirrors, displaces each beam so that it combines at the beam splitter with the beam of the other frequency.

The research in this report was supported by the Joint Services Electronics Program and the Office of Naval Research.

2. Broad-Band Time-Delayed Four-Wave Mixing

(M. Arend and S. R. Hartmann)

a. General

The time-delayed four-wave mixing (TDFWM) technique has been exploited to measure ultra-fast optical dephasing phenomena in organic dyes and semiconductor doped glasses. This technique originated from the incoherent photon echo experiment by Beach et al[3] and the work by Morita et al.[4] The experimental apparatus is shown in Figure 1. Our source is obtained by transversely ¬umping a flow through dye cell with the 2nd harmonic from a pulsed YAG laser (7 nsec pulse duration). A mirror is placed to one side of the cell to provide single pass amplification of the spontaneous emission. The light is then split in

---

2 M. G. Littman, Applied Optics, Vol. 23, No. 24, (15 Dec. 1984)

3 R. Beach, S. R. Hartmann, Phys. Rev. Lett. 53, 663 (1984)

4 N. Morita and T. Yajima, Phys. Rev. A 30, 2525 (1984)

an interferometer with one arm fixed while the other may be moved with a resolution of 50 nm by means of a Melles Griot Nanomover. This resolution in positional delay corresponds to a 0.33 fsec resolution in time delay. The two beams are made to be parallel as they leave the delay line and are subsequently focused so that they overlap in the sample. Interference of the light at the sample causes the ground state population to be modulated along the direction transverse to the excitation beams so that a spatial grating gets produced in the sample. Light which arrives at the sample at a latter time during the pulse duration can then scatter off this grating. The energy of the scattered pulse as a function of delay is what we call the time delayed four wave mixing response.

Experimetal Apparatus For Incoherent Time-Delayed Four-Wave-Mixing

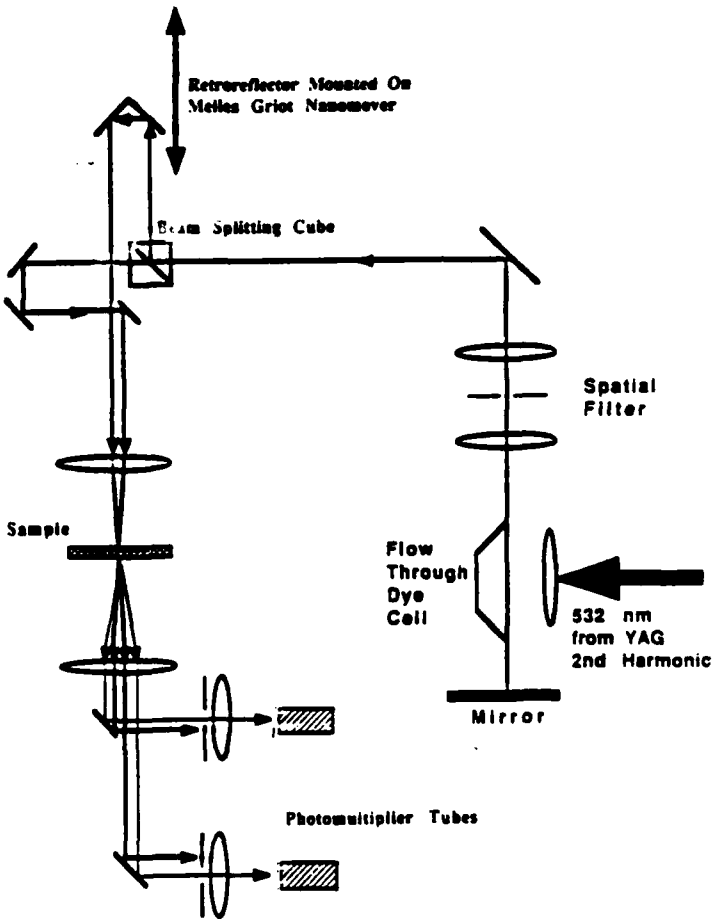

Figure 1: Experimental Apparatus

b. Nile Blue

We have utilized our broad band tunable source to excite wide regions of the Nile Blue absorption spectrum. In Figure 2 we show the transmission spectrum of Nile Blue together with the intensity spectra of several sources we have used to generate TDFWM responses. Our TDFWM measurements indicate that the Nile Blue S_0-S_1 transition is homogeneously broadened at room temperature. In Figures 3, 4 and 5 we show the TDFWM response for the sources centered at 6200Å, 6300Å and 6600Å. The TDFWM response for both the 6200Å and the 6300Å sources is symmetric as is the response, not shown, for the 5800Å source. The former, shown in Figure 3, is identical with the square of the auto correlation function while the second, shown in Figure 4, shows definite broadening which can be characterized by a value of T_2=18 fsec. These results are the basis of our statement that the Nile Blue transition is homogeneously broadened at room temperature. Our result at 6600Å, which is at the edge of the band, shows evidence of a small amount of inhomogeneous broadening.

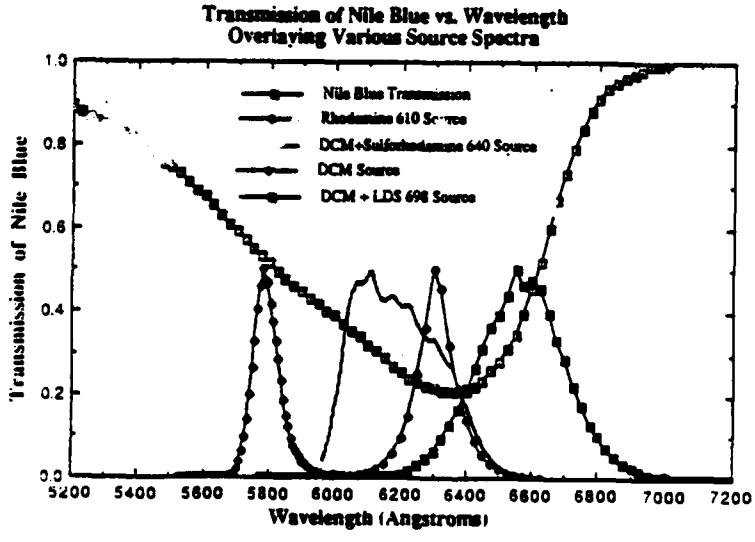

Figure 2: The power spectrum of four different sources is shown on the same wavelength axis as the transmission spectrum of nile blue. The sources which correspond to Figures 3, 4, and 5 are DCM+Sulforhodamine640, DCM, DCM+LDS698 respectively.

These results are relevant to the recent report of Becker et al[5] in which 6 fsec pulses were used in a photon echo experiment in Nile Blue. Dramatic beating effects which modulated an exponential decay were observed. They attribute the beating to system modes at 555 cm^{-1} and 1850 cm^{-1}. They assumed that their system was inhomogeneously. broadened so that the observed exponential decay implies a homogeneous relaxation time T_2 of 65 fsec. However, another interpertation is possible. If one assumes homogeneous broadening their experiment implies a homogeneous relaxation time T_2 of 33 fsec which is not out of line with our experimental results. In a separate study by Weiner et al[6], 70 fsec pulses were used to do three pulse scattering experiments. Their scattering curves for Nile Blue are indistinguishable from the instantaneous response which they claim indicates that the system is homogeneously broadened with an apparent dephasing time less than their 20 fsec experimental resolution. This is also consistent with our experimental results and inconsistant with the results of Becker et al. In addition we have made a modal analysis of our data using the system modes of Becker et al and it does not seem possible to account for both the narrowing we observe with the 6200Å source and the broadening with the 6300Å source.

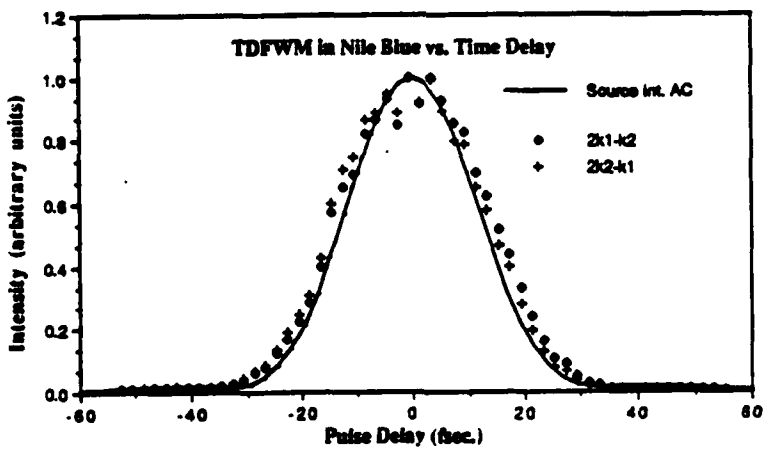

Figure 3: TDFWM in Nile Blue at room temperature in both the 2k2-k1 and 2k1-k2 directions. Also shown is the square of the autocorrelation trace of the light used. The light source for this data is the DCM+Sulforhodamine640 source shown in Figure 2.

---

5 P. C. Becker, H. L. Fragnito, J. Y. Bigot, C. H. Brito Cruz, and C. V. Shank, Phys. Rev. Lett. 63, 5 (1989)

6 A. M. Weiner, S. De Silvestri, and E. P. Ippen, J. Opt. Soc. Am. B 2,4 (1985)

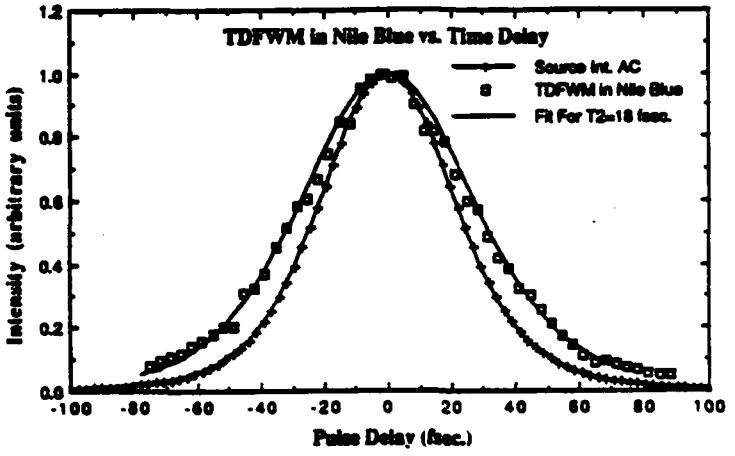

Figure 4: TDFWM in Nile Blue at room temperature. A fit yielding T2 = 18 fsec. is shown. Also shown is the square of the autocorrelation trace of the light used. The light source for this data is the DCM source shown in Figure 2.

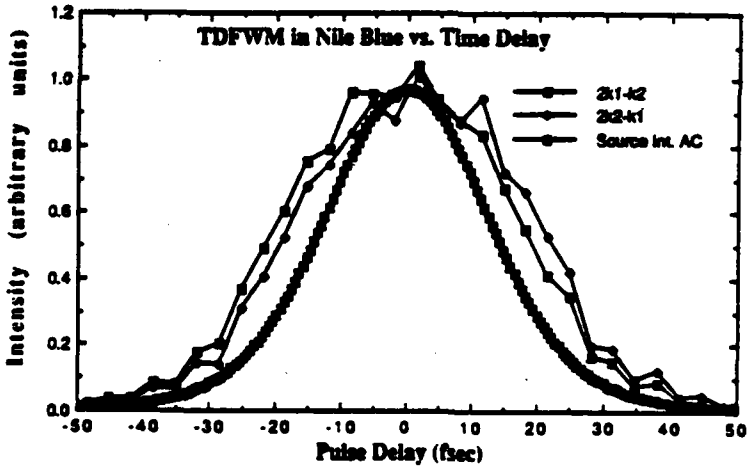

Figure 5: TDFWM in Nile Blue at room temperature in both the 2k2-k1 and 2k1-k2 directions. Also shown is the square of the autocorrelation trace of the light used. The light source for this data is the DCM+LDS698 source shown in figure two.

In order to theoretically analyze the TDFWM problem for a multilevel system in as simple a manner as possible we restricted the analysis to the case where two delayed incoherent fields are directed along k_1 and k_2 while a third field directed along k_3 is

relatively coherent. For extreme inhomogeneous broadening we are able to write the resulting intensity scattered along $\mathbf{k}_3 + \mathbf{k}_2 - \mathbf{k}_1$ in terms of elementary functions as[7]

$$I(\tau) \propto \left(4\pi^2 T_1^2 T_c^2 T_2^{*2} E_o^4 E_3^2\right)\left|\sum_{m,n}|p_m|^2|p_n|^2 \exp\left(\frac{-\tau^2}{4T_c^2}\right)\right.$$

$$\times\left[\exp\left\{\left[\left(\frac{2T_c}{T_2}-\frac{\tau}{2T_c}\right)-i(\omega_m-\omega_n)T_c\right]^2\right\}\right]$$

$$\times\left\{1-\mathrm{Erf}\left[\left(\frac{2T_c}{T_2}-\frac{\tau}{2T_c}\right)-i(\omega_m-\omega_n)T_c\right]\right\}\Bigg|^2. \qquad (1)$$

E_o refers to the amplitude of the two delayed fields while E_3 refers to the amplitude of the third pulse. T_c, T_1, and T_2 correspond respectively to the correlation time of the excitation field and the longitudinal and transverse relaxation times.

Using the modal analysis of Becker et al and using the source centered at 6200Å we use expression (1) to obtain the result shown in Figure 6. This result has the asymmetric signature of inhomogeneous broadening and is inconsistent with our experimental result shown in Figure 3. It is interesting to note that the beats should be washed out because of the shortness of T_2.

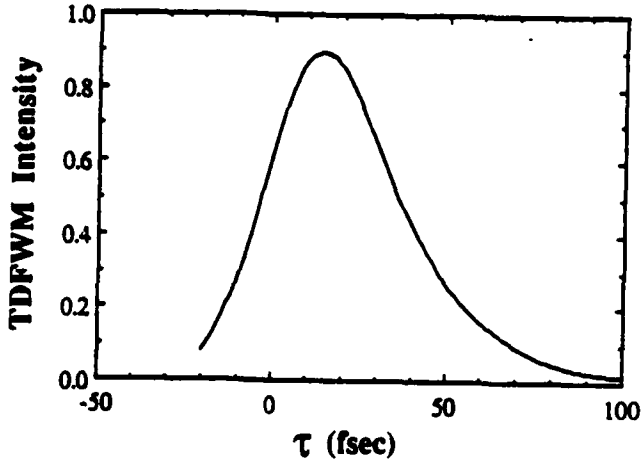

Figure 6: The theoretical TDFWM response using the source centered at 6200Å and assuming the parameters for Nile Blue which are given by Becker et al. Notice the asymmetric response.

---

7 S. R. Hartmann and J. T. Manassah, submitted to J. Phys. B.

If we assume homogeneous broadening then the appropriate response is

$$I^h(\tau) \propto \left| \frac{\pi}{2} T_2 \sum_n |p_n|^2 \exp\left(-\frac{\tau^2}{4T_c^2}\right) \right.$$
$$\times \left\{ \exp\left[\left[\left(\frac{T_c}{T_2} - \frac{\tau}{2T_c}\right) + i(\omega_L - \omega_n)T_c\right]^2\right]\left[1 - \mathrm{Erf}\left[\left(\frac{T_c}{T_2} - \frac{1}{2}\frac{\tau}{T_c}\right) + i(\omega_L - \omega_n)T_c\right]\right]\right.$$
$$\left. \left. + \exp\left[\left[\left(\frac{T_c}{T_2} + \frac{\tau}{2T_c}\right) - i(\omega_L - \omega_n)T_c\right]^2\right]\left[1 - \mathrm{Erf}\left[\left(\frac{T_c}{T_2} + \frac{\tau}{2T_c}\right) - i(\omega_L - \omega_n)T_c\right]\right]\right\}\right|^2 \quad (2)$$

In this expression we take T_2=33 fsec instead of 65 fsec. There is some arbitrariness in choosing the location of the modes. However all reasonable choices we consider lead to a situation where we can make a fit to the data of either Figure 3 or 4 separately but not to both simultaneously.

We have made improvements in our experimental setup in an effort to reconcile the two experimental techniques. Our sample is now identical to the one used by Becker et al. Previously, we had dissolved Nile Blue in ethanol and placed it in a 1mm thick sample cell. Now, we are flowing Nile Blue dissolved in ethylene glycol through a .1mm dye jet. This insures that the sample is not hole burned and that any discrepancies in dephasing due to dye concentration or type of solvent are eliminated. Also, we have made improvements in our data acquisition software which take into account fluctuations in the source intensity. This helps us account for a fluctuating signal and also allows us to properly subtract off background generated from the excitation pulses.

We have succeeded in making measurements of TDFWM at 4.5 degK and have found that the response which was homogeneous when the 6200Å source was used is now inhomogeneous (Figure 7). A fit to the 2k2-k1 direction is made using T_2=13 fsec and T_2^*=15 fsec. This is the first time that inhomogeneous broadening has been detected in Nile Blue. We attribute it to strains induced in the dye molecule by the freezing of the solvent.

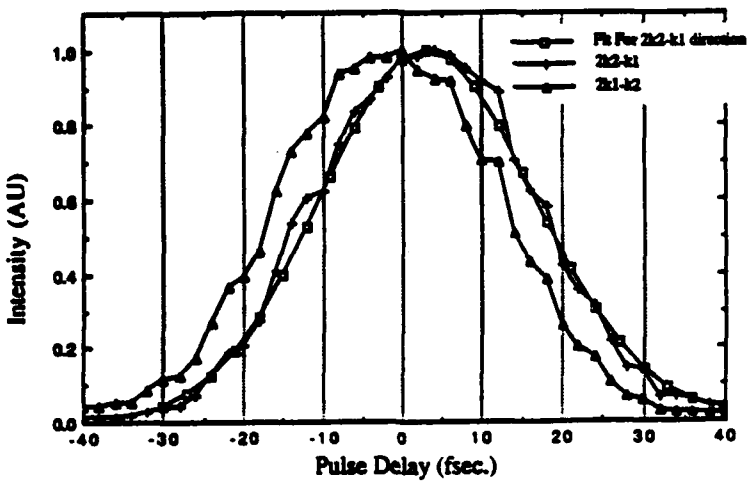

Figure 7: TDFWM in Nile Blue at 4 deg K in both the 2k2-k1 and 2k1-k2 directions. Also shown is a fit to the 2k2-k1 direction with T_2=13 fsec and T_2^*=15 fsec.

c. <u>CdS_xSe_{1-x} in glass</u>

Our TDFWM results in color filters, i.e., host glasses doped with small semiconductor (CdS_xSe_{1-x}) crystallites possessing large and fast third order nonlinearities (10^{-8} esu), indicate that regardless of the optical density or the source T_2 is approximately 30 fsec. The change in the TDFWM character we had observed in going to higher optical density (OD) we have been able to attribute to modification of the source spectrum. We now find that the lower energy transitions are inhomogeneously broadened while the higher energy transitions are homogeneously broadened. A possible explanation for this effect may be that the line width of the higher energy transitions in the microcrystallites are not as sensitive to the microcrystallite size variations as the lower energy transitions near the emission edge of the microcrystallites. Perhaps this can be attributed to quantum confinement effects. We use the equation[8]

$$\Delta E = \frac{h^2}{8\mu a^2} - \frac{1.8e^2}{\varepsilon a}$$

where a, μ, and ε are respectively the radius of the microcrystallite, the reduced electron hole mass, and the dielectric constant of the microcrystallite. For an average value of a of 50Å and a distribution of particle sizes with a standard deviation of 25Å[9] we obtain a distribution of energy shifts for the lowest energy optical transition with a standard

---

8 J. Warnock and D. Awshalom, Phys. Rev. B 32, 5529(1985).

9 N. F. Borrelli, D. W. Hall, H. J. Holland, and D. W. Smith, J. Appl. Phys. 61, 5399 (1987)

deviation of between 9.6 to 26.1 mev depending on whether the crystallites are pure CdS or CdSe. This translates to a T_2^* lying between 69 and 25 fsec. Since the selenium fraction in the samples studied is greater than .64 we expect a value of T_2^* in the lower end of this range and thus in agreement with our measurements.

This research was supported by the Joint Services Electronics Program and the Office of Naval Research.

3. Two-photon Cooperative Cascade Superfluorescence

(D. DeBeer, X. Lu, S. R. Hartmann)

We are in the early stages of a new experiment studying cascade superfluorescence. This will be the first experiment to study superfluorescence to the ground state. Superfluorescence is a type of superradiant phenomena. As described by Dicke[10] superradiance is cooperative spontaneous emission. An ensemble of atoms radiating cooperatively radiate with intensity proportional to N^2 where N is the number of cooperating atoms. When not cooperating the radiating atoms radiate incoherently and the resulting intensity is proportional to N.

Consider an ensemble of N two level systems which are initially incoherently inverted. They will initially fluoresce with an intensity proportional to N. If the ensemble is dense it will exhibit gain and the fluorescence will be amplified to produce a coherence within the system which manifests itself by the intensity becoming proportional to N^2. The first experiment in which one can observe this effect was performed by Feld *et al.* in 1973.[11]

The experiment we have started focusses on an aspect of superradiance which is cascade superfluorescence. Consider a three-level atom which is initially two-photon excited from the ground state, |a>, to the upper excited state, |c>. Then, under the conditions appropriate for superfluorescence, coherent emission will build up on the |c> - |b> and |b> - |a> transitions as we will describe. One difficulty in such an experiment is ensuring that one in not simply observing parametric four-wave mixing. However, by making the two-photon excitation short enough we can avoid that difficulty. In this case we will see the following:

---

10 R. H. Dicke, Phys. Rev. 93, 99 (1954).

11 N. Skribanowitz, I. P. Herman, J. C. MacGillivray, M. S. Feld, Phys. Rev. Lett. 30, 309 (1973).

1. No radiation will be observed on the cascade transitions simultaneously with the presence of the two-photon excitation pulse.

2. All superfluorescence bursts will be delayed from the two-photon excitation pulse.

3. At low excitation intensities, superfluorescence will only be seen on the upper transition, and it would only appear in the wrong (backward) direction.

4. As the excitation intensity increases, superfluorescence in the forward direction will begin to appear, and simultaneously with it, a superradiant burst on the lower transition. (This assumes that superfluorescence in the backward direction is suppressed.)

In order to observe the build up of the superfluorescence we must artificially narrow the linewidth of sample. We are working with Cs vapor. The gas is prepared by optically pumping the D-line transition in such a way that the m_j=-1/2 level of the ground $6S_{1/2}$ state only contains atoms in a small velocity group. With the sample thus prepared, a short, circularly polarized pulse of 5 ps duration at 8851.5Å is then applied which coherently populates the m_j=3/2 level of the $6D_{3/2}$ state via a two photon process. Superfluorescence now develops on the $6D_{1/2}$-$6P_{1/2}$ transition. Neglecting depletion effects we would expect to observe superradiance in both the forward and backward directions. Since the excited velocity group is narrow our expected T_2^* will be of the order of or greater than the 30 ns lifetime of the $6P_{1/2}$ state (the lifetime of the $6D_{3/2}$ state is 60 ns and does not limit the response of the system) and thus the evolution of the superfluorescence can be followed. As has been predicted by Okada et al.[12] the superfluorescence in the forward direction can be inhibited below a certain inversion threshold in which case a superfluorescence burst should only be seen in the backward direction. The observation of this superfluorescence inhibition and its associated threshold is one of the major goals of these experiments. Beyond this threshold, superfluorescence should develop along the forward direction and simultaneously with it a superradiant burst on the $6P_{1/2}$-$6S_{1/2}$ transition should appear, also in the forward direction. The simultaneous observation of superfluorescence on both cascading transitions is the central object of this experiment. Below the threshold mentioned above a second superfluorescence mode can be activated because of dephasing effects with the result that a delayed superfluorescence burst will appear. By decreasing the amount by which we narrow the resonance line in our optical pumping scheme, we will be able to have a handle on this dephasing induced superfluorescence.

This research was supported by the Joint Services Electronics Program, the National Science Foundation and the Army Research Office.

---

12 Jumpei Okada, Kensuke Ikeda, and Masahiro Matsuoka, Opt. Comm. 26, 189 (1978).

4. Local Field Contribution To The Nonlinear Response

(R. Friedberg, J. T. Manassah, S. R. Hartmann)

a. Abstract

We have developed a general formalism that incorporates local-field corrections into Bloch's equations and have used it to calculate the nonlinear strong-field susceptibility of a pressure-broadened gas consisting of two-level atoms.

b. General

We have found[13] that the nonlinear strong-field susceptibility of a pressure-broadened gas consisting of two-level atoms can be written as

$$\chi = \frac{\eta\beta/\pi}{\omega_o - \eta\omega_L - \omega - i\gamma_2}$$

where ρ is the number density of gas atoms, $\eta = (\rho_+ - \rho_-)/\rho$ is the fractional population difference between the excited (indicated by +) and the ground (indicated by -) states, $\beta = \pi\rho p^2/\hbar$, p is the transition dipole moment and, the bare atom resonance frequency is ω_o, and the local field term is given for a j=0 to j=1 transition by $\omega_L = \left(\frac{4}{3} - .22\right)\beta$, the number 4/3 is the Lorentz factor[14] and -.22 comes from nonpeturbative quantum effects[15]. The quantity η is determined by

$$[(1-\eta)/\eta]\left[1 + (\omega_o - \eta\omega_L - \omega)^2/\gamma_2^2\right] = I$$

where $I = \omega_R^2/\gamma_1\gamma_2$ is a normalized intensity

We note that η depends nonlinearly on the intensity I. For weak fields η = 1 and the susceptibility χ reduces to its normal form. For stronger fields η decreases. The effect of the local field correction on χ can be summarized in the following manner: In the wings of the resonance the response is shifted by the constant ω_L while at line center the shift is

---

13 R. Friedberg, S.R.Hartmann and J.T.Manassah, Phys. Rev. A40, 2446, (1989)

14 H. A. Lorentz, Theory of Electrons (Dover, New York, 2nd ed., 1952) sections 117-124 and Note 54

15 R. Friedberg, S.R.Hartmann and J.T.Manassah, Phys. Rpts. 7C, 101 (1973) and references therein

only $\omega_L/(1+I)$. At low intensities then the effect of the local field correction is to shift the susceptibility by a constant amount while at high intensities the effect is to distort the susceptibility near line center. These nonlinearities can lead to mirrorless bistability but they require that $\omega_L/\gamma_2 > 1$.

We have also calculated the susceptibility associated with a weak probe field in the presence of a strong pump field. Here the effect of the local field correction on the probe susceptibility is similiar to its effect on the pump susceptibility except that at moderate pump intensities there is a significant distortion of the probe susceptibility for the component of the probe field which is 90 degrees out of phase with the pump field.

This research was supported by the Joint Services Electronics Program and the Office of Naval Research.

II. SOLID-STATE ELECTRONICS (MATERIALS AND PROCESSING)

A. ELECTRONIC STATES AT METAL/SEMICONDUCTOR INTERFACES

Edward S. Yang, Principal Investigator (212) 854-5019

Research Area II, Work Unit 1

1. Fermi-level Movement in GaAs Bimetal Schottky Diodes

(X. Wu and E. S. Yang)

a. Introduction

For ordinary Schottky diodes having a single metal in contact with the semiconductor, the barrier height (BH) is fixed, i.e., its value is determined largely by the contact metal and the substrate semiconductor. Although some processing conditions could affect the BH to a certain extent,[1] most of them are not well-controlled. This forms a challenge to the fabrication of MESFETs with desired threshold voltages. This problem has been resolved by using a new kind of Schottky diode which has two different metal overlayers with one on top of the other. The inner metal layer is thin and in intimate contact with the semiconductor. On top of this thin layer a thick metal overlayer is deposited. The structure of the bimetal Schottky diode is shown in the inset of Figure 1. We use the notation B/A/GaAs to describe the composition of the diode, where A represents the thin inner metal and B denotes the top thick metal. The measured BH of such a device as a function of metal A thickness is depicted in Figure 1. The two diodes are Pt/Ti/GaAs and Ti/Pt/GaAs. As we see from the figure that with increasing thickness of metal A the Schottky BH of the device varies from the value associated with the metal B to that belonging to the metal A. This novel result shows us that controlling the Schottky BH in a wide range is practical. With different inner layer thickness and a proper combination of metals, we can virtually obtain any pre-specified BH value from the highest to the lowest available on a continuous basis. In addition, it is also discovered that the transition of the BH exhibits an exponential behavior extending over several monolayers of coverage. These observations provide new information to the understanding of the Schottky barrier formation.

This experiment raises a basic question on the Schottky barrier mechanism. Namely, what is the role of metallic screening in determining the Fermi-level position at metal-semiconductor interfaces. According to Mott-Jones' theory, the ideal screening length of metal is typically 0.7 Å.[2,3] If that is true in Schottky diodes, the band bending

inside the metal would be trivial and we should not be able to see any BH variation beyond d = 3 Å, since a monolayer of metal A would be thick enough to shield the effects of metal B. However, our result is evidently against this expectation. For both diodes the BH change continues even after 10 Å. Based on the above discussion, we propose a model invoking a finite metal screening length, which well explains the experimental data.

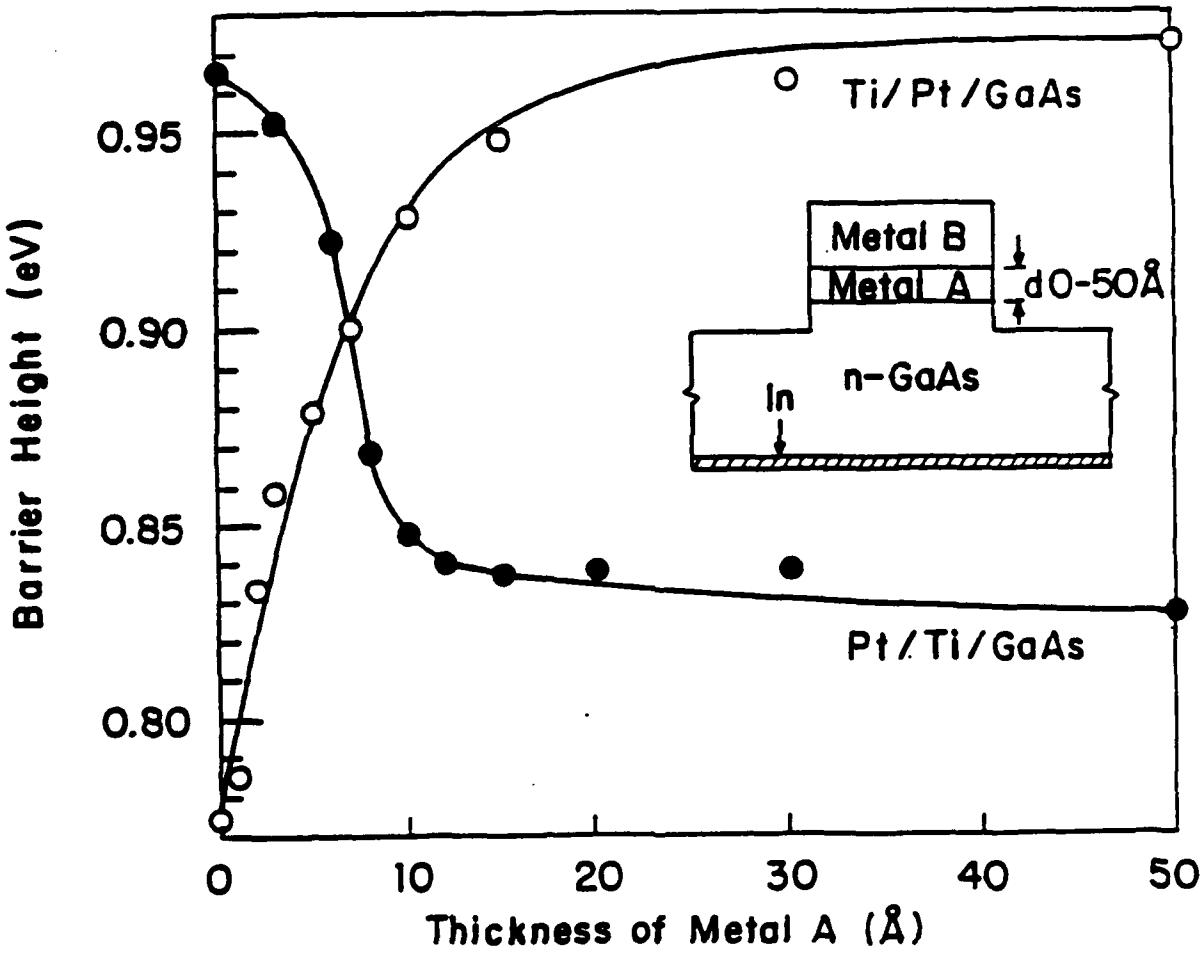

Figure 1: Barrier heights versus the inner metal thickness for Pt/Ti/GaAs and Ti/Pt/GaAs bimetal Schottky diodes. The dots and the circles are experimental data and the lines are fitted curves. The inset illustrates the structure of the device.

b. Theoretical Model

The energy-band diagrams of the bimetal Schottky diode are depicted in Figure 2.

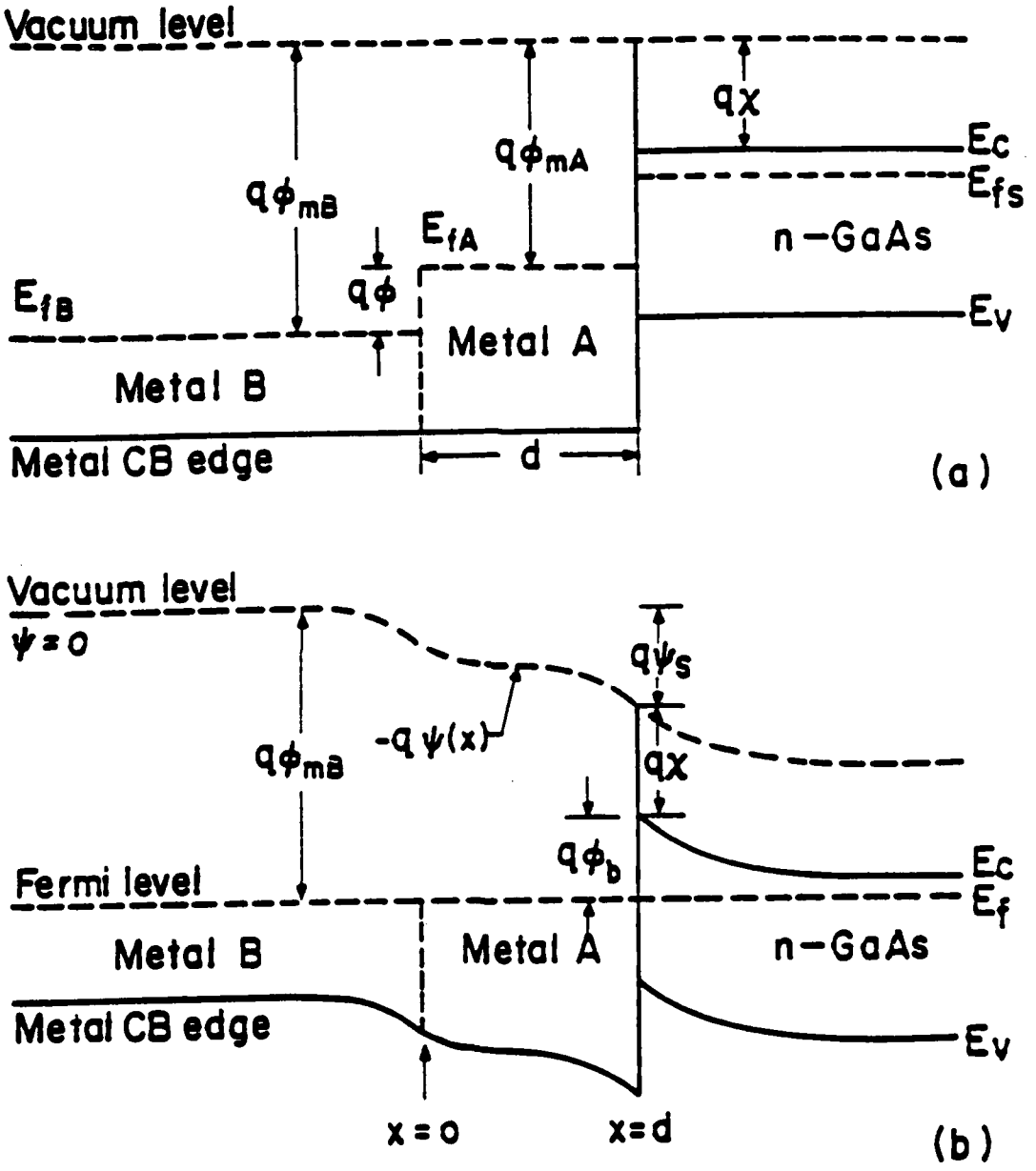

Figure 2: Energy-band diagram of the bimetal Schottky diode. The possible band discontinuity between the two metals is ignored. (a) The system is not in equilibrium. (b) After equilibrium is established, the metal band is bent by the contact potential, altering the ideal Schottky barrier height.

We use the jellium model to describe the metals such that they are treated as continuous media.[4] In the upper part, the three materials are in contact but not yet in equilibrium. This is represented by each part of the diode having its own Fermi level while the vacuum level is flat. Because of the difference in work function, electron diffusion occurs until the Fermi level in the system lines up. At equilibrium the vacuum level is no longer flat. Rather, it is bent by the contact potentials due to charge transfer among the media (Figure 2b). The band bending, $\psi(x)$, inside the metal can be derived from the local net charge, $-q\Delta n$, through Poisson's equation. Δn represents the excess electrons at position x in the metal, which in turn depends on $\psi(x)$. If the electronic density of states at the Fermi level is N/cm^3-eV and is approximately constant over the range of ϕ (the difference of the metal work function $\phi_{mB} - \phi_{mA}$), Δn can be written as $N(\Delta E_f + q\psi)$, where ΔE_f is the increase of the Fermi level in eV. Since metal B is very thick (400 Å) compared with the metal screening length, the Fermi level at the far left of Figure 2b should not be affected by the contact potential. Taking the interface of B/A as $x = 0$ and $\psi(-\infty) = 0$, we obtain

$$\frac{d^2\psi_B}{dx^2} = q\frac{N_B}{\varepsilon_{mB}}\psi_B, \qquad x < 0 \qquad (1)$$

for metal B. Similarly, for metal A, we have

$$\frac{d^2\psi_A}{dx^2} = q\frac{N_A}{\varepsilon_{mA}}(\psi_A - \phi) \qquad 0<x<d \qquad (2)$$

ε_{mA} and ε_{mB} are the lattice permittivities of the two metals respectively. These two equations are joined at $x = 0$ by the requirement of continuity for the potential as well as the electric field. The boundary condition at $x = d$, the A/GaAs interface, is

$$\varepsilon_{mA}\frac{d\psi_A}{dx}\Big|_{x=d} = Q_{it} + Q_{sc}, \qquad (3)$$

where Q_{it} and Q_{sc} are the interface charge and the semiconductor space charge per unit area, respectively. However, Q_{sc} ($\sim 4 \times 10^{11} q/cm^2$) turns out to be orders of magnitude smaller than Q_{it} ($\sim 10^{13} q/cm^2$, see results below), therefore we can neglect Q_{sc} in the analysis. Solving Eqs. (1) and (2) with the boundary conditions, we find that the potential drop at $x = d$ is

$$\psi_s(d) = \phi - \frac{\phi - Q_{it}\frac{\lambda_A}{\varepsilon_{mA}}\left[\gamma\cosh\left(\frac{d}{\lambda_A}\right)+\sinh\left(\frac{d}{\lambda_A}\right)\right]}{\left[\cosh\left(\frac{d}{\lambda_A}\right)+\lambda\sinh\left(\frac{d}{\lambda_A}\right)\right]}, \qquad (4)$$

where $\lambda_A(\lambda_B)$ is the effective screening length of metal A (B) which is defined as $\lambda \equiv \sqrt{\varepsilon_m / qN}$, and $\gamma \equiv \sqrt{(\lambda_B/\varepsilon_{mB})/(\lambda_A/\varepsilon_{mA})}$. Using Figure 2b, the BH can be written as

$$\phi_b = \phi_{mB} - \chi - \psi_s(d). \qquad (5)$$

Here we did not include the image force lowering since it is small compared with ϕ_b. Thus, for a given thickness d, the BH of the diode can be calculated from Eqs. (4) and (5) if λ, ε_m for both metals and the interface charge Q_{it} are known. The permittivity, ε_m, describes the polarizability of the atomic cores of the metal in response to an external electric field. Since the electrons in the inner shell (core) are tightly bound, ε in metal is expected to be small compared with those of dielectrics. In most cases, $\varepsilon_m = \varepsilon_0$ is a good approximation.[3] The interface charge, Q_{it}, in Eq. (4) depends on the position of the Fermi level. Namely, it is a function of $\psi_s(d)$:

$$Q_{it} = Q_0 - q\int_0^{q[\psi_s(d)-\psi_s(0)]} D_s\,dE, \qquad (6)$$

where D_s is the density of interface states (cm^{-2}-eV^{-1}) and the zero energy has been chosen as the Fermi level when d = 0. For simplicity, the Fermi distribution function in the above equation has been replaced by a step function. $Q_0 = \psi_s(0)\varepsilon_{mB}/\lambda_B$ is the initial interface charge in the absence of metal A. This accounts for $\psi_s(0)$ in an ordinary B/GaAs diode (see Eq. (5)). Combining Eqs. (4)-(6) together with the data in Figure 1, we have solved for λ_A, λ_B and the density of states, D_s.

Eq. (4) as a function of d is specified by three parameters: λ_A, λ_B and D_S. If D_S is constant, Q_{it} becomes linearly proportional to $\psi_S(d)$, i.e., $Q_{it} = Q_o - qD_S[\psi_S(d)-\psi_S(0)]$. For d = 0, $\psi_S = Q_o\lambda_B/\varepsilon_{mB}$ corresponding to the BH of B/GaAs. When $d >> \lambda_A$, ψ_S is given by $\phi + Q_{it}\lambda_A/\varepsilon_{mA}$, which corresponds to the BH of A/GaAs. For d between these two limits, ψ_s varies exponentially from one limit to the other. The characteristic decay-length of ϕ_b depends on both λ_A and λ_B but not on D_s. D_s only affects the magnitude of this transition. Further study shows that λ_A is more influential to the decay-length than λ_B. This is

because λ_B appears only in γ. In fact, varying γ from 0.2 to 5 has virtually no effect on the shape of the resulting curve. Therefore, letting $\gamma = 1$ as an initial choice allows us to find λ_A without much error. Under this situation, $\psi(d)$ reduces to a simple exponential function of d/λ_A. This was indeed what we found in the Ti/Pt/GaAs samples. Using work functions of 5.65 eV and 4.33 eV for Pt and Ti, respectively,[5] and $\chi = 4.07$ eV for GaAs, we obtained that the effective screening length of Pt is 6.5 Å and $D_s = 4.5 \times 10^{13}/cm^2\text{-eV}$ within the energy $0.78\ eV < E_c\text{-}E < 0.97\ eV$. These values have been refined with the actual value of λ_B for Ti (see below). The result is plotted in Figure 1. It fit he experimental data surprisingly well.

When D_s is non-uniform over the transition energy range, the natural exponential relation will be deformed by the interface state distribution. This is the situation for the Pt/Ti/GaAs samples. However, we can still estimate from Figure 1 that λ for Ti is ~7Å. Knowing λ for Ti, we may calculate Q_{it} in terms of $\psi_s(d)$ from Eq. (4). Then the density of interface states, according to Eq. (6), is

$$D_s = -\frac{1}{q}\frac{dQ_{it}}{d\psi_s}. \qquad (7)$$

The result of the calculation is shown in Figure 3. In contrast to the Ti/Pt/GaAs sample, we found a large density of interface states, up to $3.2 \times 10^{14}/cm^2\text{-eV}$ at ~ 0.97 eV below the conduction band in the Pt/Ti/GaAs diode. The resultant Fermi level pinning is seen as a slow variation of the BH for the first 6 Å of interfacial Ti.

c. Discussion

From the forgoing analysis, we found that the effective screening lengths for both metals differ sharply from the ideal values of Mott and Jones. Such a disagreement has also emerged from an earlier experiment. Mead once measured the capacitance of a planar capacitor as the dielectric spacing shrank toward zero.[6] He found that λ for Ta and Bi is 2.75 Å and 5.5 Å, respectively. These results, although obtained from a different approach, are consistent with our observations. The physical reasons for observing a large effective screening length are not yet clear. In order to examine the possible presence of interdiffusion or island formation at the interface, an Auger signal profile vs the metal coverage and a TEM structural analysis were carried out. The Auger profile revealed an exponential decrease of both Ga and As signal with the increasing coverage of Ti (Figure 3 inset) indicating a uniform growth of Ti overlayer and no significant diffusion of the

substrate species. The interface morphology between the Pt and the Ti was found very similar to the Ti/GaAs situation. These results were further confirmed in TEM characterization where no island structure was observed.[7] The interfacial chemical reaction, on the other hand, may create interface states, nevertheless cannot account for the observed screening length since no bulk reaction was detected by Auger. It seems to us that the properties of the metal films formed by deposition are different from those of bulk crystalline metals such as in the crystal structure and, hence, the free-electron density of states. In spite of the physical explanation, the existing evidence shows that the ideal case of metal screening does not apply to practical Schottky diodes. Therefore the actual potential drop in the metal side of a GaAs Schottky contact should not be ignored. This could very well be true for all Schottky diodes. A recent report has shown that Au and Al on ZnSe have similar behavior.[8] Finally, we would like to point out that the distributions of interface states found for the Pt/Ti/GaAs and Ti/Pt/GaAs samples are very different. This suggests that interface states are metal-dependent, though at this stage we are not able to identify the origin of these states.

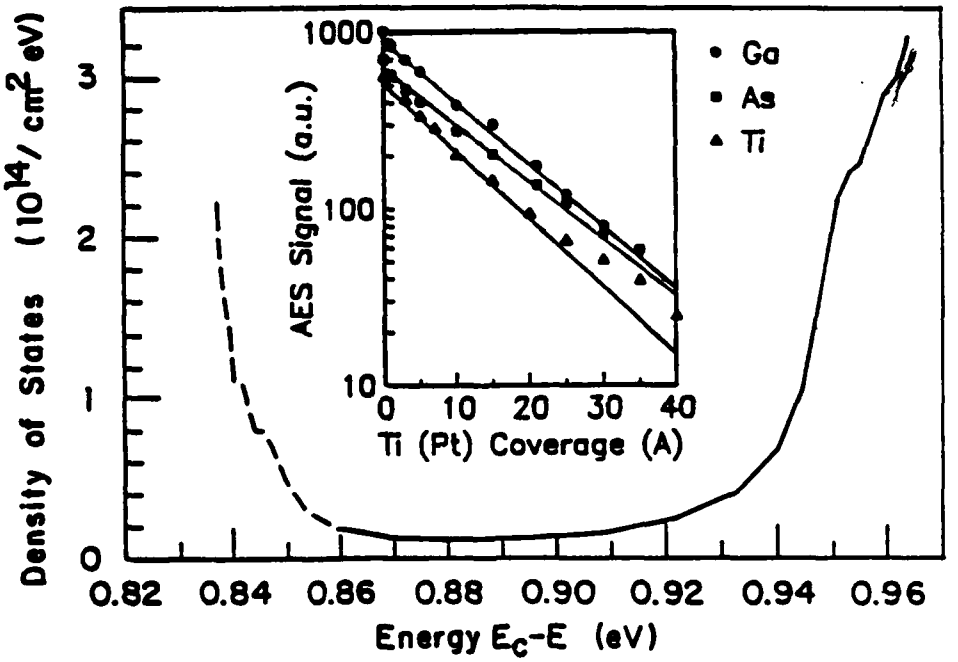

Figure 3: The density of interface states D_s obtained in Pt/Ti/GaAs sample. For Ti/Pt/GaAs sample, a constant $D_s = 4.5 \times 10^{12}$/cm^2-eV was found. The inset shows an exponential attenuation of the Auger signal for Ga and As vs. Ti coverage and Ti vs. Pt coverage. They indicate a uniform growth of metal overlayers and no interdiffusion.

d. Acknowledgements

The authors are grateful to their colleagues, especially W. I. Wang, for valuable discussions. They would also like to acknowledge M. T. Schmidt, P. Mei and Q. Y. Ma for their assistance. This work is supported by the Joint Services Electronics Program contract No DAAL03-88-C-0009.

References

1. J. M. Woodall and J. L. Freeouf, *J. Vac. Sci. Technol.* **19**, 794 (1981).
2. N. F. Mott and H. Jones, Theory of the Properties of Metals and Alloys, (Dover Publications Inc., New York, 1958), pp. 86-88.
3. C. R. Crowell, H. B. Shore, and E. E. LaBate, *J. Appl. Phys.* **36**, 3843 (1965).
4. S. G. Louie and M. L. Cohen, *Phys. Rev. B* **13**, 2461 (1976).
5. H. B. Michaelson, *J. Appl. Phys.* **48**, 4729 (1977).
6. C. A. Mead, *Phys. Rev. Lett.* **6**, 545 (1961).
7. X. Wu and E. S. Yang, submitted to *Appl. Phys. Lett.*
8. M. Vos, F. Xu, J. H. Weaver, and H. Cheng, *Appl. Phys. Lett.* **53**, 1530 (1988).

B. NEW OPTICAL MATERIALS AND SOURCES

Irving P. Herman, Principal Investigator (212) 854-4950

Research Area II, Work Unit 2

The main objective of this JSEP work unit is to understand the optical, electronic, and structural properties of II-VI semiconductor heterostructures and superlattices, using optical probing and pressure tuning techniques. Another objective of this work unit is to examine the effect of processing on compound semiconductors by using optical techniques. This research will help in the development of new optical and electronic technologies based on these semiconductor materials.

1. Optical Studies of II-VI Semiconductor Structures

We measured the near bandgap photoluminescence of ZnSe epilayers grown on GaAs substrates for pressures up to ~30 kbar using a diamond anvil cell at T = 9 K. Specifically, we measured the bandgap changes with pressure, dE/dp, for pseudomorphic and nonpseudomorphic films and compared these results with with those from similar studies we conducted for bulk crystalline ZnSe. We also began the examination of photoluminescence (PL) from $ZnSe/ZnMn_xSe_{1-x}$ superlattices. In these studies, we used MBE grown films from R. Gunshor at Purdue University and from D. Cammack at Philips Laboratories, who is a new collaborator for this JSEP effort. Our bulk crystalline ZnSe samples were also obtained from Philips (M. Shone).

Commensurate growth of ZnSe on GaAs has been achieved previously for thicknesses up to ~0.15 μm.[1-3] Elastic strain due to the lattice mismatch (0.25% at room temperature) is accommodated until the critical thickness is obtained. For larger thicknesses misfit dislocations lower the total energy of the system and incommensurate growth ensues. Previous studies have demonstrated the relation of this strain to epilayer thickness, with its concomitant effect on the density of misfit dislocations [2,4]. Moreover, photoluminescence (PL) studies have demonstrated the effect of this strain on band-edge emission. [4-6] The presence of biaxial strain in very thin films is also expected to alter the effect of applied hydrostatic pressure (p) on the band-edge photoluminescence relative to its effect on the PL from bulk material. Previous reports have determined dE/dp, the change in bandgap energy with pressure, to be in the range 6.0 – 7.5 meV/kbar for bulk ZnSe at room temperature down to 77 K.[7-9]

Photoluminescence measurements were made during this year on 0.1 and 2.1 μm-thick ZnSe epilayers grown on GaAs by MBE and on bulk ZnSe grown by zone melting.

The "thin" epilayer was commensurately grown, while the "thick" layer was thicker than the critical thickness for commensurate growth. Experiments were conducted at a temperature of T = 9 K and at pressures up to ~30 kbar. The GaAs substrate was initially ~300 μm thick, and was thinned down to ~50 μm by mechanical polishing.

High pressure measurements were made in a gasketed Merrill-Bassett diamond anvil cell (DAC) described in the previous JSEP progress report,[10,11] contained within a closed cycle refrigerator (9 K). The ZnSe sample was loaded with ruby chips in a liquid argon bath within the DAC to obtain near-hydrostatic pressure conditions at low temperature.[12] ZnSe and ruby photoluminescence were excited using the 4067 Å line from a krypton ion laser, and were detected using a 0.85 m double spectrometer and a cooled PMT. Photon counting electronics were interfaced to an IBM AT for A/D data conversion, storage, and analysis.

The pressure in the DAC was determined using the calibration scale for ruby fluorescence vs. pressure.[13] This was in turn calibrated using the 6929.468 Å line from a neon discharge lamp, together with the 6965.430 Å line from an argon lamp. The pressure determination is accurate to < 0.15 kbar, and energy measurements for the ZnSe photoluminescence are accurate to < 0.6 meV. The resultant uncertainty in the values of dE/dp is less than 0.21 meV/kbar.

Near band-edge PL spectra are shown for the three samples at ambient pressure (1 bar) and T = 9 K, as the lower spectra in each of the three parts of Figure 1. For the bulk crystalline sample in Fig. 1a, the dominant feature at 2.7973 eV (I_{2O}) is associated with a neutral bound donor exciton, attributed to either an In or Ga impurity. A neutral bound acceptor accounts for the exciton feature at 2.7924 eV (I_1). The feature at 2.7829 eV (I_1^{DEEP}) is due to a deep level acceptor, commonly attributed to Cu. The phonon replica, $I_1^{DEEP-LO}$, is found 31.6 meV lower in energy than I_1^{DEEP}. Finally, the two weak features higher in energy than I_{2O}, are due to the excited state (n=2) of a donor bound exciton at 2.8014 eV (I_{2D}) and the free exciton transition at 2.8039 eV (FE).

Identification of the PL peaks is less certain for the epilayers. For the "thick" film in Fig. 1b, the ambient pressure peak at 2.8009 eV (FE) is attributed to the ground state free exciton peak. The red shift from the bulk value may be due to a slight tensile strain.[3] The peak at 2.7958 eV (I_{2O}) is associated with an exciton bound to a neutral donor and the peak at 2.7728 meV (I') is as yet unidentified. For the "thin" film in Fig. 1c, one large peak is obtained. This corresponds to the ground state free exciton transition with energy 2.8055 eV (FE). The blue shift from the bulk value corresponds to an in-plane compressive strain due to a lattice mismatch at 9 K of ~0.23%. A very small peak is found near 2.7998 eV (I_x), which is usually attributed to a neutral bound exciton.

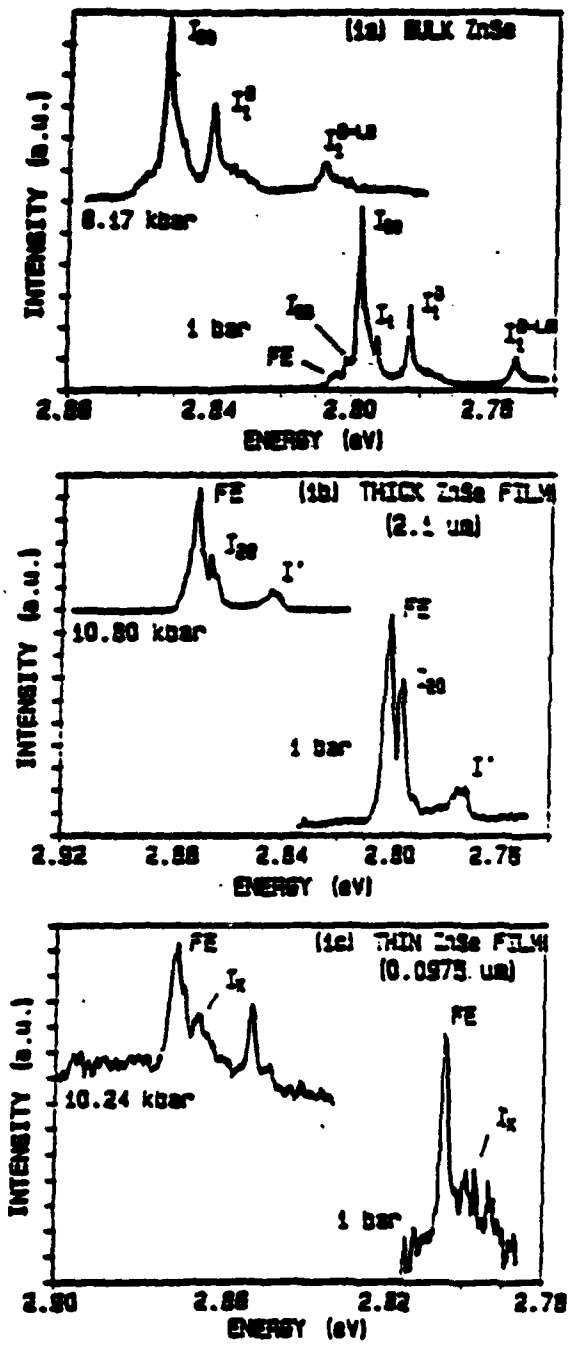

Figure 1. Photoluminescence spectra at T - 9 K

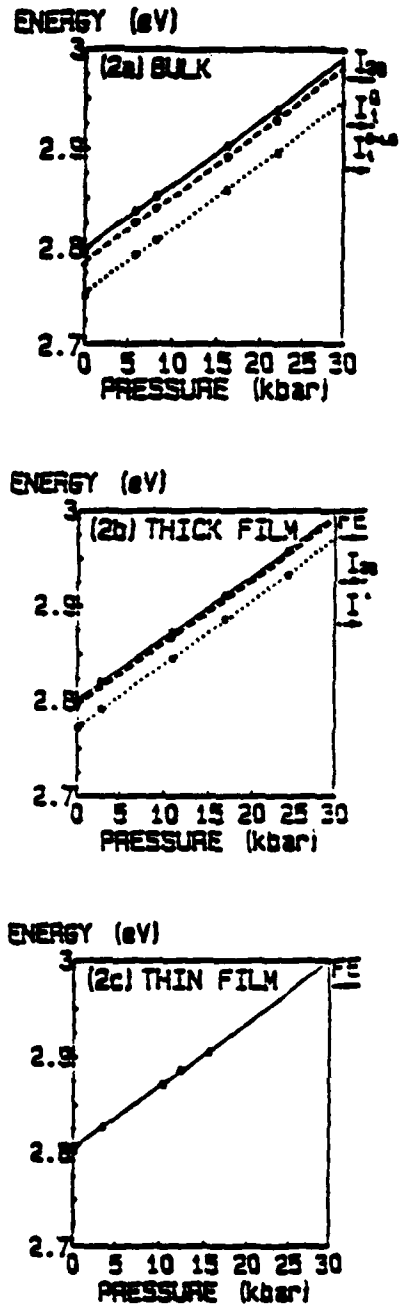

Figure 2. Plots of energy vs pressure for the various exciton peaks.

The photoluminescence was monitored with increasing pressure for all three samples. A representative plot for each sample at a higher pressure is provided by the upper spectra in the three parts of Figure 1. For the "thick" epilayer, the I_{20} peak intensity decreases with increasing pressure and disappears altogether at approximately 16 kbar. At approximately the same pressure, a new feature begins to grow at 2.9170 eV, which is 6.4 meV higher in energy than the FE peak. As pressure is increased the exciton energies I_{20}, I_1^{DEEP}, and $I_1^{DEEP\text{-}LO}$ are monitored for bulk ZnSe, the FE, $I_{20}^{Cl,In,Ga}$, and I' peaks are monitored for the "thick" sample, and the free exciton transition (FE) is monitored for the "thin" sample. The resultant plots of energy vs. pressure are shown in Figure 2. Least square lines are plotted for these data, yielding values for dE/dp. For bulk crystalline ZnSe, a value of dE/dp = 6.45 ± 0.12 meV/kbar is obtained for the dominant I_{20} peak, with dE/dp = 6.59 ± 0.12 meV/kbar for I_1^{DEEP} and 6.58 ± 0.15 meV/kbar for $I_1^{DEEP\text{-}LO}$. For the "thick" sample, dE/dp = 6.50 ± 0.13 meV/kbar for the dominant free exciton (FE) peak, 6.54 ± 0.13 meV/kbar for I_{20}, and 6.67 ± 0.15 meV/kbar for I'. For the "thin" sample, dE/dp = 6.48 ± 0.21 meV/kbar (FE).

The effect of hydrostatic and uniaxial pressure on a semiconductor is to shift the conduction and valence band edges by changing the volume and crystal symmetry. For ZnSe with its direct bandgap at Γ_1, the conduction band is only subject to hydrostatic components of strain. However, in addition to the effect of hydrostatic strain on shifting the valence bands (Γ_8), tetragonal distortion splits the degeneracy of the four-fold $P_{3/2}$ multiplet into heavy hole (hh: J = 3/2; $m_J = \pm 3/2$) and light hole (lh: J = 3/2; $m_J = \pm 1/2$) bands. The effect of biaxial stress due to lattice mismatch may therefore be separated into hydrostatic and nonhydrostatic components,[14,15] which when considered together with externally applied hydrostatic pressure may be shown to affect energy bandgap shifts, according to:

$$\Delta E_g = -(a_c - a_v)\frac{3p}{C_{11} + 2C_{12}} + \left[2(a_c - a_v)(1 - \frac{C_{12}}{C_{11}}) \mp b(1 + \frac{2C_{12}}{C_{11}})\right]e_{xx}^{ZnSe}(T,p) \qquad [1]$$

The first term is the hydrostatic pressure component, while the first component of the second term is due to the hydrostatic portion of the strain and the second component is due to tetragonal deformation, with – for heavy holes and + for light holes. Spin-orbit splitting has been included in the overall bandgap term. Here, a_c and a_v are the hydrostatic deformation potentials for the conduction and valence bands respectively, b is the uniaxial deformation potential for a strain of tetragonal symmetry, and C_{11} and C_{12} are elastic

constants for ZnSe. The strain $\varepsilon_{xx}^{ZnSe}(T,p)$ is evaluated for a given temperature and pressure and has the form:

$$\varepsilon_{xx}^{ZnSe}(T,p) = \frac{a'_x(T,p_0)}{a_x(T,p_0)} \left(\frac{1 - \frac{p}{C'_{11} + 2C'_{12}}}{1 - \frac{p}{C_{11} + 2C_{12}}} \right) - 1 \qquad [2]$$

where $a_x(T,p_0)$ is the lattice constant for ZnSe at temperature T and ambient pressure (p_0 = 1 bar), and the primed quantities correspond to the respective parameters for GaAs.

The resultant shift in bandgap energy with pressure for a strained layer may be related to $(dE/dp)_{bulk} = -\{3(a_c - a_v)/(C_{11}+2C_{12})\}$ for bulk material by:

$$\left(\frac{dE}{dp}\right)_{\substack{hh \\ lh}} = \left(\frac{dE}{dp}\right)_{bulk} - \left[2(a_c - a_v)\left(1 - \frac{C_{12}}{C_{11}}\right) \mp b\left(1 + \frac{2C_{12}}{C_{11}}\right)\right] \frac{a'_x(T,p_0)}{a_x(T,p_0)} \left[\frac{1}{C'_{11} + 2C'_{12}} - \frac{1}{C_{11} + 2C_{12}}\right] \qquad [3]$$

The variation of the exciton binding energy with applied hydrostatic pressure is not significant here.

The values for dE/dp may be evaluated using C_{11} = 929 kbar, C_{12} = 562 kbar, C'_{11} = 1221 kbar, C'_{12} = 566 kbar,[16,17] a_x(298 K,p_0) = 5.6676 Å, and a'_x(298 K,p_0) = 5.6533 Å.[5,17]. The elastic constants are for T = 77 K. For 9 K, the elastic constants are estimated to be 940, 570, 1234, and 577 kbar, respectively, extrapolating from the constants at 77 and 300 K by using an exponential fit. A wide range of deformation potential values are reported in the literature. The theoretical values $(a_c - a_v) = -4.17$ eV and $b = -1.20$ eV[3,18] can be used as reference parameters. Then the expected values of dE/dp are 6.09 meV/kbar for bulk crystalline ZnSe, and 6.05 and 5.72 meV/kbar for the hh and lh bands for strained layer ZnSe on GaAs, using the elastic constants at 77 K. At 9 K, the respective values are 6.01, 5.98, and 5.65 meV/kbar. Using the previously determined experimental values[6] as a second reference, $(a_c - a_v) = -4.87$ eV and $b = -1.05$ eV, then the three expected values for dE/dp are 7.11, 7.02, and 6.73 meV/kbar, respectively at 77 K, and 7.02, 6.93, and 6.64 meV/kbar at 9 K. The value of $(a_c - a_v)$ determined here is –4.47 eV, using dE/dp measured for the I_{20} peak in bulk crystalline ZnSe and using the elastic constants estimated for 9 K.

The heavy hole band is higher in energy than the light hole band for compressed films, while for films under tensile stress the light hole band is higher. However, since dE/dp for hh is greater than that for lh, increasing the pressure will cause the bands to cross. Thus films initially under compressive stress, such as "thin" ZnSe films, will become tensile beyond some pressure, and the value of dE/dp will change from the hh to the lh value. The "thick" films, on the other hand, are always either relaxed or under tensile stress, and will therefore follow the lh value throughout.

Low temperatures (9 K) will affect the film strain and the relative energies of the valence bands. Specifically, for ZnSe films on GaAs, a temperature decrease relaxes the compressive strain due to lattice mismatch, since the thermal expansion coefficient for ZnSe is larger than that for GaAs.[15] Nonetheless, the "thin" films here remain compressively strained even at low temperature for $p \lesssim 34$ kbar, so that the heavy hole band will therefore always be at the higher energy. Hence, the model suggests that dE/dp for the "thin" film hh excitons and for excitons in the bulk should be within 0.1 meV/kbar of each other. Within experimental uncertainty, this is seen here. The "thick" ZnSe films, however, are always under tensile stress, since it is assumed that the compressive strain has been completely relaxed at room temperature. As a result, dE/dp for these films is expected to be the lh value which, according to the model, is ~0.3-0.4 meV/kbar lower than the bulk and "thin" film values. This is in contrast to the reported measurements.

Representative PL traces for the $ZnSe/ZnMn_xSe_{1-x}$ pressure tuning studies conducted this year are given in Fig. 3, along with a preliminary determination of dE/dp, shown in Fig. 4. Note that the width of the PL spectrum decreases with increasing pressure.

We also designed a new diamond anvil cell this year, using the cell in ref. 19 as a model, which should permit operation at even higher pressures within the cryostat than is currently possible with the Merrill-Bassett cell. Moreover, use of this new DAC will enable us to tune pressure while the cell is in the cryostat, which is not possible with our current system. Two of these new cells have been constructed and they will be tested and used in the upcoming reporting period.

2. Optical Studies of Compound Semiconductors after Processing

Raman microprobe scattering was used to probe GaAs surfaces after local laser doping by Zn. Figure 5c shows a typical Raman spectrum, along with reference samples shown in Fig. 5a and b. Of particular interest is the fine lateral resolution achievable with this microprobe, which is demonstrated in Fig. 6 and shows that the width of the doped

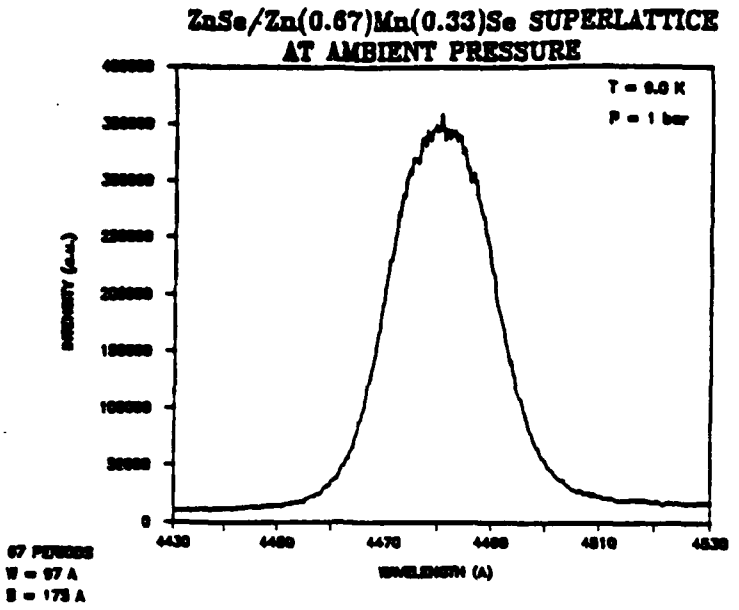

Figure 3.

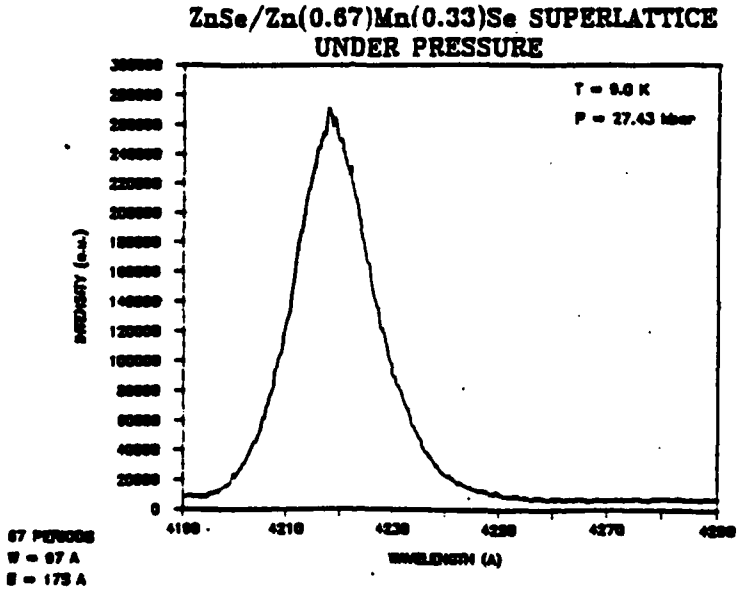

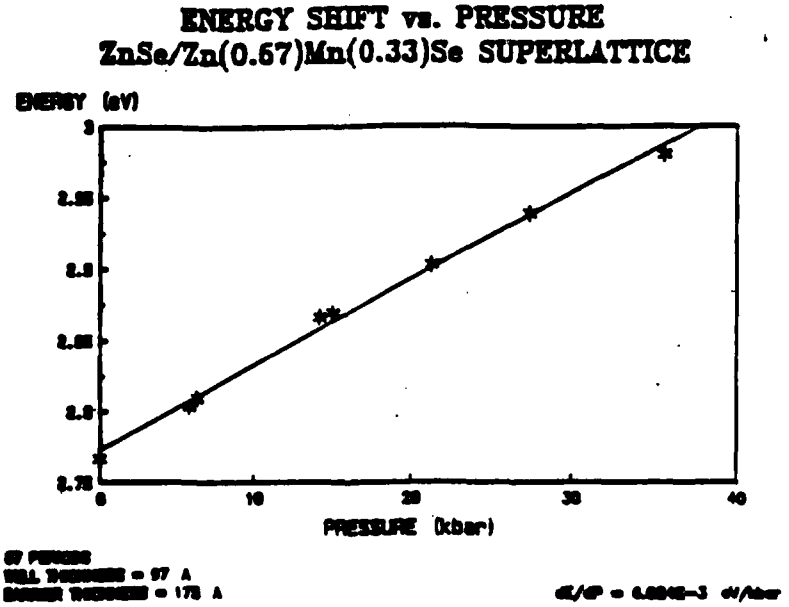

Figure 4.

region is ~ 2 μm. (The Raman probing part of this work was done in I. Herman's laboratory and was JSEP-supported. The laser doping part of this work was performed in R. Osgood's laboratory with non-JSEP support.)

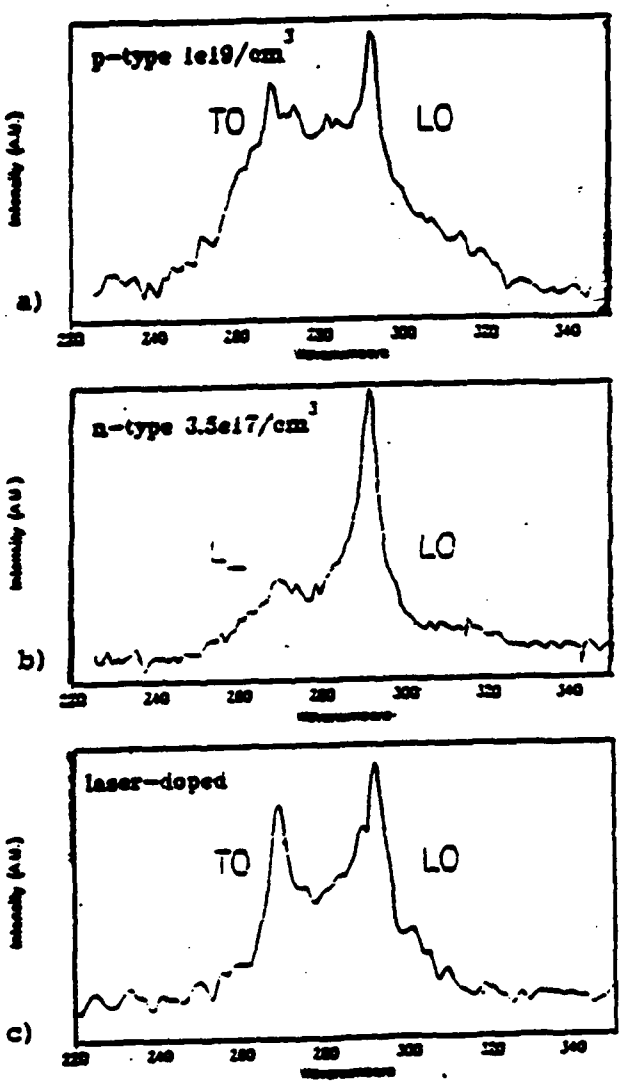

Figure 5.

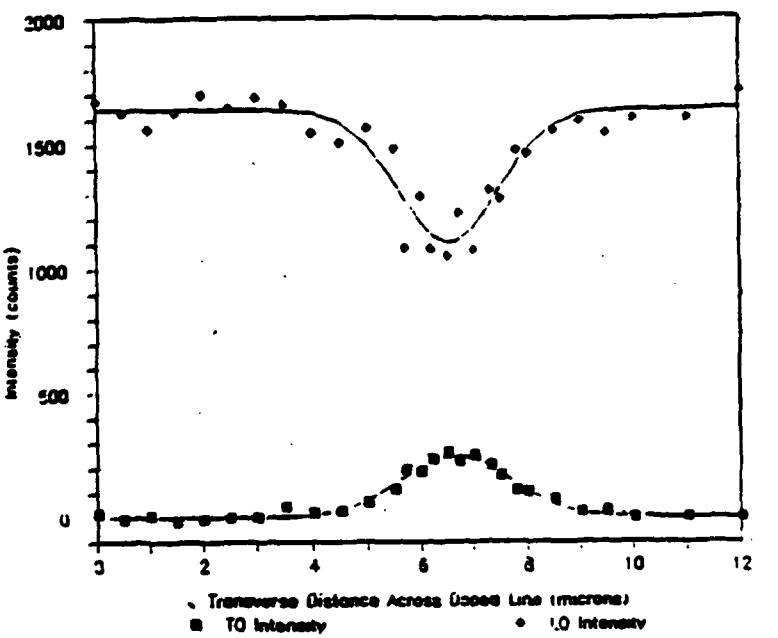

Figure 6.

References

1. J. Kleiman, R.M. Park, and S.B. Qadri, J. Appl. Phys. 61, 2067 (1987).
2. J. Petruzzello, B.L. Greenberg, D.A. Cammack, and R. Dalby, J. Appl. Phys. 63, 2299 (1988).
3. T. Yao, Y. Okada, S. Matsui, K. Ishida, and I. Fujimoto, J. Crystal Growth 81, 518 (1987).
4. T. Yao, Jpn. J. Appl. Phys. 25, L544 (1986).
5. K. Mohammed, D.A. Cammack, R. Dalby, P. Newbury, B.L. Greenberg, J. Petruzzello, and R.N. Bhargava, Appl. Phys. Lett. 50, 37 (1987).
6. R.L. Gunshor, L. A. Kolodziejski, M.R. Melloch, M. Vaziri, C. Choi, and N. Otsuka, Appl. Phys. Lett. 50, 200 (1987).
7. A.L. Edwards, T.E. Slykhouse, and H.G. Drickamer, J. Phys. Chem. Solids 11, 140 (1959).
8. S. Ves, K. Strossner, N.E. Christensen, C.K. Kim, and M. Cardona, Solid State Commun. 56, 479 (1985).
9. P. Jaszczyn-Kopec, B. Canny, G. Syfosse, and G. Hamel, Solid State Commun. 49, 795 (1984).
10. A. Jayaraman, Rev. Mod. Phys. 55, 65 (1983).
11. L. Merrill and W.A. Bassett, Rev. Sci. Instrum. 45, 290 (1974).
12. A.P. Jephcoat, H.K. Mao, and P.M. Bell, J. Geophys. Res. 91, 4677 (1986).
13. R.A. Noack and W.B. Holzapfel, in *High Pressure Science and Technology*, ed. K.D. Timmerhaus and M.S. Barber (Plenum) 1, 748 (1979).
14. H. Asai and K. Oe, J. Appl. Phys. 54, 2052 (1983).
15. C.G. Van de Walle, K. Shahzad, and D.J. Olego, J. Vac. Sci. Technol. B6, 1350 (1988).
16. S.S. Mitra and N.E. Massa, in *Handbook on Semiconductors*, ed. T.S. Moss (North Holland) 1, 96 (1986).
17. Landolt-Bornstein, *Numerical Data and Functional Relationships in Science and Technology* (Springer, New York) Group III, 17 a-b, (1982).
18. D.W. Langer, R.N. Euwema, K. Era, and T. Koda, Phys. Rev. B2, 4005 (1970).
19. D.J. Dunstan and W. Scherrer, Rev. Sci. Instrum. 59, 627 (1988).

C. ULTRAVIOLET LASER INDUCED ELECTRON AND ION EMISSION FROM SEMICONDUCTORS

Richard M. Osgood, Jr., Principal Investigator (212) 854-4462

Research Area II, Work Unit 3

1. Photoemissive Scanning Microscopy of Doped Regions on Semiconductor Surfaces

(B. Quiniou, R. Scarmozzino, Z. Wu, and R. M. Osgood, Jr.)

Photoemission from semiconductor surfaces has been extensively used to determine the energy levels in semiconductor materials,[1] and their bulk material properties such as doping.[2,3] Photoemission from metal conductors in integrated circuits has recently been used as a microscopic probe of circuit performance.[4] Here we describe the first use of photoemission scanning spectroscopy to map the doping and surface properties of semiconductors. A focused UV (ultraviolet) laser beam is scanned across a patterned semiconductor, and differences in surface properties such as doping or oxide/metal deposits are observed as differences in emitted photocurrent. Although the technique is applied to silicon, it has direct applicability to mapping of doped regions in compound semiconductors as well.

This technique has several potential advantages over other possible methods for mapping out microscopic surface properties. For instance, micro-SIMS (secondary ion mass spectroscopy) has an excellent spatial resolution but it is a destructive technique which must be used in ultrahigh vacuum. When implemented in a practical system, our technique can provide an in situ probe of doping levels or doping patterns in a semiconductor wafer, with a spatial resolution of a few wavelengths of the probing beam. The experimental apparatus consists of a cryopumped stainless steel vacuum chamber which maintains the sample and collector at a pressure of 10^{-8} to 10^{-6} Torr. The collection arrangement is shown in Figure 1.

The laser wavelength used for most experiments was 257 nm (4.82 eV) and is obtained from an argon-ion laser using an intracavity frequency doubler. The laser beam is translated by a set of X-Y stages with 0.1 -μm resolution, and is focused by a 16X UV transmitting microscope objective to a spot size of about 1.7 μm full-width-at-half-maximum. The samples used were strongly doped (100) p-type silicon (10^{20} cm^{-3}), and weakly doped (100) p-type silicon (10^{14} cm^{-3}) patterned with 25 -μm lines of p^+ (10^{18} - 10^{19} cm^{-3}) or n^+ (10^{19} -10^{20} cm^{-3}) regions. Because near-threshold photoemission is known to be very sensitive to surface conditions, several different surface preparations

were tested. Note that it is not necessary to remove the native oxide prior to loading the samples.

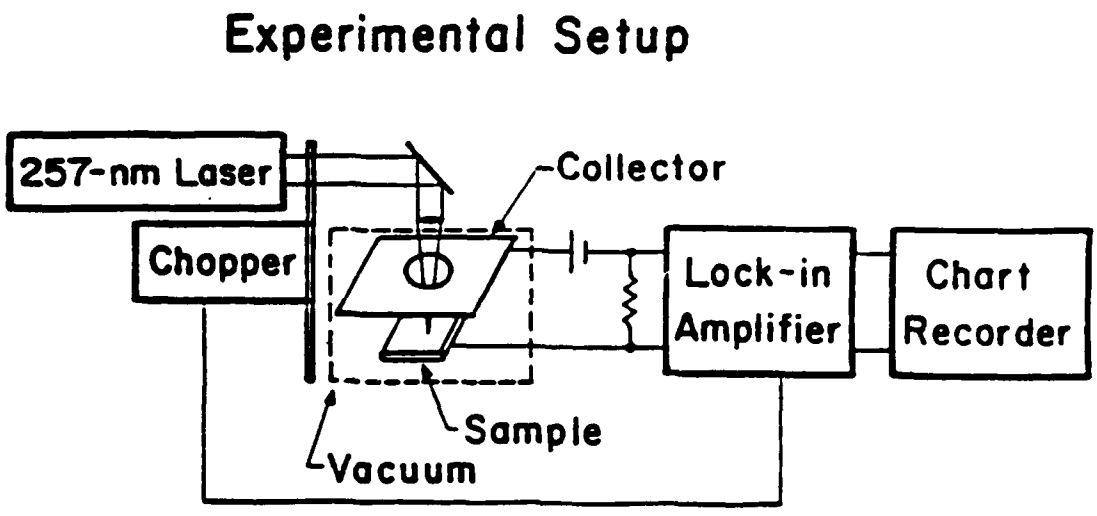

Figure 1. The collection arrangement for the detection of photocurrent. Inset: Typical plot of photocurrent versus laser power for a weakly doped p-type sample.

Our photon energy of 4.82 eV is slightly below the published photoelectric threshold for lightly doped bare Si (100) (5.11 eV).[5] Despite this energy deficiency, photoemission was seen for samples of all doping levels. A measurement of the photoelectric current was seen for samples of all doping levels. A measurement of the photoelectric current versus laser power exhibited a linear dependence, which is consistent with a single-photon photoemission process. The linear power dependence also indicates that space-charge effects are not limiting the photocurrent.

The absolute yield for the weakly doped p-type silicon with the native oxide layer was of the order of 10^{-7} electrons/photon, higher than would be expected from the data in [5], particularly when one realizes that the surface is covered with the thin layer of native oxide. This magnitude of yield was routinely obtained on silicon surfaces prepared with the simple degreasing procedure. We believe the larger-than-expected yield to be the result of adsorbed gases (possibly water vapor), which are known to affect the work function of a surface considerably.[6] Consistent with this is our observation that the yield on the

chemically inert, hydrogen-passivated surface was significantly less. Thus, despite the fact that our surfaces are far from bare, adequate yields of photoelectrons can be obtained.

Figure 2 shows a typical trace of the photocurrent versus time for a stationary laser spot on the weakly doped p-type silicon region. Figure 3 shows plots of photocurrent versus time obtained while scanning the beam across the p^+ on p and n^+ on p samples. The strongly doped regions give a higher signal than the weakly doped regions, and are clearly evident in the figure. The measured widths of the doped regions are ≈ 26 - 31 μm, in agreement with the patterned widths (these numbers differ from 25 μm due to the tilt of the samples). The signal peaks at the edges of the line are superficially similar to edge effects seen in other optical studies. The effect could be due to crystallographic-sensitive emission, electromagnetic-field edge enhancement, or doping gradient effects. In particular, since the highly doped lines are normally recessed about 400 - 800 Å due to the fabrication procedure, different crystallographic planes might be exposed at the edge of the line. The Si (100) surface, which was the surface we used, has the largest photoemission threshold (5.11 eV for the (100) surface, 4.73 eV for (110) and 4.60 eV for (111)[5] and the exposure of surfaces other than (100), due to the recessing, could give a larger signal than for the purely (100) surface in the center of the doped region. The same recess discontinuity could cause an enhanced electromagnetic field at the edge due to surface roughness. To gain some insight into the mechanism of edge enhancement, grooves of similar width were etched to depths of ≈ 300 Å on a p-type substrate. No photoemission enhancement was seen at the edges of the grooves. This result appears to rule out the enhancement due to crystallographic or optical electromagnetic field effects. We tentatively

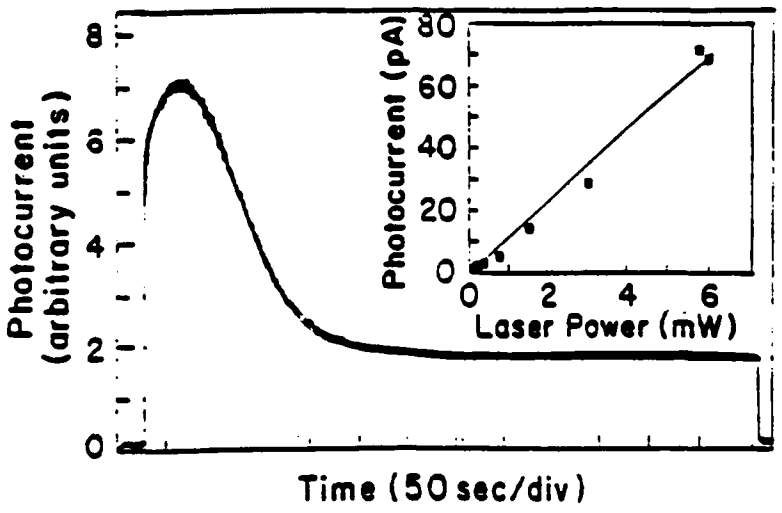

Figure 2. Photocurrent versus time for stationary illumination. Sample: weakly doped p-type silicon.

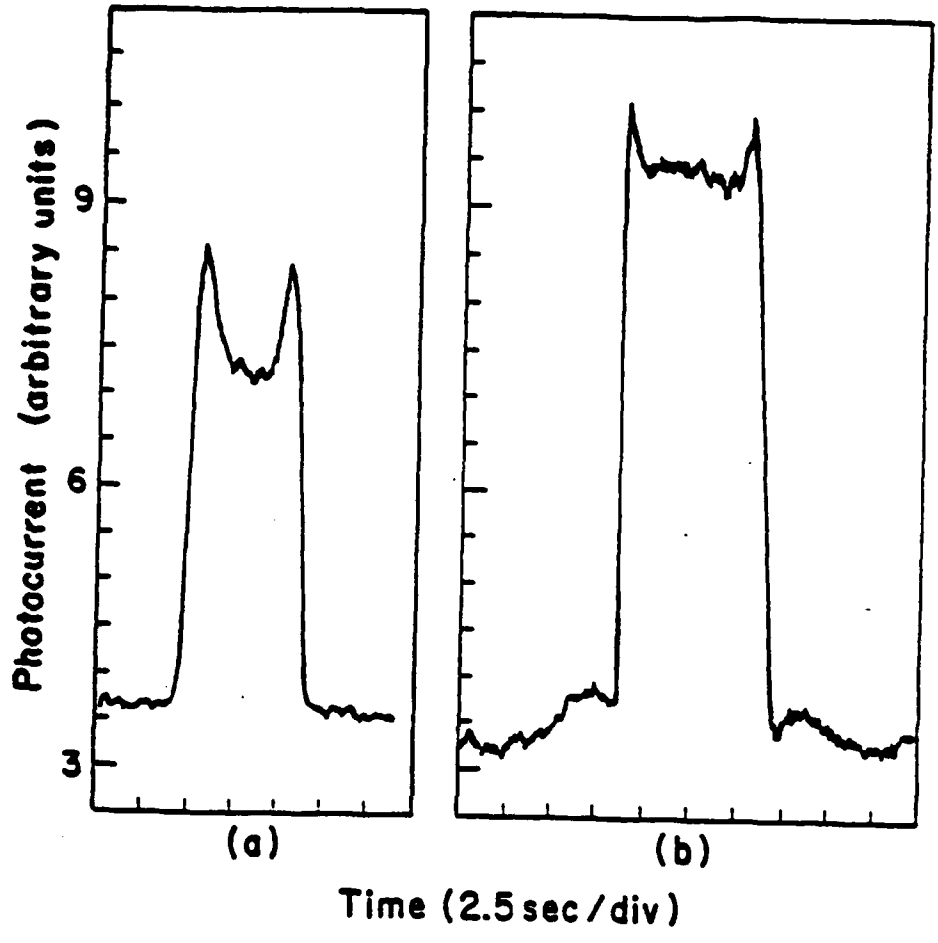

Figure 3. Photocurrent versus time while scanning the laser beam 4 μm/sec. Samples: (a) p^+ on p. (b) n^+ on p.

ascribe the edge effect to the doping gradient, most probably associated with its built-in static internal field.

On a freshly cleaved Si (111) surface, the doping dependence of photoemission yield has been observed and explained by Gobeli and Allen.[2,3] In that work they measured the apparent threshold for photoemission versus bulk doping and found that the threshold is highest for weakly doped p-type samples, while for strongly doped p or n-type samples the threshold is reduced by 0.35 - 0.40 eV. For p-type material this doping dependence arises from the upward bending of the valence band relative to the surface, which for high doping occurs within the penetration depth of the photon and the escape depth for electrons, and therefore reduces the emission threshold of electrons emitted from the bulk. For n-type material, the bands bend in the opposite direction and the threshold for emission from the valence band in the bulk is increased, thus one would expect a decrease in the yield. However, surface states lying just below the conduction band will move below the

Fermi level and become occupied, and increased yield will result due to emission from these states. As the n-type doping is increased even further, the conduction band in the bulk will move below the Fermi level, and a lower threshold will result from emission from the conduction band.

In contrast, our samples, Si (100) surfaces, are not ideal since they are covered with a thin layer of natural oxide. Further, due to our sample cleaning procedure our sample surface is covered with -OH groups. It is probable that these -OH groups lower the photoelectric threshold (5.11 eV) for Si (100) surface so that we still observe photoemission even though our photon energy is only 4.82 eV. The presence of the oxide on the Si surface drastically changes the Si/SiO_2 interface electonic states, as well as the band bending.[7] However, using arguments similar to those used for cleaved surfaces, one can still show that the photoemission yield is higher for n^+ and p^+ type than for weakly doped n or p type, in agreement with our observations. Note that the known thickness of such native oxides is less than the escape depth of the electrons, thus permitting emission from the material beneath the oxide layer.

In conclusion, we have demonstrated that photoemission induced by a focused UV laser beam can be used to map doping patterns on a semiconductor surface. We have shown that even though the photon energy is slightly below the bulk emission threshold, differences in photoemission yield from different doping regions are still clearly observable. The spatial resolution was limited only by the width of the focus UV probing beam, to be ~ 1 - 2 μm for our optics; more attention to the optical train and processing can yield submicrometer values. This probing technique is shown to be applicable to Si samples covered with a natural oxide layer, therefore it has the potential of being a practically useful tool to probe semiconductor surfaces. The technique can potentially be extended to observing other surface sensitive properties such as defects or surface roughness.

This research was supported by the Joint Services Electronics Program; the laser scanning instrumentation was funded by SRC.

References

1. R. C. Eden, J. L. Moll, and W. E. Spicer, *Phys. Rev. Lett.* 18, 597 (1967).
2. G. W. Gobeli and F. G. Allen, *Phys. Rev.* 127, 141 (1962).
3. F. G. Allen and G. W. Gobeli, *Phys. Rev.* 127, 150 (1962).
4. A. M. Weiner, P. S. D. Lin, and R. B. Marcus, *SPIE* 795, 292 (1987).
5. R. M. Broudy, *Phys. Rev. B* 1, 3230 (1970).
6. J. A. Ramsey, *Surface Science* 8, 313 (1967).
7. L. F. Wagner and W. E. Spicer, *Phys. Rev. B* 9, 1512 (1974).

2. UV Laser Photoemission Studies of Compound Semiconductor Surfaces

(B. Quiniou, R. M. Osgood, Jr., and Z. Wu)

a. Introduction

One photon photoemission spectroscopy has proved to be an extremely valuable technique for investigating electronic structures of materials and especially semiconductors. However, this technique does not allow the probing of states with an energy laying between the Fermi energy and the vacuum level, and therefore normally unoccupied. These states happen to play very important roles or are directly involved in chemical and physical processes at surfaces such as molecular/atomic adsorption and Fermi level pinning in electronic devices.

Although there are several different spectroscopic techniques which allow direct probing of these states including inverse photoemission, negative electron affinity and partial yield spectroscopies, two photon photoemission spectroscopy, based on laser sources, recently appeared as most interesting in terms of energy resolution, surface sensitivity and has also benefitted from the long developed one photon photoemission spectroscopy. In this technique an electron is ejected by a first photon from an initial state to an intermediate state, then to a final state by a second photon.

We have recently proposed to use two-photon photoelectron spectroscopy to study semiconductor surfaces and their interfaces with their respective insulators. Our goal is to extract the relevant concepts associated with surface and interface electronic phenomena and to gain a working knowledge of these phenomena, for which there is a real need.

The following is a brief description of our experimental set-up and a report of our progress.

A schematic representation of our experimental set-up is shown below.

EXPERIMENTAL SET-UP

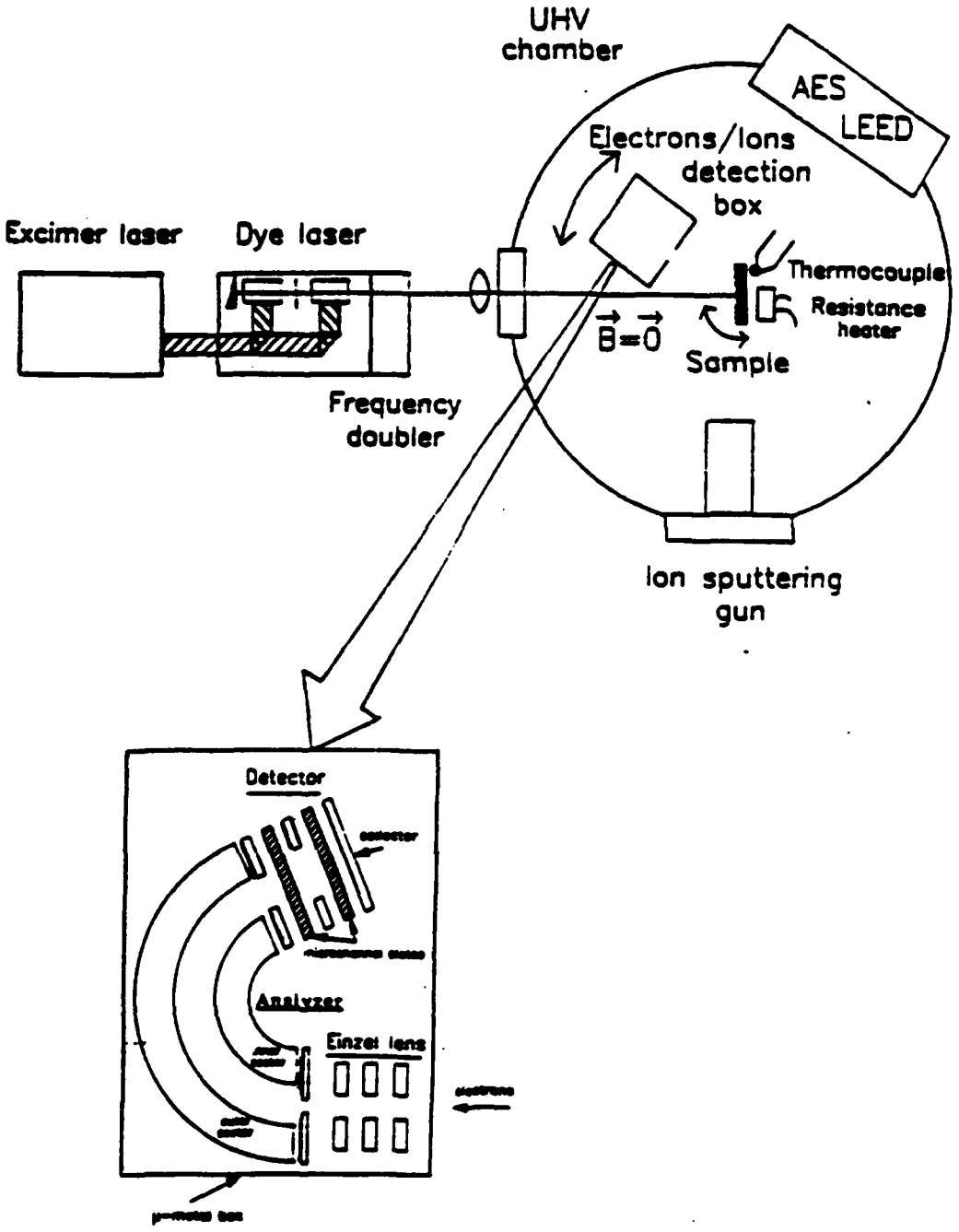

Tunable, pulsed excitation laser radiation is provided by the frequency-doubled output of a dye laser pumped by an excimer laser. Using several sets of dyes the photon energy is tunable from the far infrared to the ultraviolet ranges. The pulses are typically 20 nanoseconds long and can carry 0.1 joules in energy.

The sample sits on a rotatable rod in a vacuum chamber with base pressure less than 10-10 Torr. The rotation of the rod as well as the loading of the sample are made possible, without any venting of the chamber, by a three stage differential pumping unit. The analyzer/detector box is also attached to a rotatable flange. Prior to being studied the sample can be cleaned by repeated cycles of argon ion sputtering and high-temperature annealing. The chemical composition and the atomic structure at the surface of the sample are monitored by Auger spectroscopy (AES) and low energy electron diffraction (LEED).

The weakly focused laser beam impinges on to the sample at an incidence angle of 45°. The photoelectrons emitted are collected by the analyzer within a solid angle of less than 0.002 steradians. When necessary the electrons can be focused on to the analyzer entrance slit by an electrostatic Einzel lens. The analyzer is operated in a constant transmission energy mode, typically 40 electron-volts. The electrons are either accelerated or deccelerated to the transmission energy. The energy resolution is constant and equals 0.4% of the transmission energy, i.e., 150 meV.

The analyzed electrons, at the transmission energy, are then multiplied by a pair of microchannel plates (MCP) in a chevron configuration. This configuration ensures a high gain of about one million, a reduced noise as well as a high saturation level, which is desirable in our pulsed light experiment. Once multiplied by the microchannel plates the electrons are collected by a metallic end-plate collector.

These charges, Q, are analyzed by the following electronics:

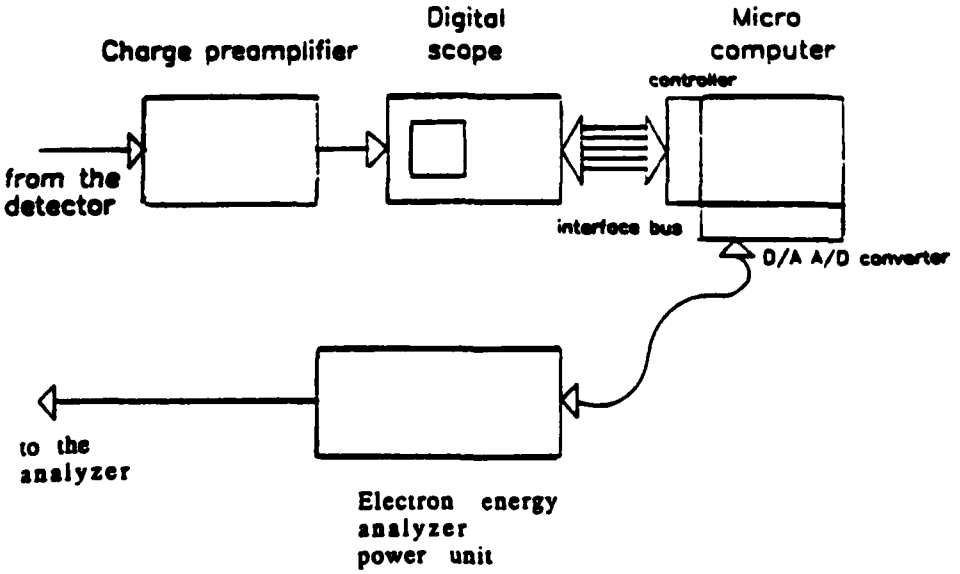

A charge preamplifier transforms the roughly 20 nanoseconds long packet containing the Q charges into a voltage which has a peak directly proportional to Q (0.3 volts per picocoulomb) and then decays on a millisecond scale. A fast digital scope with internal data processing capabilities captures the signal from the preamplifier, digitizes it and transmits the relevant information to the memory of a microcomputer via an interface bus. The microcomputer also controls the digital scope and the electron analyzer power unit which implements the potential differences to be maintained between the different parts of the analyzer.

b. Results

Our initial experiments with the above apparatus were designed to test the sensitivity of the detection system and the control of the dye and pump laser beams. To do this we used a sample of polycrystalline aluminum, a material having the relatively low work function of ~4.1 eV. We irradiated this sample with 43 eV from the doubled-dye laser at an intensity of about 1 MW/cm^2 and measured the energy of the photoelectrons. Photoelectrons were easily seen, and a measurement of the electron energy distribution showed a feature originating from a simple, single-photon emission as well as a feature at higher electron energies which we believe originates from a two-photon process.

The second set of "calibration' experiments involved Si (111). This material has a carefully studied band structure and a clearly delineated method of surface preparation. In addition, Steinmann et. al.[1] and Moison and Bensoussan[2] have made some previous studies of its near threshold-photon emission using various laser sources. Finally, the yield from Si is expected to be low so that the sensitivity of our spectrometer could be tested under more rigourous conditions than for Al.

In this experiment, we used low B-doped (111) oriented material. Since we irradiated it with 4.03 eV light, well below its threshold photon energy of 5.1 eV, the photoemission process involved two-photon emission. A plot of the integrated electron number versus laser intensity is shown in Figure 1. The results show that at low energies (or intensities) photoemission varies linearly with the light intensity. This result may appear unexpected for a two-photon process which might be expected to proceed as the square of the laser intensity, however, it can be shown that it is, in fact, in accord with a sequential two-photon process in which one of the steps has a much larger cross section than the other. At higher intensities in Fig. 1, the linearity is lost at which point space charge limit emission occurs. At still higher energies (inset), linearity is again regained. We believe based on previous experiments, that the space-charge limitation is broken by the onset of positive ions. A major goal of this JSEP project is to understand the effect of

surface preparation on emission of positive ions. This determination will be undertaken in the next several months.

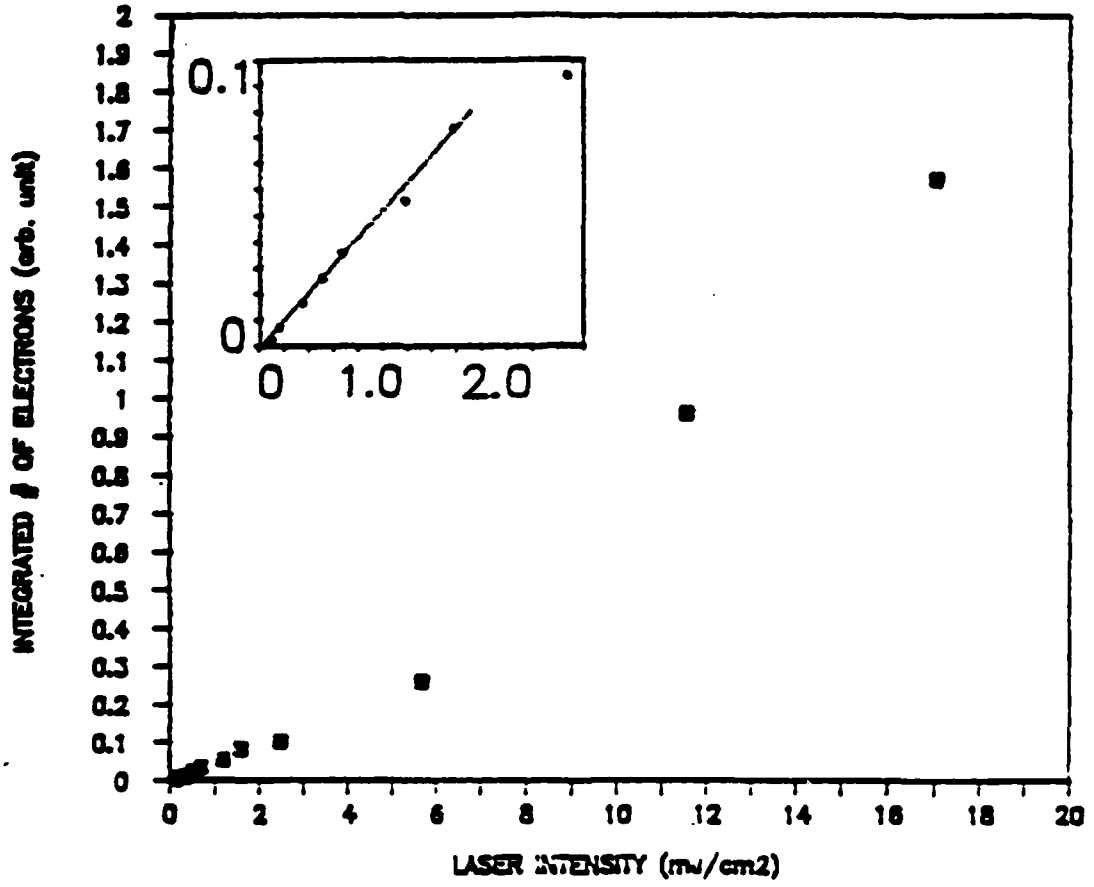

Figure 1. Integrated number of emitted electrons versus laser intensities.

A second experiment which we have begun is to investigate the evolution of space-charge broadening in the electron energy distribution. The experimentally obtained electron distributions are shown in Figure 2 for three different irradiation intensities. ($\theta = 0^0$, 308 nm, Si (111)). The results show that as the electron density increases above the surface, electron-electron collisions broaden the electron distribution and increase the maximum electron kinetic energy. We are analyzing this data and attempting to develop a theoretical treatment.

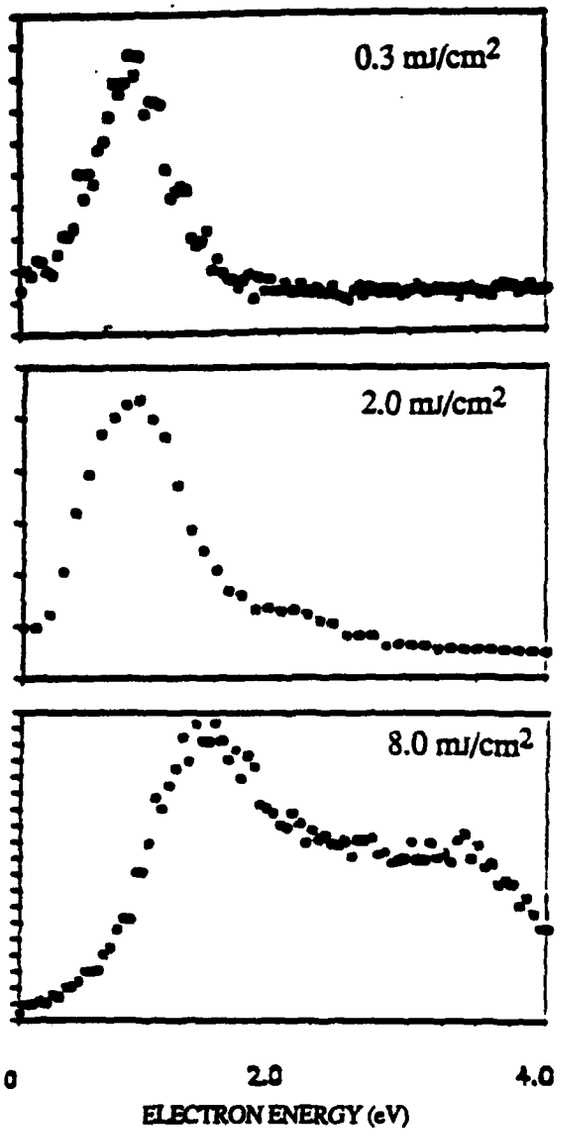

Figure 2. Normalized electron energy distribution curves for different laser intensities. Note the shift in peak energies between different curves, due to a change in contact potential.

c. Future plans

Our current research plan is to first demonstrate good control over semiconductor surface quality, and then begin investigation of two-photon photoemission in compound semiconductors and insulator semiconductor interfaces.

This research was supported by the Joint Services Electronics Program and the instrumentation funded in part by the ARO and by an instrumentation grant from AFOSR.

References

1. W. Steinmann, K. Giesen and F. Have, Ann. Isr. Phys. Soc. 6, 446 (1984).
2. M. Bensoussan and J. M. Moison, Phys. Rev. B 27, 5192 (1983).

D. GENERATION AND DYNAMIC PROPERTIES OF METASTABLE SPECIES FOR QUANTUM ELECTRONICS AND LASER MICROPROCESSING

George Flynn, Principal Investigator (212) 854-4162

Research Area II, Work Unit 4

1. Diode Laser Probing of CO_2 Vibrational Excitation Produced by Collisions with High Energy Electrons from 193nm Excimer Laser Photolysis of Iodine

(Arthur S. Hewitt, Lei Zhu, and George W. Flynn)

a. Introduction

The elucidation of electron-molecule interactions is of fundamental importance in the chemistry and physics of electron-rich environments such as plasmas, discharges, gas discharge lasers, the upper atmosphere, and planetary atmospheres. There have been many studies of direct electron-molecule inelastic scattering as well as of the formation of temporary negative ion states.[1-3] The typical electron scattering experiment consists of energy selected electrons from an electron gun which collide with a molecular beam. The scattered electrons are detected with a rotatable energy analyzer. The energy resolution of these experiments has been limited to ~11.5 meV (~93 cm^{-1}). As a result, the state-selective investigation of molecular rotational excitation by electrons is only possible for electron-H_2/D_2 scattering.[4-7]

The use of narrow bandwidth lasers to produce monoenergetic electrons and to probe the excited species following electron-molecule interaction holds much promise for providing new insights into electron collisions with diatomic and small polyatomic molecules. By varying the pump laser wavelength and the electron precursor, resonances in electron-molecule scattering can be observed.[1] Bergmann, *et al.* have recently used laser-induced fluorescence to probe rotational excitation in sodium dimers from the impact of 150-300 eV electrons produced from an electron gun.[8,9] Diode laser absorption spectroscopy, a super high resolution technique,[10,11] allows the vibrational, rotational, and translational energy of molecules excited by direct electron scattering or produced by decay of temporary negative ion states to be determined.

Due to its importance in CO_2 lasers, electron-CO_2 scattering has been studied in considerable detail by electron energy loss techniques. Each of the fundamental vibrational modes is excited at threshold (*i.e.*, when the translational energy of the electron matches the

vibrational frequency) with a cross section of ~1 $Å^2$.[12,13] Direct inelastic scattering[13,14] and the influence of a virtual state[15-18] are found to contribute to the vibrational excitation of CO_2. However, electron energy loss techniques are not able to resolve various vibrational modes of CO_2. In this report, the first high resolution (0.0003 cm^{-1}) studies of electron-CO_2 scattering are described. Hot electrons, e-*, are produced by I_2 multiphoton ionization (MPI) at 193 nm:

$$I_2 + nh\nu(193\ nm) \rightarrow I_2^+ + e^{-*} \qquad (1)$$

Vibrationally excited CO_2 molecules are then produced by inelastic scattering:

$$e^{-*} + CO_2(00^00;J',V') \rightarrow e^- + CO_2(mn^lp;J,V) \qquad (2)$$

where m, n, and p are the number of quanta of symmetric stretching, bending, and antisymmetric stretching motion; J and l are the rotational and vibrational angular momentum quantum numbers; and V is the velocity of the CO_2 molecule. Time-resolved diode laser absorption spectroscopy is then used to monitor the nascent excited ro-vibrational states populated in the scattering process:

$$CO_2(mn^lp;J,V) + h\nu(\sim 4.3\mu m) \rightarrow CO_2(mn^lp+1;J-1,V) \qquad (3)$$

In addition, time-resolved laser "Doppler spectroscopy" is employed to determine the translational recoil of the CO_2 molecules following a collision. The rotational distribution, transient linewidths, power dependence, and the ratio of the number of vibrationally excited molecules to the number of photons initially absorbed are determined for excitation of the $CO_2(00^01)$ antisymmetric stretching state. Preliminary studies of vibrational excitation into the 00^02, 10^00, 02^00, and 02^20 levels of CO_2 as well as the v=1 level of CO are also discussed here. Electron-CO inelastic scattering is studied with time-resolved diode laser absorption spectroscopy by monitoring transitions of the type:

$$CO(v=1;J,V) + h\nu(\sim 4.7\mu m) \rightarrow CO(v=2;J-1,V) \qquad (4)$$

b. Experimental

The experimental apparatus has been described in detail elsewhere,[19,20] and only a brief summary will be given here. 193 nm pulses from an ArF excimer laser are propagated down a 2.76m sample cell which contains a 1/10 mixture of I_2/CO_2 or I_2/CO at a total pressure of 27.5 mTorr. Tunable cw radiation from a diode laser at ~4.3 μm (to probe CO_2) or ~4.7 μm (to probe CO) is collinearly propagated through the cell with the excimer beam. The diode laser is tuned to various ro-vibrational transitions in CO_2 or CO. Time-resolved changes in the transmitted IR intensity are measured with an InSb detector. The signals are digitized and averaged on a digital oscilloscope and sent to a computer for storage and later analysis. The diode laser modulation, excimer laser firing sequence, and data aquisition are controlled by a PC. For transient linewidth measurements, the diode laser is modulated at ~250 Hz over several linewidths of a specific CO_2 absorption line. The Doppler lineshape is determined by firing the excimer laser at different delay times with respect to the start of the modulation cycle. A Fabry-Perot etalon with a free spectral range of 0.0097 cm^{-1} is used for frequency calibration.

The size of the signals is found to decrease as a function of the number of excimer laser shots due to the build-up of photoproducts on the cell windows and due to the loss of I_2. In order to make accurate relative measurements, an "indicator" line is employed to correct for all these factors. Transient absorption signals are also observed when the diode laser is tuned off-resonance due to thermal lensing and/or schlieren effects. The off-resonance signals are decreased in amplitude relative to the on-resonance signals by using gas mixtures with a low I_2 mole fraction and by careful alignment of the excimer and diode lasers. After realigning the laser beams, if the off-resonance signal is more than 5% of the on-resonance signal, then the off-resonance signal is subtracted from the on-resonance signal.

A capacitance manometer (range: 0-1 Torr) monitors the gas pressure in the sample cell. The CO_2 (Matheson, 99.8%) is freeze-pump-thawed at liquid nitrogen temperatures before preparing a CO_2 bulb. The I_2 crystals (Aldrich, 99.999%) are placed in a gas bulb which is pumped on for several hours before use. 1/10 mixtures of I_2/CO_2 are made by consecutively flowing each gas into the sample cell. Before filling the cell with an I_2/CO_2 gas mixture, the cell is seasoned with ~200 mTorr of I_2 for an hour (the I_2 gas pressure decreases substantially with time when put into a clean cell due to adsorption on the cell walls).

c. Results

(c.1) $CO_2(00^01)$ Antisymmetric Stretch Excitation

A typical time-resolved signal observed while monitoring a specific rotational state of the 00^01 antisymmetric stretching mode of CO_2 is shown in Figure 1. The observed signal exhibits a detector-limited (~700 ns) fast rise corresponding to the direct excitation of $CO_2(00^01,J)$ followed by slow decay due to diffusion of the excited CO_2 molecules out of the diode laser beam path. To obtain the relative nascent rotational distribution of the 00^01 state of CO_2 shown in Figure 2, the fast rise amplitudes are normalized by the excimer and diode laser powers and the fast rise amplitude of the "indicator" line. It is clear from Figure 2 that an approximately room temperature (T=316 K) Boltzmann distribution fits the observed rotational distribution well. The nascent transient linewidths of several $CO_2(00^01,J) \rightarrow CO_2(00^02,J-1)$ transitions are measured following vibrational excitation. The observed linewidths correspond to room temperature Doppler linewidths (Figure 3).

The dependence of the $CO_2(00^01)$ transient absorption signals on excimer laser power is determined by varying the amount of I_2 gas in a 30 cm glass cell placed in the excimer beam path. The excimer laser power dependence of the $CO_2(00^01)$ transient absorption signal is found to be n=2.4±0.5 for excimer fluences from 2-20 mJ cm^{-2}, where the fast rise amplitude is proportional to the excimer intensity to the nth power (Signal proportional to I^n). The ratio of the number of excited $CO_2(00^01)$ molecules to the number of photons absorbed is determined from diode laser and excimer absorption measurements and is found to be $3.8\pm1.1\times10^{-2}$.

(c.2) CO_2 Symmetric Stretch and Bend Excitation

In addition to vibrational excitation of the antisymmetric stretching mode of CO_2, vibrational excitation is also observed for 10^00, 02^00, 02^20. "10^00" and "02^00" are respectively the upper level (1388 cm^{-1}) and the lower(1285.5 cm^{-1}) levels of the Fermi dyad. The 02^20 vibrational state is a "pure" bending mode. Time-resolved signals observed while monitoring specific rotational states of the 10^00, 02^00, and 02^20 vibrational modes of CO_2 are shown in Figure 4. It is found that there is much more excitation into the "10^00" upper level than into the "02^00" lower level. The relative excitation cross section between the upper and lower Fermi mixed levels is determined to be $\pi\sigma^2_{10^00}/\pi\sigma^2_{02^00}=9\pm4$. This is a very surprising result since the vibrational wavefunctions for these states are almost identical due to the Fermi resonance. The excitation cross sections for 10^00 and 02^20 relative to 00^01 are found to be $\pi\sigma^2_{10^00}/\pi\sigma^2_{00^01}=0.7\pm0.3$ and

$\pi\sigma^2_{02^20}/\pi\sigma^2_{00^01}$=0.3±0.2, respectively. The relative excitation cross section data for the 00^01, 10^00, 02^00, and 02^20 vibrational states of CO_2, as well as the v=1 vibrational state of CO, are presented in Table I. Preliminary measurements suggest that the rotational and translational temperatures for all these vibrational states of CO_2 are ~300 K.

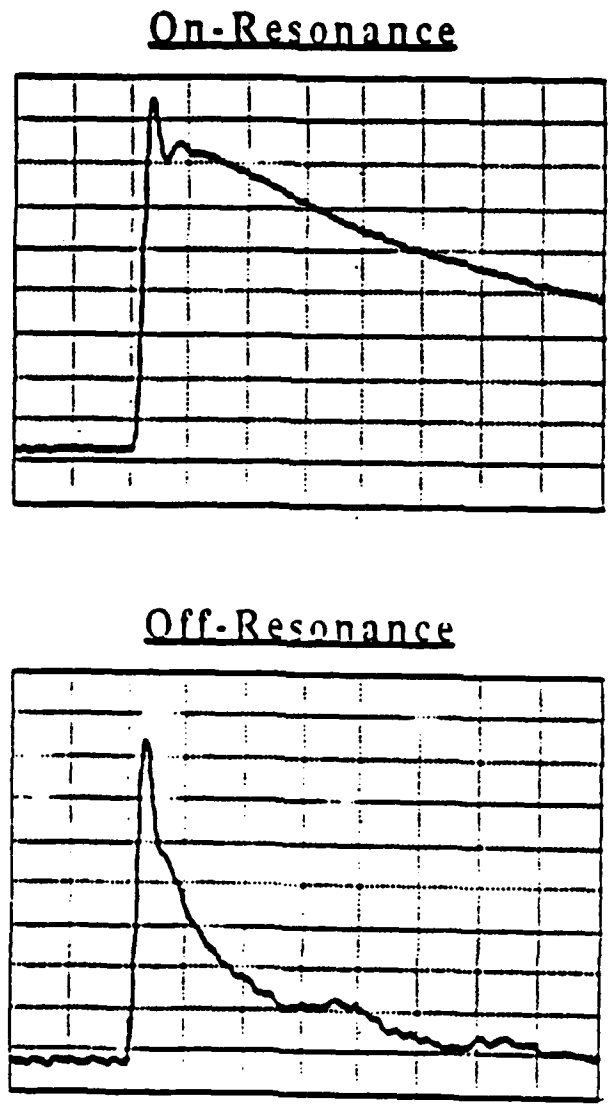

Figure 1: Changes in the absorption of the diode laser probe beam are shown following 193 nm photolysis of I_2 in a 1/10 mixture with CO_2 at a total pressure of 27.5 mTorr. The diode laser monitors the 00^01, J=13→00^02,J=12 ro-vibrational transition of CO_2 in the upper trace. The diode laser is tuned off the absorption line in the lower trace. Each trace is 20 μs full scale. The vertical axes are not scaled relative to one another.

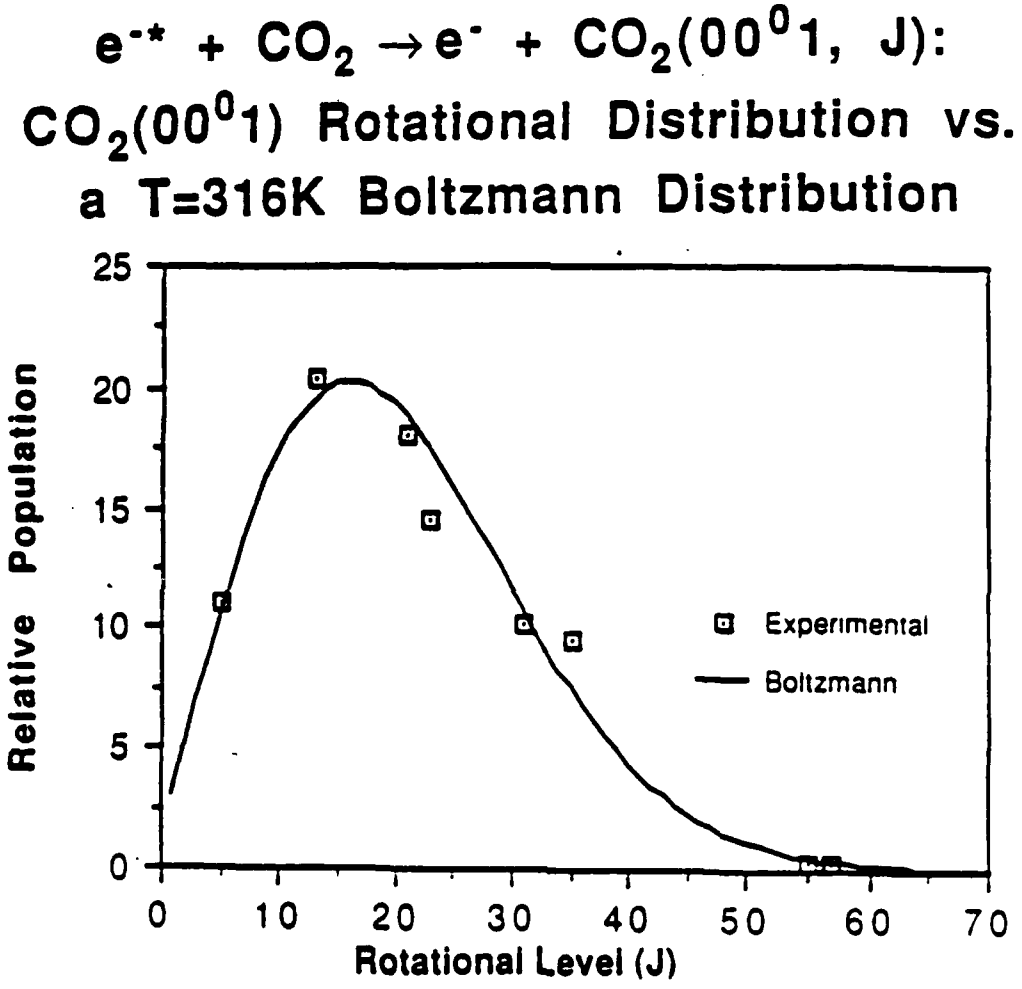

Figure 2: The experimentally determined rotational population distribution of $CO_2(00^01)$ for a 1/10 mixture of I_2 in CO_2 at a total sample pressure of 27.5 mTorr. The squares represent the experimental data points. The solid line represents a 316K Boltzmann distribution.

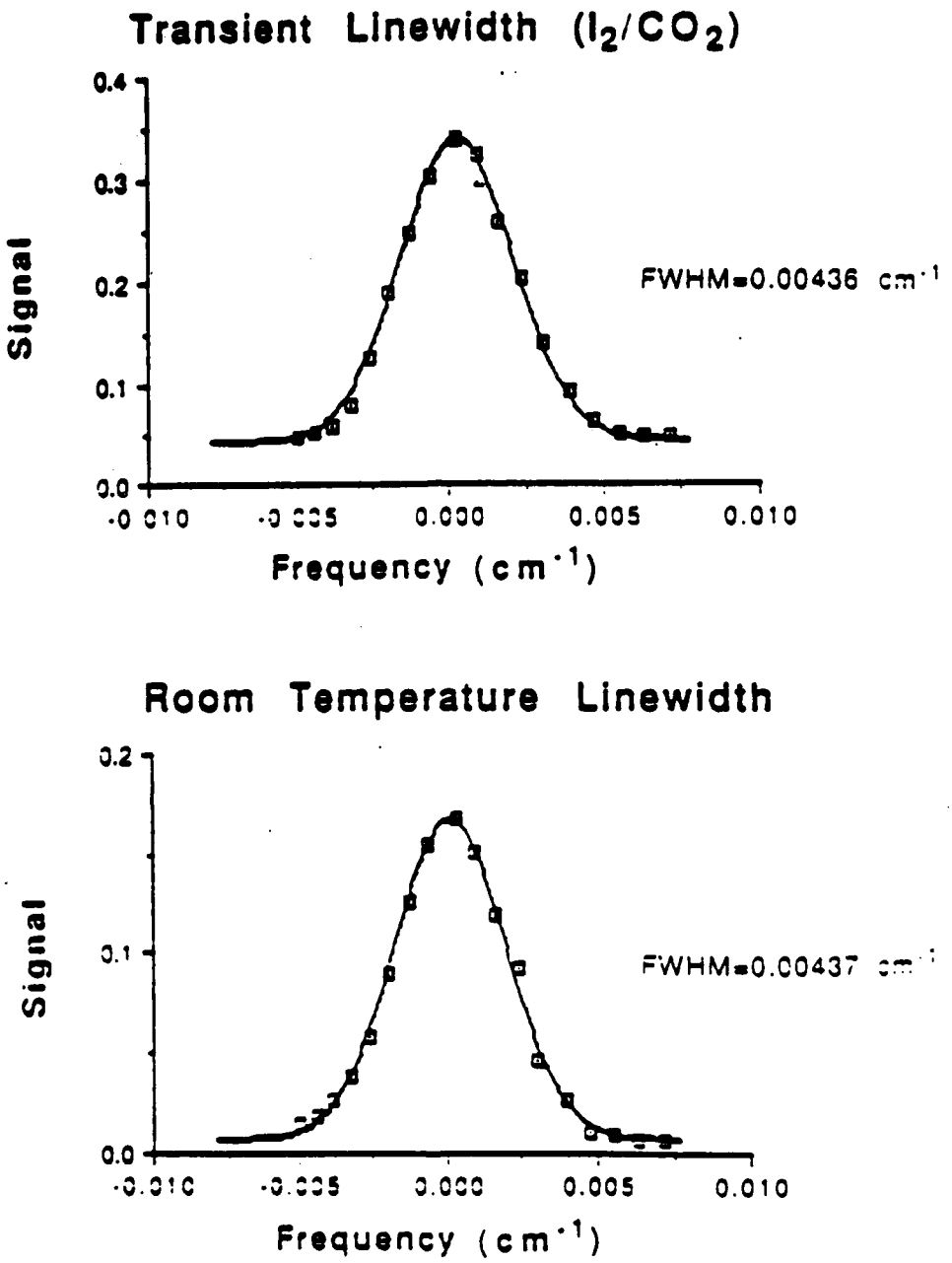

Figure 3: Lineshape profiles for 00^01 P(35) following excimer laser photolysis of I_2. The squares are experimental data: the curves are best fits to a Gaussian lineshape. The upper trace shows the nascent lineshape, 700 ns after the excimer laser fires, before collisional relaxation. The lower trace shows the lineshape 15 μsec after the excimer laser fires, after ~4 gas kinetic collisions. A total pressure of 27.5 mTorr of a 1/10 I_2/CO_2 mixture was employed.

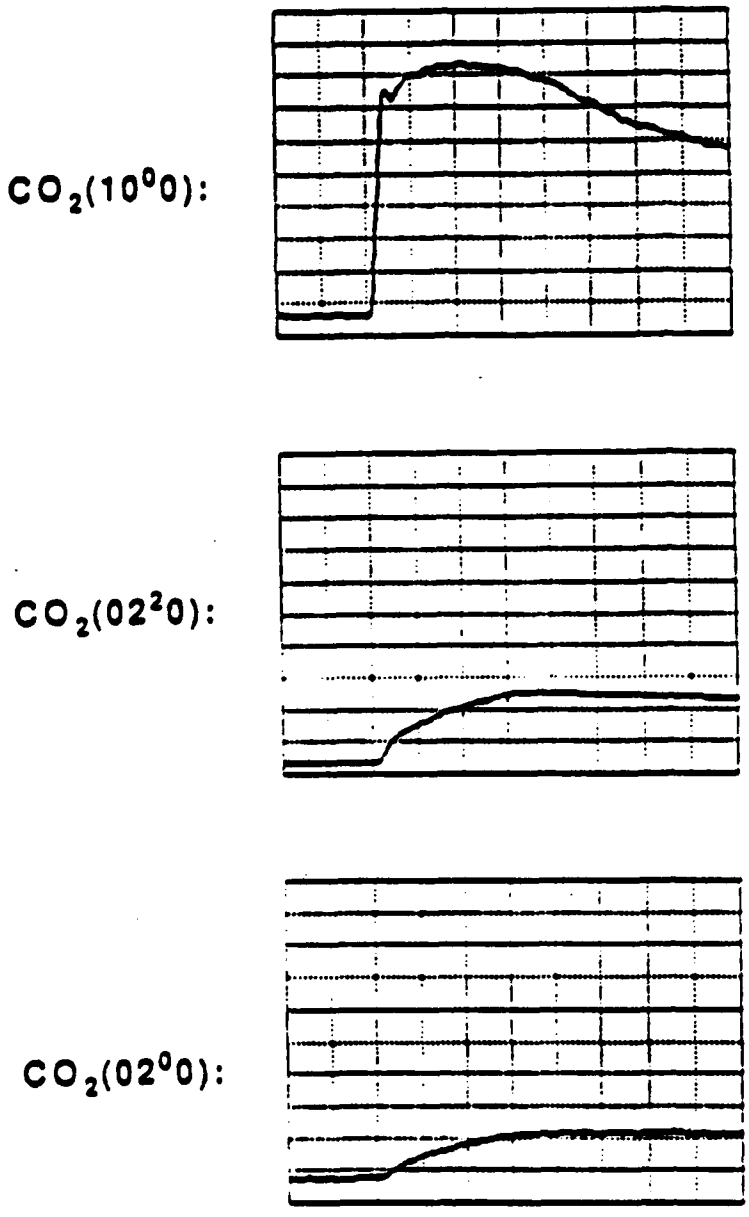

Figure 4: Changes in the absorption of the diode laser probe beam are shown following 193 nm photolysis of I_2 in a 1/10 mixture with CO_2 at a total sample pressure of 27.5 mTorr. The diode laser monitors the 10^00,J=18→10^01,J=17; 02^00,J=18→02^01,J=17; and 02^20,J=15→02^21,J=14 ro-vibrational transitions of CO_2. Each trace is 20 μs full scale. The vertical scales are the same for the three traces.

TABLE I: Excitation of CO_2 and CO vibrational modes by electrons which are produced from excimer laser photolysis of I_2.

Vibrational Excitation Process	Probability
$e^{-*} + CO_2(00^00) \rightarrow e^- + CO_2(00^01)$	1
$e^{-*} + CO_2(00^00) \rightarrow e^- + CO_2(\text{“}10^00\text{”})(\text{Upper})^a$	0.7
$e^{-*} + CO_2(00^00) \rightarrow e^- + CO_2(\text{“}02^00\text{”})(\text{Lower})^a$	0.08
$e^{-*} + CO_2(00^00) \rightarrow e^- + CO_2(02^20)$	0.3
$e^{-*} + CO(v=0) \rightarrow e^- + CO(v=1)$	1.1

[a]The “10^00” and “02^00” refer to the upper and lower Fermi mixed symmetric stretch/overtone bend states.

(c.3) CO(v=1) Stretch Excitation

Transient absorption signals are also measured for 1/10 mixtures of I_2/CO. By repeatedly switching back and forth between a CO_2 diode and CO diode, the cross section for excitation of CO_2 00^01 P(17) relative to CO v=1 P(16) is found to be 1.3±0.6. Assuming that the rotational distributions and transient linewidths of CO(v=1) are room temperature Boltzmann, the relative excitation cross section is found to be $\pi\sigma^2_{CO_2(00^01)}/\pi\sigma^2_{CO(v=1)}$=0.9±0.4. In addition, there is clear evidence that CO is being produced in the cell from I_2/ω_2 mixtures; *frequency-resolved* diode laser absorption shows that the CO v=0 P(22) absorption line increases with the number of excimer laser shots fired into the sample cell.

d. Discussion

Electron-CO_2 scattering appears to hold the most promise for explaining the above experimental results. The negligible translational and rotational momentum transfer to CO_2 during electron-CO_2 collisions can be explained as a result of the small mass of the electron. The relative vibrational excitation cross sections are also consistent with an electron excitation mechanism, though it may appear at first glance that the present relative excitation cross section results are inconsistent with an electron scattering process. From a simple perturbation argument, it is expected that electrons will collisionally excite the 00^01 antisymmetric stretching mode but not the 10^00 symmetric stretch/bend mode of CO_2. The fast electrons will weakly interact with CO_2, and the vibrational excitation cross sections will scale as the radiative oscillator strength.[21] In other words, the fast electron appears to the molecule to be a time dependent electric field. However, the cross sections for vibrational excitation of $CO_2(00^01)$ and $CO_2(10^00)$, as well as CO(v=1), by low energy electron scattering have been determined in electron energy loss experiments to be similar (~1 $Å^2$).[12, 13, 22, 23] Thus, the relative cross sections measured in this study are consistent with an electron excitation mechanism. For electron kinetic energies below ~10 eV, the molecular electrons can no longer be considered to be motionless during the interaction time.[21, 24-25] At these low energies, the molecular electrons respond to the approaching electron, creating an induced dipole. Furthermore, when resonances occur, the free electron is temporarily bound on a timescale of the same order of magnitude as molecular vibrations.[26] Consequently, the electron scattering process cannot be considered a weak interaction. The strong electron-molecule interaction may lead to a breaking of the Fermi resonance and subsequent preferential excitation of the 10^00 upper level of the Fermi dyad.

At present, all our experimental evidence is in accord with an electron scattering excitation mechanism; however, it is not possible at present to make quantitative comparisons with previous electron-CO_2 studies because the electron velocity, number density, and quenching mechanisms are not yet accurately known. Due to the uncertainties in the 193 nm multiphoton ionization of I_2 and the complexity of the electron-CO_2 interaction, further experimental evidence is required before it can be definitively stated that the observed vibrational excitation is due to electron-CO_2 scattering. Experiments are presently under way to determine the relative cross sections, transient linewidths, and rotational profiles of various other modes of CO_2 (E.A.≈-0.6eV)[27] and CO (E.A.≈ -1.3eV).[2] In addition, other small polyatomic molecules can be probed such as CS_2 (E.A.≈+0.7eV)[28] or OCS (E.A.≈+0.5eV)[28] in order to determine the dependence of the vibrational excitation on the electron affinity. The production of electrons with well-defined

kinetic energies, such as from ionization of cesium,[29,30] would allow a much better comparison with electron energy loss data.

A key and novel feature of these experiments is the resolution, $0.0003cm^{-1}$ or approximately $4X10^{-8}$ eV! This compares with standard electron scattering experiments which have a typical energy resolution of about 80 cm^{-1} or 10 meV. The high resolution is, of course, obtained by observing the molecular collision partner rather than the scattered electron as is normal in most electron scattering experiments. Such studies can provide fundamental insight into the mechanisms and processes which are important in plasma etching reactors. Considerable interest in this technique has been exhibited by scientists working on plasma etching diagnostics at the IBM East Fishkill facility.

This work was supported by the Joint Services Electronic Program, the National Science Foundation and the Office of Naval Research.

References

1. S.C. Brown, Electron-Molecule Scattering (Wiley, New York, 1980).
2. L.G. Christophorou, Electron-Molecule Interactions and their Applications (Academic Press, New York, 1984).
3. G.J. Schulz, Rev. Mod. Phys. **45**, 423 (1973).
4. E.S. Chang and S.-F. Wong, Phys. Rev. Lett. **38**, 1327 (1977).
5. S.F. Wong and G.J. Schulz, Phys. Rev. Lett. **32**, 1089 (1974).
6. G. Joyez, J. Comer, and F.H. Read, J. Phys. B**6**, 2427 (1973).
7. F. Linder and H. Schmidt, Z. Naturforsch **26a**, 1603 (1971).
8. G. Ziegler, S.V.K. Kumar, P. Dittmann, and K. Bergmann, Z. Phys. D**10**, 247 (1988).
9. G. Ziegler, M. Radle, O. Putz, K. Jung, H. Ehrhardt, and K. Bergmann, Phys. Rev. Lett. **58**, 2642 (1987).
10. J. O. Chu, C. F. Wood, G. W. Flynn, and R. E. Weston, Jr., J. Chem. Phys. **80**, 1703 (1984).
11. J. O. Chu, C. F. Wood, G. W. Flynn, and R. E. Weston, Jr., J. Chem. Phys. **81**, 5533 (1984).
12. J.J. Lowke, A.V. Phelps, and B.W. Irwin, J. Appl. Phys. **44**, 4664 (1973).
13. A. Stamatovic and G.J. Schulz, Phys. Rev. **188**, 213 (1969).
14. C.R. Claydon, G.A. Segal, and H.S. Taylor, J. Chem. Phys. **52**, 3387 (1970).
15. K.-H. Kochem, W. Sohn, N. Hebel, K. Jung, and H. Erhardt, J. Phys. B**18**, 4455 (1985).
16. M.A. Morrison, Phys. Rev. A**25**, 1445 (1982).

17. J. Ferch, C. Masche, and W. Raith, J. Phys. B14, L97 (1981).
18. M.A. Morrison and N.F. Lane, Chem. Phys. Lett. 66, 527 (1979).
19. J. A. O'Neill, C. X. Wang, J. Y. Cai, G. W. Flynn, and R. E. Weston, Jr., J. Chem. Phys. 88, 6240 (1988); 85, 4195 (1986).
20. J. A. O'Neill, J. Y. Cai, G. W. Flynn, and R. E. Weston, Jr., J. Chem. Phys. 84, 50 (1986).
21. N.F. Lane, Rev. Mod. Phys. 52, 29 (1980).
22. G.J. Schulz, Phys. Rev. A135, A988 (1964).
23. H. Ehrhardt, L. Langhans, F. Linder, and H.S. Taylor, Phys. Rev. 173, 222 (1968).
24. M.A. Morrison, Aust. J. Phys. 36, 239 (1983).
25. Y. Itikawa, Phys. Rev. A3, 831 (1971).
26. M.J.W. Boness and G.J. Schulz, Phys. Rev. A9, 1969 (1974).
27. R.N. Compton, P.W. Reinhardt, and C.D. Cooper, J. Chem. Phys. 63, 3821 (1975).
28. P.S. Drzaic, J. Marks, and J.I. Brauman, Gas Phase Ion Chemistry, Vol. 3 (ed. by M.T. Bowers), Academic Press, New York, 1979, p. 200.
29. C.D. Cooper and R.N. Compton, J. Chem. Phys. 59, 3550 (1973).
30. C.D. Cooper and R.N. Compton, Chem. Phys. Lett. 14, 29 (1972).

2. Chemical Dynamics of the Reaction Between Chlorine Atoms and Deuterated Cyclohexane

(J. F. Hershberger, J. M. Hossenlopp, Y. Lee, and G. W. Flynn)

a. Introduction

Product energy disposal in chemical reactions has been widely studied both experimentally and theoretically.[1] Modern laser spectroscopic techniques allow the determination of both rotational and vibrational quantum states of nascent product molecules, while molecular beam experiments provide information on angular and translational energy distributions. Reactions of chlorine atoms have important applications in atmospheric chemistry,[2,3] in chemical etching of surfaces,[4] and in organic chemistry.[5] We report here the spectroscopic observation of vibrationally and rotationally cold, but translationally hot DCl molecules produced by the reaction of chlorine atoms with deuterated cyclohexane.

b. Experimental

The experimental method employs an excimer laser as pump and an infrared diode laser as probe. Details have been described previously.[6,7] Briefly, chlorine atoms are produced by excimer laser photolysis of S_2Cl_2 precursor molecules:

$$S_2Cl_2 + h\nu\ (248\ nm) \rightarrow Cl + \text{other products} \qquad (1)$$

This precursor produces a mixture of 78% ground state $^2P_{3/2}$ and 22% excited state $^2P_{1/2}$ Cl atoms[8] with an average translational energy estimated to be approximately 9.2 kcal/mole (0.4 eV).[7] the chlorine atoms then react with C_6D_{12} to form DCl:

$$Cl + C_6D_{12} \rightarrow C_6D_{11} + DCl \qquad (2)$$

The rate constant for the corresponding hydrogen atom reaction is 3.1×10^{-10} cm^3-$molec^{-1}$-sec^{-1} at room temperature.[3] DCl products are probed by time-resolved infrared absorption spectroscopy with a high resolution ($\sim$0.0003 cm^{-1}) lead-salt tunable diode laser:

$$DCl(v,J,V) + h\nu\ (\sim 4.9\mu m) \rightarrow DCl(v\pm1,J\pm1,V) \qquad (3)$$

where v,J, and V are the vibrational quantum number, rotational quantum number, and translational velocity, respectively. The excimer and diode laser light were made collinear by a dichroic beamsplitter and passed through a 2-meter absorption cell containing 30 mtorr of a flowing 1:1 mixture of S_2Cl_2 and C_6D_{12}. Excimer laser repetition rates were kept low (0.05-0.1 Hz) to allow product DCl molecules to be pumped out of the reaction cell between laser shots. Transient changes in infrared absorption were measured by an InSb detector, amplified, and signal averaged on a digital oscilloscope.[6]

c. Results

When the diode laser was tuned to a DCl v=0 absorption line, large transient signals were observed. At the low pressures used, the time between gas kinetic collisions is roughly 3-3.5 μsec, slower than the observed rise times of 1.5 μsec, and much slower than the detector response time of ~700 nsec. Thus the observed transients are due to direct production of nascent, unrelaxed DCl by reaction (2). Much smaller signals were observed when probing DCl v=1 lines, indicating that 90% of the products are formed in the vibrational ground state.

The signal amplitudes for different rotational levels of the vibrational ground state were measured at t=700 nsec after the excimer pulse. These data were normalized by diode laser power and relative transition matrix elements[9] to obtain the rotational distribution shown in figure 1(a). The best fit to a Boltzmann distribution gives a temperature of T_{Rot}=135°K. An average of several experimental runs provides the value T_{Rot}=156±35 °K. In addition, transient Doppler lineshape profiles were measured by taking absorption signals while the diode laser was slowly scanned over an absorption line. The lineshape is shown in figure 1(b) for the v=0 P(2) line. The lineshape was well fitted to a Gaussian profile with full width at half maximum (FWHM)=0.0092±0.001 cm^{-1}, which corresponds to a temperature of T_{Trans}=1420±300 °K. An average of several runs provides the value T_{Trans}=1290±300 °K. The linewidth for the v=0,P(5) line was found to be identical within experimental error to that of v=0,P(2).

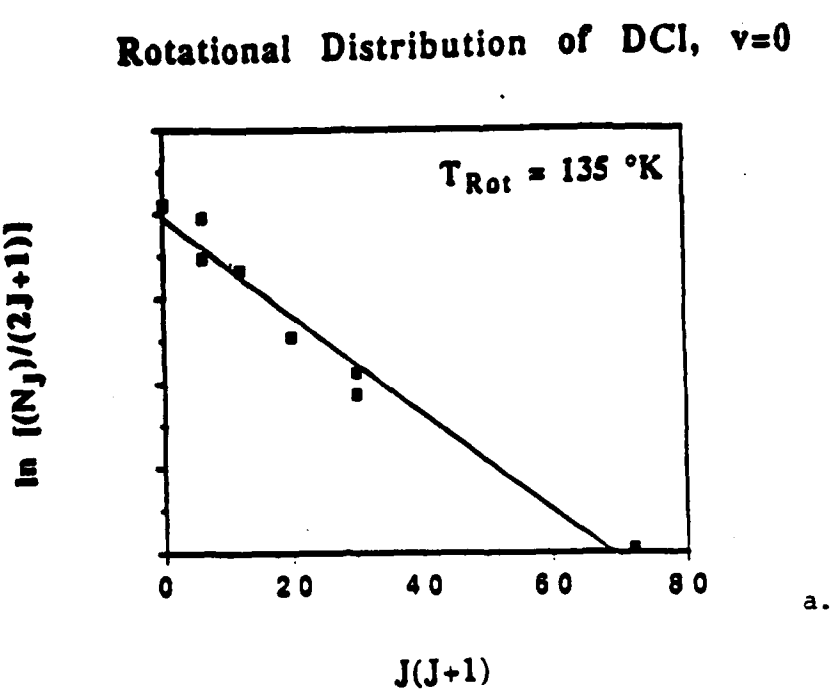

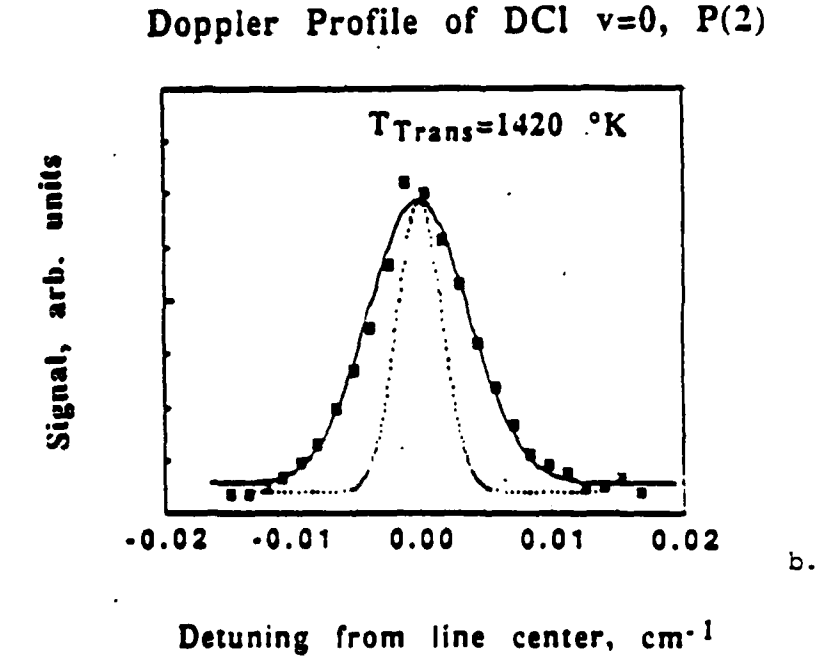

Figure 1. a: Boltzmann plot of the nascent rotational distribution of DCl (v=0) produced by reaction (2). The line is a best fit to a rotational temperature of 135 °K. b: Nascent Doppler lineshape of the DCl v=0 P(2) line. The solid line is a best fit to a Gaussian lineshape. The fitted full width at half maximum (FWHM) is 0.0092 cm^{-1}, which corresponds to a translational temperature of 1420 °K. The room temperature lineshape (FWHM=0.0042 cm^{-1}) is shown for comparison as a dotted line.

d. Discussion

These results clearly represent nonstatistical partitioning of energy into rotationally cold, but translationally hot DCl molecules. This reaction has an exothermicity of 7.9 kcal/mole, with an activation energy estimated at less than 0.5 kcal/mole by comparison with the reaction of Cl with C_5D_{10}.[10] The Cl atom reagent translational energy of 9.2 kcal/mole is easily enough to overcome the activation barrier. The energy available to the reaction products is therefore roughly E_T (Cl) - ΔH = 17.1 kcal/mole, neglecting C_6D_{12} internal energy and Cl atom spin-orbit energy. DCl product rotation accounts for only a fraction f_R (DCl) = 0.02 of the available energy. The fraction in DCl translation is f_T (DCl) = 0.26, determined from the linewidth data. Momentum conservation allows a rough estimate of $f_T(C_6D_{11}) = 0.10$, leaving $f_I = 0.62$ left for internal motion of C_6D_{11} radical. The collision thus appears to be too short-lived to allow energy randomization of internal and translational degrees of freedom. These results strongly suggest a direct abstraction mechanism with a collinear C····D····Cl recoil geometry. The Cl atom does not necessarily have to approach in a linear configuration; even with non-collinear approach, a very small motion of the light D atom can produce a collinear transition state which then rapidly falls apart. The departing DCl products move rapidly away with minimal torque being exerted by the large cyclohexyl radical. Alignment effects such as this have been predicted in trajectory calculations on simple systems.[11] Furthermore, similarly cold rotational distributions have been previously observed in hydrogen abstraction reactions of $O(^3P)$ with hydrocarbons.[12] A mechanism in which Cl inserts between C and D would be expected to produce low rotational excitation in DCl even for a nonlinear C····D····Cl geometry; however, such a mechanism is expected to have a high barrier and therefore to be unimportant in the present study. If the collinear hypothesis is correct, a molecular beam experiment should show predominantly backward scattering in the DCl product.

The observation of such a simple mechanism for a reaction between a large gas phase molecule and an atom raises the question as to whether reactions between atoms and thin film surface polymers might also exhibit similar behavior. Efforts to answer this and other questions regarding the reactivity of Cl atoms are continuing in our laboratory.

This work was supported by the Joint Services Electronics Program, the National Science Foundation , the Department of Energy, and the Office of Naval Research.

References

1. Robinson, G. N.; Continetti, R. E.; Lee, Y. T. *J. Chem. Phys.* **1988**, *89*. 6226. Schmatjlo, K. J. and Wolfrum, J. *Ber. Bunsenges. Phys. Chem.* **1978**, *82*, 419/ Kruus, E. J.; Niefer, B. I.; Sloan, J. J. *J. Chem. Phys.* **1988**, *88*, 985. Aker, P.M., Germann, G. J., Valentini, J. J. *J. Chem. Phys.* **1989**, *90*,4795. Häusler, D.; Rice, J.;Wittig, C. *J. Phys. Chem.* **1987**, *91*, 5413. Rakestraw, D. J.; McKendrick, K. G.; Zare, R. N. *J. Chem. Phys.* **1987**, *87*, 7341.
2. Molina, M. J.; Rowland, F. S. *Nature* **1974**, *249*, 810.
3. Atkinson, R.; Aschmann, S. M. *Int. J. Chem. Kinet.* **1985**, *17*, 33.
4. Danner, D. A.; Hess, D. W. *J. Appl. Phys.* **1986**, *59*, 940. Ritsko, J. J.; Ho, F.; Jurst, J. *Appl. Phys. Lett.* **1988**, *53*, 79. Wormhoudt, J.; Stanton, A. C.; Richards, A. D.; Swain, H. H. *J. Appl. Phys.* **1987**, *61*, 142.
5. Breslow, R.; Brandl, M.; Hunger, J.; Turro, N.; Cassidy, K.; Krogh-Jespersen, K.; Westbrook, J. J. *Am. Chem. Soc.* **1987**, *109*, 1205.
6. O'Neill, J. A.; Cai, J. Y.; Wang, C. X.; Flynn, G. W.; and Weston, R. Jr. *J. Chem. Phys.* **1988**, *88*, 6240. Hershberger, J. F.; Chou, J. Z.; Flynn, G. W.; Weston, R. E. Jr. *Chem. Phys. Lett.* **1988**, *149*, 51; Hossenlopp, J. M.; Hershberger, J. F.; Flynn, G. W., submitted to *J. Phys. Chem.*
7. Hershberger, J. F.; Hewitt, S. A.; Sarkar, S. K.; Flynn, G. W.; Weston R. E. Jr. *J. Chem. Phys.*, in press.
8. Tiemann, E.; Kanamori, H.; Hirota, E. *Annual Review*, Institute for Molecular Science, Okazaki, Japan **1988**, 37.
9. Oba, D.; Agrawalla, B. S.; Setser, D. W. *J. Quant. Spectrosc. Radiat. Transfer* **1985**, *34*, 283.
10. Davis, D. D.; Braun, W.; Bass, A. M. *Int. J. Chem. Kinet.* **1970**, *2*, 101
11. Kornweitz, H.; Persky, A. *Chem Phys.* **1989**, *132*, 153. Mayne, H. R. *J. Chem. Phys.* **1980**, *73*, 217. Tan, K. G.; Laidler, K. J.; Wright, J. S. *J. Chem. Phys.* **1977**, *67*, 5883.
12. Andersen, P.; Luntz, A. C. **J. Chem. Phys. 1980**, *72*, 5842. Luntz, A. C.; Andersen, P. *J. Chem. Phys.* **1980**, *72*, 5851. Kleinrmanns, K.; Luntz, A. C. *J. Chem. Phys.* **1982**, *77*, 3533.

3. Diode Laser Probe of Vibrational, Rotational, and Translational Excitation of CO_2 following Collisions with $O(^1D)$: I. Inelastic Scattering

Lei Zhu, Thomas G. Kreutz, A. Scott Hewitt, and George W. Flynn
Department of Chemistry and Columbia Radiation Laboratory, Columbia University, New York, NY 10027

Time domain diode laser absorption spectroscopy has been used to obtain detailed information about state-specific energy deposition in the vibrational, rotational, and translational degrees of freedom of CO_2 following the 248 nm photolysis of a low pressure mixture of CO_2 and ozone. Nascent rotational population distributions have been measured in a number of low-lying CO_2 vibrational levels, including 00^00, 01^10, 02^20, 02^00, 03^30, 10^00, and 00^01. In addition, measurements of CO_2 translational excitation have been obtained for most of these ro-vibrational states. The results suggest that the observed absorption signals arise *only* from T→VRT inelastic scattering between CO_2 and the translationally hot $O(^1D)$ and $O_2(^1\Delta)$ photofragments rather than from E→VRT electronic quenching of $O(^1D)$ to $O(^3P)$ by collisions with CO_2. New evidence suggests that the latter process [$O(^1D)$ deactivation] deposits energy primarily into the CO_2 rotational and translational - *not* vibrational - degrees of freedom. This finding has important implications about the nature of the electronic deactivation process and the presence (or absence) of an intermediate CO_3 complex.

I. INTRODUCTION

The first electronically excited state of atomic oxygen, $O(^1D)$, plays an important role as an intermediate in radiative and photochemical systems, in the chemistry of the earth's stratosphere, and in the chemistry of planetary atmospheres. Since this state is optically metastable (τ_{rad}=140 s for the magnetic-dipole allowed transition $^1D \rightarrow {}^3P$ at 630 nm[1]), $O(^1D)$ may undergo many encounters with atmospheric molecules before relaxing radiatively to the ground state. Typically, the deactivation of $O(^1D)$ to the ground electronic state $O(^3P)$ by collisions with atmospheric species is quite fast, requiring from 1-10 gas kinetic collisions.[2] As a result, molecular collisions are expected to be the most important route for deactivation of $O(^1D)$.

There have been a large number of studies of the quenching of $O(^1D)$ by diatomic and polyatomic molecules.[2-12] The rate of depletion of $O(^1D)$ atoms has been detected either by measuring the weak $O(^1D) \rightarrow O(^3P)$ emission at 630 nm[6-8] or by monitoring the atomic absorption spectrum of the ground state oxygen atom.[4,5,9] However, very little is known about the specific vibrational states of the quencher molecules into which the electronic energy of $O(^1D)$ is channeled during the deactivation process. Such state specific information can provide insight into the nature of the potential energy surfaces involved and the mechanism of the quenching processes. Although theoretical models of E→V transfer have become quite sophisticated,[13-18] state specific experimental information which can be used to test these theories is scarce and usually limited to diatomic molecules. Polyatomic molecules, which have more than one vibrational degree of freedom, can provide additional information about these quenching processes and can therefore serve as a more accurate test of the theories used in describing these phenomena.

The deactivation of $O(^1D)$ to $O(^3P)$ by collisions with CO_2:

$$O(^1D)+CO_2(^1\Sigma) \rightarrow O(^3P)+CO_2(^1\Sigma)^* ,$$

(where '*' indicates CO_2 vibrational, rotational and translational excitation) is an important quenching process about which relatively little is known. Numerous experimental investigations have shown that the quenching rate is extremely fast, occurring in approximately 1-3 gas kinetic collisions.[2,5,6] The high efficiency of this spin forbidden deactivation process has been attributed to the formation of an intermediate CO_3 complex in the bound region of a singlet surface. If the configuration space accessible to such a complex includes a region where crossing to a triplet surface can occur, multiple passes through this region during the lifetime of the complex should eventually lead to a crossing to the triplet surface yielding $O(^3P)$ and CO_2.[19] The most direct evidence for the existence of a CO_3 complex in the quenching process comes from isotope exchange reactions of $O(^1D)$ with CO_2.[20-22] Further evidence comes from matrix isolation experiments in which an infrared spectrum assigned to CO_3 was observed following ultraviolet photolysis of a solid CO_2 and O_3 mixture.[22,23] Theoretical studies of the geometry and electronic structure of CO_3 seem to favor a planar structure, with either C_{2v} or D_{3h} geometry.[24-30] On the other hand, there have been many studies which do not invoke a CO_3 intermediate.[31-33] Clearly, further investigation is necessary to understand the mechanism of this deactivation process.

This work represents the first high resolution study of translationally, rotationally, and vibrationally state-specific energy deposition in the CO_2 molecule following collisional quenching of $O(^1D)$. We report nascent rotational distributions for a number of low-lying vibrational levels (00^00, 01^10, 02^20, 02^00, 03^30, 10^00, and 00^01) as well as measurements of CO_2 translational excitation in each of these ro-vibrational states. The basic experimental approach is described in the following equations.

$$O_3+h\nu(248\text{ nm}) \rightarrow O_2(^1\Delta)+O(^1D)$$

$$O(^1D)+CO_2 \rightarrow O(^3P)+CO_2(mn^lp, J)$$

$$CO_2(mn^lp, J)+h\nu(\sim 4.3\ \mu\text{m}) \rightarrow CO_2(mn^lp+1, J\pm 1).$$

$O(^1D)$ atoms are produced in a mixture of O_3 and CO_2 by the excimer laser photolysis of O_3 at 248 nm. The $O(^1D)$ atoms are collisionally quenched by CO_2 to produce ro-vibrationally excited $CO_2(mn^lp,J)$, where m, n, and p are (respectively) the quantum numbers for the symmetric stretching (ν_1), bending (ν_2), and antisymmetric stretching (ν_3) vibrational modes; J and l denote respectively the rotational and vibrational angular momentum quantum numbers. A high resolution, cw diode laser is used to probe specific ro-vibrational states of CO_2 molecules via absorption in the strongly allowed ν_3 band. Due to the anharmonicities in CO_2 and the high resolution (~0.0003 cm^{-1}) of the diode laser, the IR absorption lines are easily resolved. Virtually *all* low lying ro-vibrational states of CO_2 can be probed using this method. In addition, the sub-Doppler resolution of the diode laser can be used to obtain the transient (nascent) absorption line profile, thus providing information about translational excitation in the CO_2 molecules.

Energy can be deposited into the internal degrees of freedom of CO_2 via two separate mechanisms, 1) electronic quenching (chemical and/or physical) of the $O(^1D)$ to $O(^3P)$, labelled here as the "E→VRT" process:

$$CO_2+O(^1D) \rightarrow CO_2(mn^lp;J,V)+O(^3P) \qquad (E\rightarrow VRT)$$

and 2) inelastic scattering between CO_2 and the translationally excited photofragments, *i.e.* "T→VRT" excitation:

* As an experiment in this section, we are attempting a different format for our report which enables us to present a more complete picture of our experimental work.

$$CO_2+O^*(^1D) \rightarrow CO_2(mnlp;J,V)+O(^1D) \quad (T\rightarrow VRT)$$

$$CO_2+O_2^*(^1\Delta) \rightarrow CO_2(mnlp;J,V)+O_2(^1\Delta) \quad (T\rightarrow VRT)$$

where '*' indicates translational excitation. In the first (E→VRT) process, the 1.97 eV electronic energy is available to the internal degrees of freedom of CO_2. In the second process, photodissociation provides 1 eV of translational energy to the O and O_2 fragments (split 67% and 33% respectively), which is available for T→VRT excitation of CO_2. In addition to the two excitation processes above, Valentini *et al.*[36] and Sparks *et al.*[37] have shown that in the photodissociation of O_3 at 266 nm, approximately 40% of the $O_2(^1\Delta)$ fragments are produced with vibrational excitation, suggesting the potential for vibration-to-vibration (V→V) energy transfer from $O_2(^1\Delta)^*$ to CO_2. The 3 eV total energy available to CO_2 is enough to excite, for example, 10 ν_3 or 36 ν_2 vibrational quanta, but is insufficient to promote CO_2 into an electronically excited level. The reactive channel producing O_2+CO accounts for less than 0.2% of all collisions.[34,35] Both the E→VRT and T→VRT processes are energetic and fast, requiring only a few gas kinetic collisions. As a result of their similar time scales, their effects are hard to separate experimentally. One method used here to selectively identify the effects of the T→VRT channel involves measuring nascent populations and line widths at a low gas temperature of 223 K, which significantly alters the initial rotational and vibrational state populations of CO_2. This procedure is likely to perturb the outcome of T→VRT inelastic scattering, but is not expected to have a significant effect upon a highly energetic and strongly coupled process like electronic quenching of $O(^1D)$.

II. EXPERIMENTAL

The excimer laser photolysis/diode laser probe double resonance apparatus has been described in detail elsewhere[38-42] and will be outlined here only briefly. An excimer laser operating at 248 nm provides a ~50 mJ photolysis pulse which is directed through a 3 m long sample cell containing a flowing mixture of O_3 and CO_2. The cw infrared radiation (at ~ 4.3 μm) from a tunable diode laser is propagated through the sample cell collinearly with the photolysis beam. During the course of a typical experiment, the frequency of the diode laser is locked to the center of a particular CO_2 absorption line. Temporal changes in the transmitted intensity of the IR probe beam after the photolysis pulse are detected with a cooled (77 K) InSb detector. The time-domain signals are digitized and averaged on a Lecroy 9400 digital oscilloscope and analyzed on an IBM PS/2 microcomputer.

In addition to room temperature measurements, the experiment was also repeated at low temperatures to alter the initial rotational and vibrational Boltzmann distributions of the CO_2. In these experiments, the gas mixture flows through a 3 m long pyrex cell which is cooled by circulating chilled methanol through an outer jacket. The temperature of the cell wall is maintained at 223 K, as determined by an iron-constantan thermocouple and verified spectroscopically.[42] In low pressure experiments (*e.g.* 50 mTorr total pressure), the sample pressure was determined spectroscopically in order to avoid systematic errors and those arising from thermal transpiration effects.[41,42]

The gas manifold, gas handling apparatus and sample cell were made of pyrex with flexible stainless steel tubing and fittings (Cajon Ultratorr). Only glass or teflon stopcocks with viton O-rings were used, and halocarbon grease was employed throughout. Ozone was produced by passing dry O_2 through a commercial "ozonizer" and collected on silica gel beads in a cold trap which was immersed in a mixture of dry ice and acetone. Before preparing gas samples, the cold trap was pumped on extensively to remove residual oxygen. The ozone was then

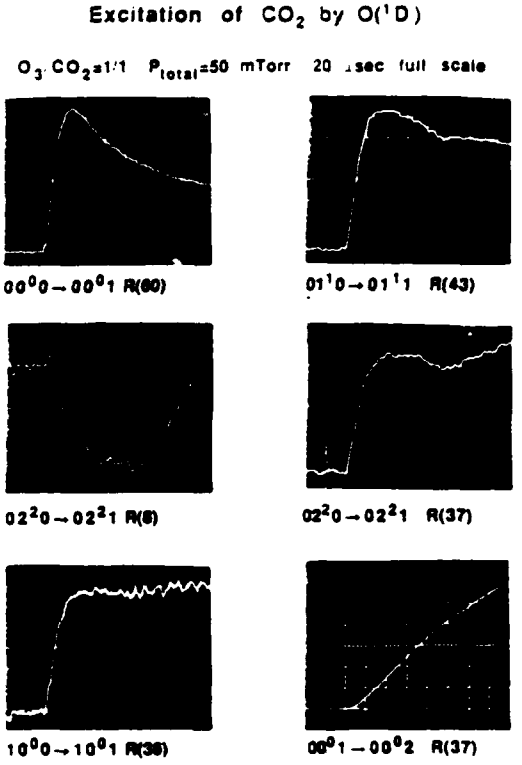

Fig. 1. Time-domain diode laser absorption signals corresponding to ro-vibrational excitation of CO_2 following the 248 nm photolysis of ozone in a 1:1 mixture of CO_2:O_3. Full horizontal scale equals 20 μs. The fast rise in signal amplitude is caused by direct excitation in that particular state; it is followed by a more slowly varying component which corresponds to subsequent rotational relaxation. The lack of a fast rise in the $00^01 \rightarrow 00^02$ R(37) signal indicates a lack of prompt excitation in the 00^01 level; the negative signal in the $02^20 \rightarrow 02^21$ R(8) signal corresponds to *depletion* of ambient population from 02^20;*J*=8 due to the excitation process. The measurements were taken at room temperature (294 K) at a total pressure of 50 mTorr.

transferred from the trap to a 'seasoned', light-tight storage bulb which was kept refrigerated when not in use. The O_3 concentration at room temperature was routinely determined in the cell by means of diode laser absorption measurements of the $000,18_{2,16} \rightarrow 101,19_{2,17}$ IR transition of O_3. Typical samples were about 70% O_3; the remainder of the sample was assumed to be O_2. Later in this paper, mixtures cited as "1/1 CO_2/O_3" are in fact 1/1 mixtures of CO_2 and this O_3/O_2 combination, *i.e.* 1/0.7/0.3 $CO_2/O_3/O_2$. All gas mixtures were prepared in gas bulbs prior to performing the experiments. The CO_2 (Matheson "bone-dry" grade) was purified by two freeze-pump-thaw cycles before use.

III. RESULTS

The 'direct probing' technique employed here provides the nascent CO_2 ro-vibrational population distributions by directly measuring the time dependent IR absorption (following the excimer laser pulse) in a *low pressure* (< 50 mTorr) mixture of CO_2 and O_3. A typical time domain absorption signal for a given ro-vibrational level (*e.g.* Fig. 1) exhibits a fast rise which corresponds to the initial excitation process. This prompt feature is followed by a more slowly varying component resulting from subsequent collisional relaxation and diffusion from the beam path. The amplitude of the fast component corresponds to the collisionally induced population change in the ro-vibrational state because the rise time is fast compared to the time scale for collisional relaxation of the CO_2 translational and rotational degrees of freedom (~4 μs at 25 mTorr). The population change can be roughly estimated by measuring the size of the signal at time *t*=700 ns (the rise time of the IR detector), or more pre-

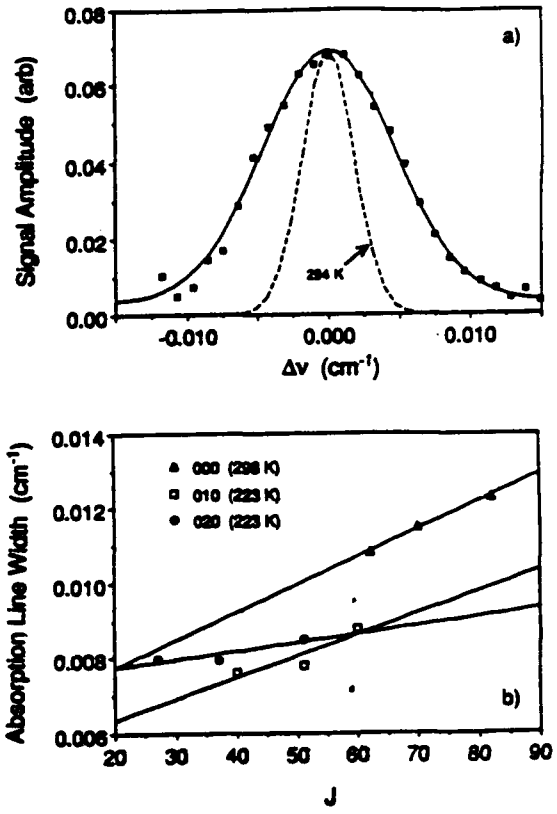

Fig. 2. a) A frequency-domain diode laser absorption signal indicating the nascent absorption line shape for CO_2 molecules which are excited into 02^20; J=51. The (frequency dependent) signal amplitude was measured 720 ns after the 248 nm photolysis pulse. The signal was fit to a Gaussian function (denoted with a solid line) having a width of 0.00831 cm^{-1} (FWHM). This corresponds to a translational temperature of 1130 K, or 785 cm^{-1} per CO_2 molecule. A room temperature Doppler-broadened absorption line (0.00424 cm^{-1} FWHM) is shown for comparison. The data was taken with a 50 mTorr flowing mixture of 1/1 CO_2/O_3 at 294 K. b) Rotational state dependence of transient line widths for representative vibrational levels of CO_2. Solid lines correspond to a least squares fit to the measured line widths. The room temperature 02^20 and 10^00 line widths (not shown) are almost equal to the 223 K 02^20 line widths.

cisely, by fitting the whole signal to a simple model containing multiple exponential decays (and/or rises) and extracting the amplitude at t=0.[41] When normalized for the J-dependent transient absorption line widths (see the following paragraph), the fitted amplitudes provide a detailed map of ro-vibrational state-specific energy deposition in CO_2 during this process.

Translational excitation of the nascent CO_2 molecules in any given ro-vibrational state is obtained by measuring the size of the absorption signal at a number of frequencies surrounding the absorption line center. It was found that the nascent absorption line shapes (at any given time after the excimer laser pulse) can be well fit to a Gaussian function, reflecting a Doppler-broadened, isotropic distribution of excited CO_2 molecules. The relative insensitivity of the apparatus to polarization effects (and the associated non-Doppler absorption profiles) is largely due to the fact that the experiment does not probe the photofragments, but rather the CO_2 quencher molecules which must suffer random collisions with the photofragments in order to become excited. In addition, the collinear geometry of the pump/probe beams and the random polarization of the excimer laser further inhibit the observation of polarization effects.[43] The width of the fitted Doppler profile, measured as a function of time after the excimer laser pulse, provides a measure of the translational temperature of the excited CO_2 molecules. A typical transient absorption signal is shown in Fig. 2.

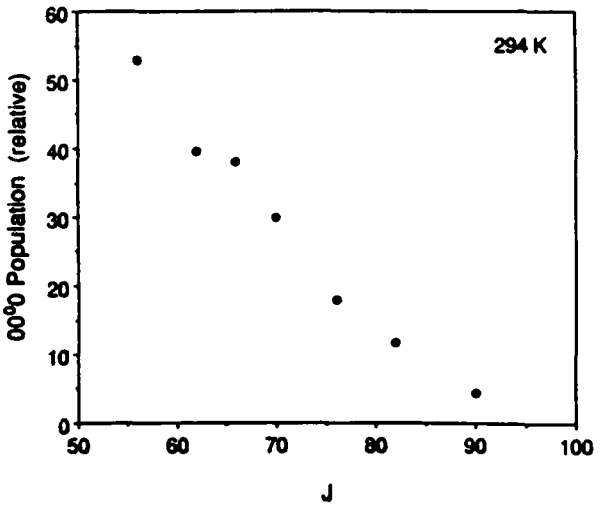

Fig. 3. Rotational state dependence of the nascent CO_2 population produced in the ground state (00^00) following the 248 nm photolysis of ozone in a 1:1 mixture of CO_2:O_3. Values for the low rotational levels are missing due to strong absorption of IR radiation by ambient CO_2 molecules. All data has been corrected for final state line width variations (see Fig. 2b) and correspond to time t=0 (see text for explanation). The measurements were made at room temperature using a 25 mTorr sample pressure; the population magnitudes are scaled relative to the measurements for the 01^10 and 02^20 states given in Figs. 4-6.

A. Excitation in the Ground Vibrational State

Time resolved absorption signals were obtained for excitation of the ground vibrational state (00^00) of CO_2 from J=60 to J=94. Obtaining signals at low rotational levels in the ground state is experimentally difficult because of strong absorption of the diode laser beam by ambient CO_2 molecules in the cell. A typical time-resolved absorption signal for a high rotational level in 00^00 is shown in Fig. 1. Such data was obtained at room temperature (294 K) using a 1/1 mixture of O_3/CO_2 at a total pressure of 25 mTorr. The observed signal exhibits a prompt, detector-limited rise (~ 700 ns), followed by a decay due to rotational relaxation and diffusion of high velocity $O(^1D)$ atoms from the diode beam. The frequency domain signal (taken at t=700 ns) is shown in Fig. 2a along with the room temperature Doppler profile. Note that the fitted width of the nascent absorption line is 0.0093 cm^{-1} (FWHM), approximately 2.2 times larger than the room temperature Doppler width of 0.00424 cm^{-1}. This corresponds to a translational temperature of ~1320 K, and is in close accord with the predictions of a simple 'billiard ball' model for collisions between translationally hot ozone photofragments and CO_2 (see Sec. IV).[44-46] The transient line widths in the ground state, shown in Fig. 2b, are substantially larger than those measured in other vibrational states, and are seen to increase rapidly with increasing final rotational level, J. As discussed in more detail the next section, this features may be signatures of significant CO_2 translational and rotational excitation from the electronic quenching process. The nascent rotational distribution in the ground state, normalized for both laser intensity and transient line widths, is given in Fig. 3; note the monotonic decay of CO_2 excitation as J increases.

B. Excitation in the Antisymmetric Stretching (ν_3) Vibrational Mode

Transient absorption signals for the 00^01 vibrational level of CO_2 are shown in Fig. 1. In contrast to the ground state (and other vibrational states; see Fig. 1), these strong signals rise only *slowly*, on a time scale of ~15-25 gas kinetic collisions. This suggests that 00^01 is *not* directly produced, either by electronic quenching of $O(^1D)$ or by collisional excitation, but

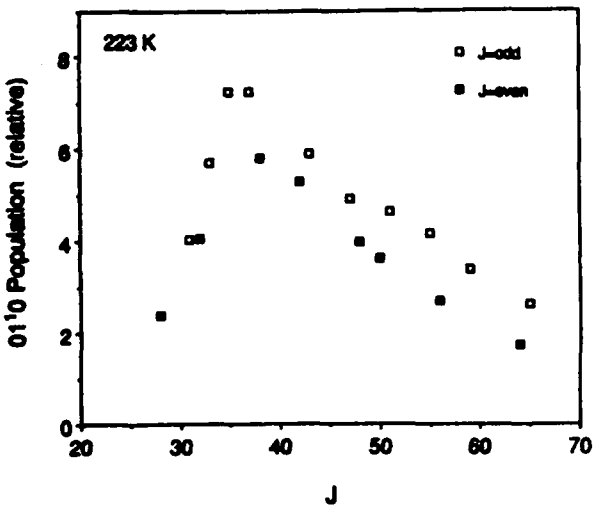

Fig. 4. Nascent rotational population distribution for the first CO_2 bending state, 01^10, following the 248 nm photolysis of ozone in a 1:1 mixture of CO_2:O_3. Values for the low rotational levels are missing due to strong absorption of IR radiation by ambient CO_2 molecules. A significant alternation in excitation between the even and odd rotational levels is clearly seen; on average, the population in the odd rotational levels is larger than the even rotational levels by a factor of 4/3. All data has been corrected for final state line width variations (see Fig. 2b) and correspond to time t=0 (see text for explanation). The measurements were made at room temperature using a 50 mTorr sample pressure; the population magnitudes are scaled relative to the measurements for the 00^00 and 02^20 states given in Figs. 3, 5, and 6.

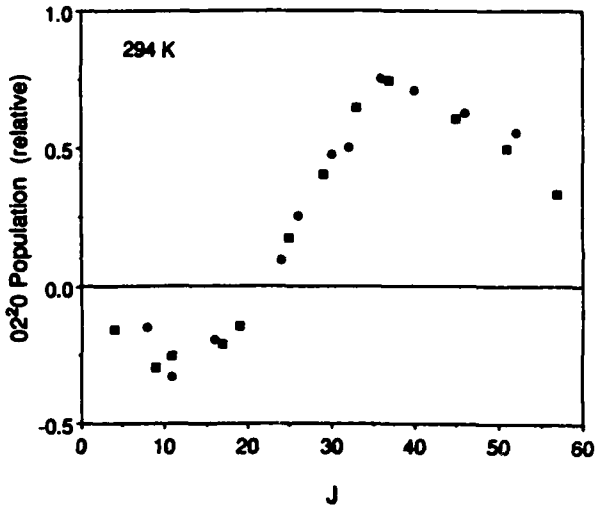

Fig. 5. Nascent rotational population distribution for the CO_2 (02^20) level following the 248 nm photolysis of ozone in a 1:1 mixture of CO_2:O_3. Negative values at low J correspond to *depletion* of the ambient population due, most likely, to pure rotational scattering within the 02^20 level from low to high rotational levels (see text). The nascent rotational population distribution for CO_2 (10^00) is virtually identical to this figure. All data has been corrected for final state line width variations (see Fig. 2b) and correspond to time t=0 (see text for explanation). The measurements were made at room temperature using a 50 mTorr sample pressure; the population magnitudes are scaled relative to the measurements for the 00^00, 01^10, and 02^20 states given in Figs. 3, 4, and 6.

rather through some intermediate species. For example, the slow rising 00^01 signal may be due to non-resonant V-V energy transfer to ground state CO_2 from either highly vibrationally excited $CO_2(nm^lp)$ or vibrationally excited $O_2(^1\Delta)$. Finally, we note that no observable signals, either prompt or otherwise, have been observed in the 00^02 state.

C. Excitation in the Bending (v_2) Vibrational Mode

Typical traces depicting time dependent changes in population of the CO_2 bending levels, 01^10 and 02^20, following the excimer laser pulse are shown in Fig. 1. These signals were acquired using a 1/1 O_3/CO_2 mixture at a total pressure of 50 mTorr. Like the ground state (but unlike 00^01), these states exhibit a *prompt* change in absorption, which decays back to the baseline on a longer time scale. Transient line widths for all of these states are quite similar (see Fig. 2b) and have a weak dependence upon the final rotational level. As in the ground state, the line widths are roughly twice as large as the room temperature Doppler line width, and are also in close accord with the 'billiard ball' collision model (see Sec. IV).

Nascent rotational population distributions for the 01^10 and 02^20 states are given in Figs. 4 and 5; the 03^30 signals are not of sufficient size to obtain a full rotational distribution. Like the ground state, the 01^10 rotational distribution is incomplete because of strong absorption by ambient CO_2 population in the low lying rotational levels. Its most significant feature is the obvious alternation of intensity depending upon whether the final rotational state, J, is even or odd (see Fig. 4). Such an effect has been predicted by Clary and Alexander[47] in a theoretical investigation of ro-vibrational excitation of CO_2 (01^10) by collisions with low energy helium atoms, and has been observed experimentally in our laboratory[48,49] during the collisional excitation of 01^10 and 01^11 by translationally hot hydrogen atoms. This oscillation may provide information about the competing effects of vibrationally inelastic scattering from 00^00 to 01^10 versus pure rotationally inelastic scattering within 01^10 (see Sec. IV).

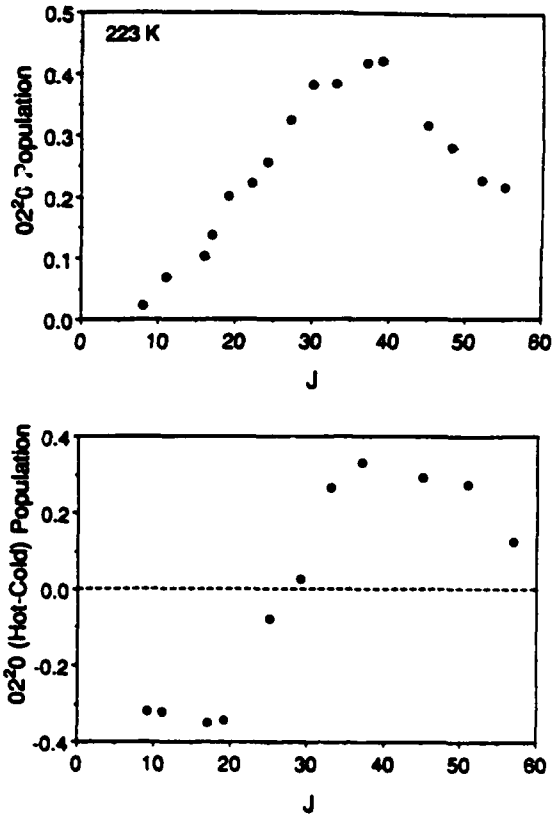

Fig. 6 a) The *low temperature* (223 K) rotational population distribution in CO_2 (02^20). Note the lack of negative values at low J, indicating the decreased importance of pure rotational scattering in the nascent distribution (as compared with Fig. 5). b) The rotational state dependence of the *difference* in nascent population at room temperature (294 K) and low temperature (223 K), *i.e.* "Fig. 5 - Fig. 6".[54] Note that the negative and positive 'lobes' of the distribution are almost identical, suggesting that this graph represents *only* pure rotational scattering within 02^20. Thus, at low temperature little rotational scattering (*i.e.* negative signals) is evident, while at room temperature it is an important feature of the nascent population distribution.

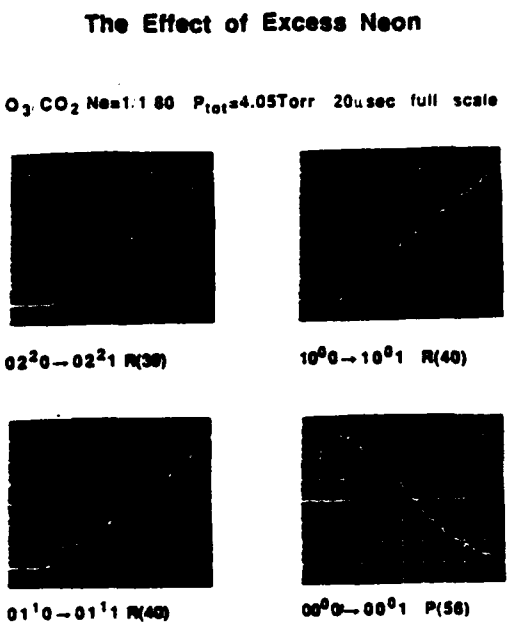

Fig. 7. Time-domain diode laser absorption signals for the ro-vibrational excitation of CO_2 following the 248 nm photolysis of ozone in a 1:1:100 mixture of CO_2:O_3:Ne. The small prompt excitation is caused by a translational/rotational temperature 'jump' which accompanies the excimer laser pulse. The rate of the slowly varying component corresponds to the electronic quenching rate of $O(^1D)$ by CO_2 at room temperature, *i.e.* 3×10^{10} cm^3 molecule^{-1} sec^{-1} (ref. 2). The measurements were taken at room temperature (294 K) at a total pressure of 5 Torr.

The 02^20 distribution is unique in that it is essentially complete, containing both negative signals at low J caused by *depletion* from low rotational levels and positive signals at high J which show a peak near J=37. As described more fully in the next section, these negative signals are believed to be caused by pure rotational scattering within the 02^20 state from collisions between CO_2 and the translationally hot photoproducts. This would cause population from the most heavily populated, low lying rotational levels to be scattered into the higher rotational states:

$$CO_2(02^20;J')+O^*(^1D) \rightarrow CO_2(02^20;J)+O(^1D) ,$$

producing negative signals at low J and positive signals at high J. With this interpretation in mind, we have also obtained a nascent 02^20 population distribution at a substantially lower gas temperature of 223 K, at which the 01^10 population is reduced by a factor of three and the 02^20 population is decreased by a factor of nine. This serves to reduce the contribution from both vibrationally and rotationally inelastic scattering. The 223 K 02^20 distribution, shown in Fig. 6a, exhibits *no* negative signals, suggesting that the negative signals are due to pure rotational scattering among the 02^20 rotational levels.

D. Excitation in the Symmetric Stretching (ν_1) Vibrational Mode

Similar experiments to those performed on the rotational levels of the 02^20 vibrational state were also carried out on the nearly isoenergetic levels, 10^00 and 02^00. Both time and frequency domain absorption signals (using a 1/1 mixture of O_3 in CO_2 at a total pressure of 50 mTorr) were found to be qualitatively similar to the 02^20 signals shown in Figs. 1 and 2. The 10^00 rotational distribution was also found to be essentially identical (within experimental error) to that shown in Fig. 5 for the 02^20 level.

E. The Effect of Adding Excess Neon

Excess neon gas (×100) was added to the CO_2/O_3 sample in order to reduce the importance of T→VRT collisional energy transfer in the observed signals. Since neon does not quench $O(^1D)$ at an appreciable rate (< 10^{-17} cm^3 molecule^{-1} sec^{-1}),[2] its only effect is to absorb the translational energy of the photofragments and to promote fast collisional relaxation among the CO_2 rotational and translational degrees of freedom. At a total pressure of ~ 5 Torr (the partial pressure of the CO_2/O_3 mixture was kept at 50 mTorr), the nascent rotational populations within each CO_2 vibrational state are completely relaxed within the 700 ns rise time of the IR detector, and thus any observed time dependence corresponds to population changes within the given *vibrational* level. As shown in Fig. 7, the previously observed 'prompt' signals essentially disappear in the presence of excess neon (compare with Fig. 1). Instead, the signals exhibit a much smaller prompt rise from the slight rotational/translational temperature 'jump' following the excimer pulse (whose size is proportional to the ambient vibrational state population), followed by a slowly changing component whose time scale corresponds to the known room temperature CO_2+$O(^1D)$ quenching rate.[2] As will be discussed in the next section, this strongly suggests that the prompt signals seen in Fig. 1 are due solely to T→VRT collisional excitation, not electronic quenching of $O(^1D)$ by CO_2.

IV. DISCUSSION

Energy can be deposited into the internal degrees of freedom of CO_2 via two separate mechanisms, 1) E→VRT electronic quenching of $O(^1D)$, and 2) T→VRT inelastic energy transfer from the photoproducts. Both processes are relatively fast, and both deposit substantial amounts of energy into the CO_2 bath molecules. Nevertheless, the data obtained so far indicates that the "prompt" signals and the nascent populations presented in the previous section are due *only* to inelastic scattering between the translationally hot photofragments and CO_2, *not* from the electronic quenching process. This implication is supported by five different experimental findings: 1) the relatively narrow transient line widths measured for all states *except* the ground state, 2) the oscillation in the magnitudes of the odd/even nascent 01^10 rotational populations, 3) the large amounts of rotational scattering in 02^20, 4) the lack of prompt signals when excess neon is added to the system, and 5) the results of 'harvesting' experiments which suggest little deposition of energy into the vibrational degrees of freedom of CO_2. We examine items 1-4 in detail below; the fifth will be discussed briefly below and more completely in a forthcoming paper.[50]

A. Transient Line Widths

The transient absorption line shapes were measured for the majority of the ro-vibrational levels which were probed in this investigation. Despite the enormous energy available in the system (1 eV translational+2 eV electronic), the line widths are fairly narrow for vibrational levels other than the ground state, only ~2 times the room temperature Doppler line width (see Fig. 2b). This level of excitation corresponds to a translational 'temperature' of ~1200 K, *i.e.* only ~830 cm^{-1} of translational energy per CO_2 molecule. It is instructive to compare the experimentally measured line width with that predicted by a simple 'billiard ball' calculation for collisional energy transfer during elastic collisions between hard spheres which have the same mass as CO_2, O, and O_2. Assuming that the the photofragments collide with CO_2 molecules which are initially at rest, the average CO_2 energy (averaged over all angles of approach) is simply given by:[44-46]

$$E^T_{CO_2} = \frac{2\mu}{M_{CO_2}+M_O} E^T_O , \qquad (1)$$

where E^T_O is the initial laboratory frame translational energy of

the O atom (or O_2). E'_{CO_2} is the final lab frame CO_2 translational energy, and $\mu = 11.733$ amu is the system reduced mass. For excitation of CO_2 (02^20) by collisions with both O and O_2 photofragments, Eq. (1) gives values for E'_{CO_2} of 1580 and 660 cm^{-1} respectively (after having first subtracted the 1334 cm^{-1} of unavailable 02^20 vibrational energy from E'_O). The average of these two values, 1120 cm^{-1}, leads to a predicted line width which is amost exactly equal to the measured value. This suggests that either 1) the E→VRT process *coincidentally* produces the same amount of CO_2 translational excitation as simple inelastic scattering, or 2) the experimental data in the upper vibrational states simply does not reflect the results of the electronic quenching process. While such a coincidence is certainly possible, the arguments which follow make it appear unlikely. Note finally that the transient line widths for rotational levels between J=60 and J=80 in the ground vibrational state of CO_2 are significantly larger (see Fig. 2b) than those seen in the vibrationally excited level; in addition, they are increasing rapidly as a function of J. As will be discussed below, this may imply that the electronic quenching process provides substantial translational and rotational but *little* CO_2 vibrational excitation.

B. Odd/Even Oscillation in 01^10

Alternations in the magnitude of the cross sections for scattering from the ground vibrational state (00^00) of CO_2 into the odd versus even rotational states of the first bending vibrational state (01^10) have been both predicted by Clary and Alexander[47] for He-CO_2 scattering and observed experimentally in H-CO_2 collisions.[48] This effect arises during the symmetry breaking which accompanies the $00^00 \rightarrow 01^10$ transition. As in He-H_2 scattering,[51] the linear, symmetric CO_2 ground vibrational state allows only ΔJ=even rotational transitions due to selection rules in the rotational coupling matrix elements. Furthermore, the ground state is missing all odd rotational levels as a result of nuclear spin statistics, whereas the bent 01^10 state has *both* even and odd rotational levels. As a result, one expects a marked propensity for scattering into a single manifold of rotational levels in 01^10 (either odd or even, depending upon the symmetry of the vibrational wavefunctions) during the vibrationally inelastic transition. In fact, it is the *odd* rotational levels in 01^10 which are populated most heavily (see Fig. 4 and ref. 44).

While oscillations in the nascent 01^10 rotational populations are well known for collisional energy transfer, such a phenomena has not, to the best of our knowledge, been described for electronic quenching processes. Because of the substantial isotopic scrambling which has been observed in this system, both in our laboratory and by other researchers,[20] *i.e.*

$$C^{18}O_2 + {}^{16}O(^1D) \rightarrow 69\%\left[C^{16}O^{18}O + {}^{18}O(^3P)\right] + 31\%\left[C^{18}O_2 + {}^{16}O(^3P)\right]$$

the electronic quenching process is thought to proceed through a CO_3 collision complex which dissociates statistically into CO_2+O. Bending excitation produced by such a mechanism is *not* likely to favor a single manifold of rotational levels, unless such an excitation occurs in the exit channel via a (half-)collision-like interaction between ground state CO_2 and the departing oxygen atom. Rather, it is more likely that the high energy electronic quenching process, which may involve the dissociation of a highly bent CO_3 complex, would populate both even and odd rotational levels with equal probability.

If the even/odd oscillation observed in 01^10 is interpreted solely in terms of inelastic scattering, the experimentally measured nascent populations shown in Fig. 4 can be used to provide an estimate of the relative importance of vibrationally inelastic scattering from the ground state versus pure rotational scattering within the 01^10 level. Such information is useful for interpreting temperature dependent measurements in the 02^20 level discussed below and may be obtained in the following manner. First, we consider the effect that pure rotational scattering within 01^10 has upon the measured 01^10 population distribution. At 223 K, ~2.7% of all CO_2 molecules are found in the 01^10 state. The number of populated rotational levels is sufficiently large (~60) that the population in any two adjacent even and odd rotational states is roughly equal. It follows that pure rotational scattering within the 01^10 state, *regardless* of any propensities which might exist, produces equal numbers of molecules in odd and even rotational states. In other words, pure rotational scattering does *not* produce oscillations in the nascent populations, and thus the excess population observed in the odd rotational levels of 01^10 at 223 K(see Fig. 4) are probably caused by vibrationally inelastic scattering from the ground state. Note that the excess molecules found in the odd rotational levels are quite a large fraction of the total nascent 01^10 population.

Although the detailed propensity rules for scattering from 00^00 into even versus odd rotational levels of 01^10 are complex and depend upon the initial rotational state,[47] the *overall* behavior of the system may be described in simpler terms. Model calculations[52] indicate that, in the absence of even/odd propensities, state-to-state ro-vibrational scattering cross sections from 00^00 to 01^10 are quite similar to cross sections for pure rotational scattering within 01^10 except for their absolute magnitude. In other words, the ro-vibrationally inelastic cross sections appear to be'dynamically separable' into cross sections for pure rotational scattering times a simple multiplicative factor to account for vibrational inelasticity. As a result, we can ascertain the 'relative importance' of these two scattering channels if their 'results' (*i.e.* nascent populations) can be separately compared. Fortunately, the even/odd scattering propensities and oscillating nascent populations in 01^10 provide such an opportunity. The relative importance of rotational versus vibrational scattering can be roughly determined by comparing nascent populations scattered into adjacent (even and odd) rotational levels in 01^10, $N^{010}_{J=even}$ and $N^{010}_{J=odd}$, for *high* values of J (as described below). In these high rotational levels, the ambient population is sufficiently small that depletion due to pure rotational scattering may be neglected, and as a result, the observed nascent population increase represents positive contributions from both rotationally and vibrationally inelastic scattering. This may be written:

$$N^{010}_{J=even} = N^{rot} + N^{vib}_{\Delta J=even} \qquad (2)$$

$$N^{010}_{J=odd} = N^{rot} + N^{vib}_{\Delta J=odd} \,. \qquad (3)$$

where N^{rot} is the contribution from pure rotational scattering, while $N^{vib}_{\Delta J=even}$ and $N^{vib}_{\Delta J=odd}$ are the vibrationally inelastic contributions from the ground state. Assuming temporarily that *all* of the vibrational scattering ends up in the odd rotational levels of 01^10, *i.e.* $N^{vib}_{\Delta J=even}=0$ and $N^{vib}=N^{vib}_{\Delta J=odd}$, then

$$N^{rot} \approx N^{010}_{J=even} \qquad (4)$$

and

$$N^{vib} \approx N^{010}_{J=odd} - N^{010}_{J=even} \,. \qquad (5)$$

In this limit, $(N^{010}_{J=odd} - N^{010}_{J=even})$ and $N^{010}_{J=even}$ are, respectively, separate measures of contributions from vibrationally inelastic and pure rotational energy transfer. We explicitly express the ratio of these quantities, R, as

$$R \equiv \frac{\textit{Vibrational inelasticity}}{\textit{Rotational inelasticity}} \approx \frac{N^{010}_{J=odd} - N^{010}_{J=even}}{N^{010}_{J=even}} \quad (6)$$

From the measured nascent 01^10 rotational distribution shown in Fig. 4, an experimental value for R is found to be ~1/3, indicating vibrational scattering is an important channel relative to pure rotational scattering, and accounts for a significant fraction of the observed nascent populations. This is the most *conservative* statement that can be made; if vibrational scattering populates *even* levels of 01^10 as well as the odd levels (*contrary to the simplifying assumption above*), then vibrational excitation plays an even larger role in the observed signals!

C. Rotational Excitation in 02^20

In a similar fashion, the room temperature 02^20 distribution shown in Fig. 5 can be interpreted as being composed of pure rotational scattering within the 02^20 level and vibrationally inelastic scattering from 01^10. The importance of the 02^20 distribution is that it is essentially complete, including both positive values at high rotational levels as well as negative values at low J which correspond to scattering *out of* these states. It is unlikely that significant scattering into 02^20 arises from the ground state of CO_2; simple S.S.H. calculations indicate that such cross sections are smaller by more than three orders of magnitude than those for scattering from 01^10.[53-55] Because the $01^10 \rightarrow 02^20$ energy gap is roughly equal to the $00^00 \rightarrow 01^10$ gap, we expect that the importance of vibrationally inelastic scattering relative to pure rotational scattering in the 02^20 distribution is roughly *twice* that seen in the 01^10 distribution. This is due to the existence of *both* even and odd rotational levels in 01^10 as compared with only even levels in 00^00 (*i.e.* $N^{020}_{odd}/N^{010}_{odd} = 2N^{010}_{even}/N^{000}_{even}$). Evidence for the domination of vibrational scattering over rotational scattering *is clearly seen* in the 223 K 02^20 distribution shown in Fig. 6a where *no* negative (*i.e.* rotationally inelastic) signals can be observed! Note finally that if the 223 K distribution, which represents as much as possible the pure vibrationally inelastic scattering distribution, is subtracted from the room temperature distribution,[56] we obtain in Fig. 6b what appears to be a distribution for pure rotationally inelastic scattering; the negative and positive populations are of almost exactly the same size. Such a procedure is not strictly valid because of uncertainties in the relative magnitudes of the two distributions, but it clearly demonstrates how the two separate scattering processes can combine to yield the observed distribution. The presence of significant negative signals, along with the substantial temperature dependence of the nascent 02^20 distribution, also argue for a T→VRT inelastic scattering mechanism rather than for an E→VRT electronic quenching process.

D. The Effect of Excess Neon

A simple and direct test to determine the origin of the fast signals observed in the present experiments was made by adding a large (×100) excess of neon buffer gas to the system. Numerous studies have shown that neon is an extremely poor quencher of $O(^1D)$, requiring more than 10^6 *Ne-$O(^1D)$ collisions* to occur. Thus, prompt CO_2 signals should continue to be evident in the presence of excess neon if the previously observed signals are caused by electronic quenching. If these signals are due to collisional energy transfer, they should disappear because the many intervening Ne-$O(^1D)$ collisions which absorb the translational energy of the photoproducts. The effect of neon is threefold: 1) it slows down the velocity of the $O(^1D)$ atoms (and thus reduces the quenching rate) by a factor of four, 2) it brings the CO_2 molecules into translational, rotational and partial vibrational equilibrium before the signal can be measured, and 3) it vastly slows the rate of diffusion of the $O(^1D)$ atoms from the beam path. If the prompt signals shown in the last section were caused by the E→VRT process, their size would be diminished (on average) by a factor of four, and the observed nascent rotational population distributions would all exhibit a well defined Boltzmann rotational temperature. Instead, the prompt signals are greatly suppressed, leaving only a small portion due to the temperature jump which accompanies the photolysis pulse. In place of the large prompt signals are only slowly varying CO_2 signals whose time scales correspond closely to the *room temperature* quenching rate of $O(^1D)$. *The combination of a slowly falling signal* in the ground state (*i.e.* depletion of 00^00 population) with the slowly *rising signals* in 01^10, 02^20, and 10^00, would appear to indicate vibrational excitation during the electronic quenching process. Nevertheless, quantitative measurements of such data show that vibrational excitation is quite small relative to excitation in the rotational and translational degrees of freedom. In fact, separate time resolved studies[50] show that the translational and rotational temperature increase dramatically with time, indicating strong dumping of energy into the rotational/translational degrees of freedom due to an as-yet-undetermined mechanism. This result suggests that the prompt signals shown in Fig. 1 are due *predominantly* to T→VRT inelastic energy transfer from the translationally hot photoproducts to CO_2 instead of the E→VRT electronic quenching process.

E. 'Harvesting' Results and Implications

The *total* amount of CO_2 vibrational energy for this system has recently been measured in a set of preliminary 'harvesting' experiments. In this technique, excess CO_2 as added to the sample in order to 'promote fast, near-resonant V-V energy transfer collisions which efficiently 'harvest' all of the CO_2 vibrational energy down into the low-lying vibrational energy levels where it is conveniently measured. These preliminary experiments, which will be the subject of a separate publication,[50] indicate that the electronic quenching process yields very little CO_2 vibrational excitation (<500 cm^{-1} per molecule) in this system. If this finding is correct, then the vast majority of the 2 eV contained in the $O(^1D)$ - as well as its additional 2/3 eV translational energy - must be partitioned between CO_2 translation and rotation during the E→VRT process. By invoking conservation of energy and angular momentum, and assuming that no energy is left as CO_2 vibration, it can be shown[52] that a CO_3 complex with an initial internal energy of E=2 eV will dissociate into CO_2+$O(^3P)$ fragments which have a final relative translational energy E' given by

$$E' = E\left[1 + \frac{\mu}{I} b_n^2\right]^{-1} , \quad (7)$$

where I = 43.1 amu Å^2 is the moment of inertia of the CO_2 molecule and b_n is the 'effective impact parameter' or moment arm of the half collision. The final CO_2 rotational and laboratory frame translational energy are given by:

$$E^{rot}_{CO_2} = E - E' ; \qquad E^{T}_{CO_2} = \frac{\mu}{M_{CO_2}} E' . \quad (8)$$

The size of b_n in Eq. (7) clearly governs how much of the initial 2 eV internal energy will be partitioned into relative translational energy; the remainder is converted into CO_2 rotation. Without knowing details of the interaction potential, it is difficult to obtain a precise value for b_n. Nonetheless, from the size of the CO_2 molecule and probable values for the position and angle of the oxygen atom "push-off", it is likely that b_n ranges from 0.7-1.4 Å. Although the majority of the energy is carried away by the oxygen atom, a substantial amount remains in CO_2 translation and rotation. The span of probable b_n values leads

to CO_2 translational/rotational energies which range from 3980 cm^{-1}/956 cm^{-1} to 2760 cm^{-1}/5530 cm^{-1}.

The primary consequence of the energy partitioning calculation presented above is that the observed line widths from the "prompt" signals are much too small to be due to the electronic quenching process. That process *alone* should provide 3000-4000 cm^{-1} per CO_2 molecule; in addition, an extra 1500 cm^{-1} per molecule is expected from the collisional recoil. These estimates suggest that the transient line widths associated with the electronic quenching process should be ~4 times greater than room temperature, and twice as large as that measured in this work. We have recently searched for such broad transient absorption lines which would indicate the electronic quenching process, but have been unsuccessful to date. This may be due to a number of causes. First, the increased absorption line width associated with the quenching process means that the maximum absorption signal (at line center) is smaller than that associated with collisional excitation. Second, while translational and rotational excitation typically require only a single gas kinetic collision, the electronic quenching process - albeit fast - requires ~3 gas kinetic collisions at room temperature. However, the rate for this process has a *negative* temperature coefficient, suggesting that the electronic quenching rate of *translationally excited* $O(^1D)$ atoms (via 248 nm photolysis of O_3) by CO_2 is slower than the room temperature rate by as much as an order of magnitude.[2] These factors may combine to substantially decrease our ability to observe the E→VRT quenching process directly in the presence of significant T→VRT collisional excitation.

An important factor which inhibits our ability to locate signals corresponding to the electronic quenching process is uncertainty about which CO_2 states to probe. Several contradictory suggestions have been proffered. Infrared fluorescence measurements by Trolier and Wiesenfeld[57] indicate that the primary vibrational levels populated are CO_2 $(0,m,p)$, where m ranges from 3-6 and p from 2-3. Similar work by Barker[58] (using 308 nm excimer radiation) suggests that p may be as high as 10! In contrast, IR fluorescence, diode laser/boxcar, and diode laser 'harvesting' studies in our lab indicate little or no CO_2 vibrational excitation! Instead, these latter measurements suggest that high rotational and translational excitation is present in the CO_2 ground state and first bending level. The energy partitioning calculations presented above indicate that dissociation of a static CO_3 intermediate would yield 1000-5500 cm^{-1} in rotational energy, *i.e.* 50-120 ħ. In addition, the complex may already have as much as $L=\mu vb \sim 75$ ħ from the original $O+CO_2$ associative collision. Thus, we might expect to observe a nascent distribution in the ground state which is bimodal, with relatively narrow transient lines at low J (J=0-80) due T→RT collisional energy transfer, and broad absorption lines at extremely high rotational levels (J=50-200) from the E→RT electronic quenching process. The unusually large transient line widths measured in high rotational levels of the ground state (see Fig. 2b) may be evidence of such a bimodal distribution.

V. CONCLUSION

Time-domain diode laser absorption spectroscopy has been used to measure state specific energy disposal in the translational, rotational, and vibrational degrees of freedom of CO_2 following the 248 nm excimer photolysis of a low pressure mixture of CO_2 and ozone. Although prompt excitation is found in many ro-vibrational levels, a large body of evidence suggests that these signals are due *only* to T→VRT inelastic scattering between the translationally hot photoproducts and CO_2, *not* from the E→VRT electronic deactivation of $O(^1D)$ by CO_2. Although this process is though to involve a highly bent (D_{3h} or C_{2v}) CO_3 intermediate, recent experiments[50] indicate that little of the 2 eV electronic energy is deposited in the vibrational degrees of freedom of CO_2. Instead, the vast majority of this energy appears in CO_2 rotation and translation. Thus, except for the observation of unusually large transient line widths in high rotational levels of the ground state, there appears to be no evidence (as yet) of *direct* energy deposition from this fast, energetic quenching process. Explanations for the apparent absence of these signals include: 1) the E→VRT process is obscured by the large T→VRT inelastic scattering signals, 2) the quenching rate is much smaller than expected because of the high velocity of the $O(^1D)$ atoms and the negative activation energy, and 3) the electronic quenching process populates high-lying ro-vibrational levels of CO_2 which have not yet been probed. In light of recent work which has found substantial *indirect* evidence of this process,[50] it is hoped that further investigation will provide a complete state-resolved map of energy deposition in CO_2 during this important interaction.

ACKNOWLEDGEMENTS

We are grateful to Professor John Wiesenfeld and Dr. Michael Trolier for communicating their IR emission data on the $O(^1D)+CO_2$ system prior to publication, and also to Professor Millard Alexander for a number of helpful discussions. Work supported by the Joint Sevices Electronics Program, the National Science Foundation, and the Department of Energy.

REFERENCES

1 R.J . Donovan and D. Husain, Chem. Rev., 70, 489 (1970).
2 *Chemical Kinetics and Photochemical Data for Use in Stratospheric Modeling*, JPL 87-41, (Jet Propulsion Laboratory, Pasadena, 1987).
3 J. R. Wiesenfeld, Acc. Chem. Res., 15, 110 (1982).
4 R. F. Heidner, III, D. Husain, and J. R. Wiesenfeld, Chem. Phys. Lett., 16, 530 (1972).
5 R. F. Heidner, III, D. Husain, and J. R. Wiesenfeld, J. Chem. Soc., Faraday Trans. II, 69, 927 (1973).
6 J. A. Davidson, C. M. Sadowski, H. I. Schiff, G. E.Streit, C. J. Howard, D. A. Jennings, and A. L. Schmeltekopf, J. Chem. Phys., 64, 57 (1976).
7 G. E. Streit, C. J. Howard, A. L. Schmeltekopf, J. A. Davidson, and H. I. Schiff, J. Chem. Phys., 65, 4761 (1976).
8 J. A. Davidson, H. I. Schiff, G. E. Streit, J. R. McAfee, A. L. Schmeltekopf, and C. J. Howard, J. Chem. Phys., 67, 5021 (1977).
9 S. T. Amimoto, A. P. Force, R. J. Gulotty, Jr., and J. R. Wiesenfeld, J. Chem. Phys., 71, 3640 (1979).
10 S. T. Amimoto, A. P. Force, and J. R. Wiesenfeld, Chem. Phys. Lett., 60, 40 (1978).
11 P. H. Wine and A. R. Ravishankara, Chem. Phys. Lett., 77, 103 (1981).
12 T. G. Slanger and G. Black, J. Chem. Phys., 60, 468 (1974).
13 E. R. Fisher and E. Bauer, J. Chem. Phys., 57, 1966 (1972).
14 J. J. Ewing, Chem. Phys. Lett., 29, 50 (1974).
15 J. C. Tully and R. K. Preston, J. Chem. Phys., 55, 562 (1971).
16 M. H. Miller and T. F. George, J. Chem. Phys., 56, 5637 (1972).
17 W. H. Miller, J. Chem. Phys., 68, 4431 (1978).
18 R. D. Levine and R. B. Bernstein, Chem. Phys. Letter., 15, 1 (1972).
19 J. C. Tully, J. Chem. Phys., 62, 1893 (1975).
20 D. L. Baulch and W. H. Breckenridge, Trans. Faraday Soc., 62, 2768 (1966).
21 K. F. Preston and R. J. Cvetanovic, J. Chem. Phys. 45,

2888 (1966).
22 E. Weissberger, W. H. Breckenridge, and H. Taube, J. Chem. Phys., 47, 1764 (1967).
23 N. G. Moll, D.R. Clutter, and W. E. Thompson, J. Chem. Phys., 45, 4469 (1966).
24 S. Canuto and G. H. F. Dickerson, Chem. Phys., 120, 375 (1988).
25 J. S. Fransisco and I. H. Williams, Chem. Phys., 95, 373 (1985).
26 B. M. Gimarc and T. S. Chou, J. Chem. Phys., 49, 4043 (1968).
27 M. Cornille and J. Horsley, Chem. Phys. Lett., 6, 373 (1970).
28 J. F. Olsen and L. Burnelle, J. Am. Chem. Soc., 91, 7286 (1969).
29 J. A. Poper, U. Seeger, R. Seeger, and P.V.R. Schleyer, J. Comp. Chem., 1,199 (1980).
30 W. J. Van de Guchte, J. P. Zwart, and J. J. C. Mulder, J. Molec. Struct. (Theochem) 152, 213 (1987).
31 T. G. Slanger and G. Black, J. Chem. Phys., 54, 1889 (1971).
32 J. F. Noxon, J. Chem. Phys., 52, 1852 (1970).
33 R. J. Donovan, D. Husain, L.J. Kirsch, Trans. Faraday Soc., 67, 375 (1971).
34 R. G. Shortridge and M. C. Lin, Chem. Phys. Lett., 35, 146 (1975).
35 A. J. Sedlacek, D. R. Harding, R. E. Weston, Jr., T. G. Kreutz, and G. W. Flynn, *Probing the $O(^1D)+CO_2$ Reaction with Second Derivative Modulated Diode Laser Spectroscopy*, submitted J. Chem Phys.
36 J. J. Valentini, D. P. Gerrity, D. L. Philips, J. Nieh, and K. D. Tabor, J. Chem. Phys., 86, 6745 (1987).
37 R. K. Sparks, L. R. Carlson, K. Shobatake, M. L. Kowalczyk, and Y. T. Lee, J. Chem. Phys., 72, 1401 (1979).
38 J. O. Chu, C. F. Wood, G. W. Flynn, and R. E. Weston, Jr., J. Chem. Phys., 81, 5533 (1984).
39 J. A. O'Neill, J. Y. Cai, G. W. Flynn, and R. E. Weston, Jr., J. Chem. Phys., 84, 50 (1986).
40 J. A. O'Neill, C. X. Wang, J. Y. Cai, G. W. Flynn, and R. E. Weston, Jr., J. Chem. Phys., 88, 6240 (1988).
41 F.A. Khan, T.G. Kreutz, G.W. Flynn, and R.E. Weston, Jr., *State Resolved Vibrational, Rotational, and Translational Energy Deposition in $CO_2(00^01)$ Excited by Collisions with Hot Hydrogen Atoms*, submitted: J. Chem. Phys.
42 F. A. Khan, T. G. Kreutz, L. Zhu, G. W. Flynn, and R. E. Weston, Jr., J. Phys. Chem. 92, 6171 (1988).
43 R. N. Zare, Mol. Photochem. 4, 1 (1972).
44 J. F. Hershberger, J. Z. Chou, G. W. Flynn, and R. E. Weston, Jr., Chem. Phys. Lett. 149, 51 (1988).
45 J. F. Hershberger, S. A. Hewitt, S. K. Sarkar, G. W. Flynn, and R. E. Weston, Jr., *Quantum State Resolved Study of Pure Rotational Excitation of CO_2 by Hot Atoms*, accepted: J. Chem. Phys.
46 W. F. Libby, J. Am. Chem. Soc. 69, 2523 (1947).
47 M.H. Alexander and D.C. Clary, Chem. Phys. Lett. 98, 319 (1983).
48 J. F. Hershberger, S. A. Hewitt, G. W. Flynn, and R. E. Weston, Jr., J. Chem. Phys. 88, 7243 (1988).
49 F. A. Khan, T. G. Kreutz, J. A. O'Neill, C. X. Wang, G. W. Flynn, and R. E. Weston, Jr., *State Resolved Vibrational, Rotational, and Translational Energy Deposition in $CO_2(01^11)$ Excited by Collisions with Hot Hydrogen Atoms*, submitted: J. Chem. Phys.
50 L. Zhu, T. G. Kreutz, and G. W. Flynn, *Diode Laser Probe of Vibrational, Rotational, and Translational Excitation of CO_2 following Collisions with $O(^1D)$: II. Electronic Quenching*, submitted: J. Chem. Phys.
51 T. G. Kreutz, L. Eno, and H. Rabitz, J. Chem. Phys. 88, 6322 (1988), and references within.
52 T. G. Kreutz, F. A. Khan, and G. W. Flynn, *Analysis of Translational, Rotational, and Vibrational Energy Transfer in Collisions between CO_2 and Hot Hydrogen Atoms; The 3-Dimensional 'Breathing' Ellipsoid Model*, submitted: J. Chem. Phys.
53 R. N. Schwartz, Z. I. Slawsky, and K. F. Herzfeld, J. Chem. Phys. 20, 1591 (1952).
54 F. I. Tanzcos, J. Chem. Phys. 25, 439 (1956).
55 J. T. Yardley and C. B. Moore, J. Chem. Phys. 46, 4491 (1967).
56 This procedure cannot be performed rigorously due to uncertainties in the relative magnitudes of the nascent populations measured at room temperature and at 223 K (see ref. 41 for a more complete discussion of this problem), but the procedure is nonetheless instructive and qualitatively correct.
57 M. Trolier, Thesis, Cornell University, 1988.
58 J. Barker, private communication.

SIGNIFICANT ACCOMPLISHMENTS

The Schottky barrier behavior of Ti/Pt/GaAs and Pt/Ti/GaAs bimetal structures has been investigated using several surface analysis techniques. Interfacial morphology of Ti and Pt thin films on GaAs(100) substrate was characterized by coverage profiling of Auger electron spectroscopy and transmission electron microscopy. The results showed no sign of clustering for both metals at room temperature deposition. A simple model explains well the bimetal Schottky behavior. Within this model, the functional dependence of the barrier height on the inner metal thickness is interpreted in terms of the metal effective screening and the interface trap states. Data analysis shows that the effective screening lengths of Pt and Ti are significantly greater than the usual estimates and that the potential drop inside the metal electrode of a Schottky contact is not negligible, in contrast to the common assumption.

Photoelectric emission induced by a focused UV laser beam (λ=257nm) has been used to probe semiconductor surfaces. It was possible to distinguish between regions of different doping levels on a silicon surface. The spatial resolution was found to be limited only by the laser beam spot size.

The photoluminescence from ZnSe epilayers on GaAs, bulk crystalline ZnSe, and $ZnSe/ZnMn_xSe_{1-x}$ superlattices, when subjected to hydrostatic pressure in a diamond anvil cell, has been studied. These measurements will aid in the development of optical and electronic devices based on wide-band-gap II-VI semiconductors.

Raman microprobe spectroscopy has been used to profile locally doped regions in GaAs with micrometer-level resolution. This is an important in-situ diagnostic technique for compound semiconductors.

A simple method for producing hot electrons and studying their collisions with molecules in the gas phase has been developed. A key and novel feature of the experiments is the resolution, $0.0003cm^{-1}$ or approximately 4×10^{-8} eV! This compares with standard electron scattering experiments which have a typical energy resolution of about 80 cm^{-1} or 10 meV. The high resolution is obtained by observing the molecular collision partner rather than the scattered electron as is normal in most electron scattering experiments. Such studies are providing fundamental insight into the mechanisms and processes which are important in plasma etching reactors. Considerable interest in this technique has been exhibited by scientists working on plasma etching diagnostics in the electronics industry.

For optical signals transmitted through random media such as the atmosphere, recursion relations, together with the generalized method of steepest descent, have been

developed to numerically evaluate the photon-counting distributions and their factorial moments to excellent accuracy.

Optical dephasing phenomena have been studied in organic dyes in solution and semiconductor doped glasses. Dephasing times as short as 18 fsec were observed at room temperature.

TECHNOLOGY TRANSITIONS

A collaboration between Columbia and Professor C. B. Carter's group at Cornell University has been established to characterize interfacial morphology of different metals on GaAs. The TEM analysis of Ti/Pt/GaAs presented in this report was achieved through this collaboration.

Laser etching of GaAs, supported for several years by JSEP, has been pursued as an industrial process by Siemens. In addition, laser etching has also been used by United Technology for trimming of integrated optical waveguides and the etching of semiconductor sensors.

A joint project with Frederico Cappaso of AT&T has yielded several new concepts for quantum well detectors to accomplish reduction in optical noise. A joint project with Bellcore has yielded a method for evaluating noise in semiconductor laser amplifiers.

PERSONNEL

Faculty

G. Flynn, Professor of Chemistry
S. Hartmann, Professor of Physics
I. Herman, Associate Professor of Applied Physics
R. Osgood, Professor of Electrical Engineering and Applied Physics
M. Teich, Professor of Engineering Science
E. Yang, Professor of Electrical Engineering

Visiting Scientists

Dr. B. Brody
Dr. Z. Wu
Mr. H. Yaowu

Research Scientists

Dr. T. Kreutz
Dr. D. Podlesnik
Dr. R. Scarmozzino
Dr. Z. Wu

Post-Doctoral Research Scientists

Dr. D. DeBeer
Dr. J. Hershberger
Dr. J. Hossenlopp
Dr. P. Mei
Dr. S. Sarkar
Dr. M. Schmidt

Graduate Research Assistants

M. Arend
B. Burke
R. Campos
T. Choi
J. Cressler
U. Gennser
N. Hakim
S. Hewitt
B. Jalali
J. Jiang
S. Keilson
F. Kahn
V. Liberman
T. Licata
S. Lowen
K. Luo
Q. Y. Ma
F. Moshary
K. Ni
J. Piao
B. Quiniou
W. Schwarz
P. Shaw
C. Shu
Z. Sui
T. Tanabe
H. Tang
A. Tuchman
E. Usadi
X. Wu
Q. Wang
L. Zhu

Undergraduate Technicians

J. Aizprua
H. Beressi
C. Berzins
R. Cardenas
C. Chen
J. Chung
J. Chow
J. Collins
A. Cowder
S. Edwards
K. Feng
A. Fleischman
D. Gnanakuru
C. Goldberg
V. Huang
L. Liu
J. Matsibekker
H. Ng
S. Ng
P. Ronen
A. Tam
R. Ting
M. Torres
B. Wendemagegnehu
X. J. Wong
J. Yves

Administration

B. Blegen
L. Morrison
M. Santoro
G. White
K. Wingate